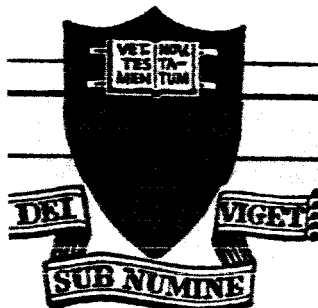


GPO PRICE \$ _____

CFSTI PRICE(S) \$ _____

Hard copy (HC) 3.00

Microfiche (MF) 1.75



653 July 65

FACILITY FORM 602

N66 35790	_____
(ACCESSION NUMBER)	(THRU)
<u>95</u>	<u>1</u>
(PAGES)	(CODE)
<u>CP-77672</u>	<u>33</u>
(NASA CR OR TRX OR AD NUMBER)	(CATEGORY)

PRINCETON UNIVERSITY
DEPARTMENT OF
AEROSPACE AND MECHANICAL SCIENCES

NATIONAL AERONAUTICS AND SPACE ADMINISTRATION
NASA Contract NASr-217

Reproduction, translation, publication, use and disposal in whole or in part by or for the United States Government is permitted.

NONLINEAR ASPECTS OF COMBUSTION

INSTABILITY IN LIQUID PROPELLANT ROCKET MOTORS

Sixth Yearly Progress Report
For the Period 1 June 1965 to 31 May 1966

Report No. 553-f

Department of Aerospace and Mechanical Sciences

Prepared by:

David T. Harrje

David T. Harrje
Senior Research Engineer

William A. Sirignano

William A. Sirignano
Research Staff Member

with contributions from:

Charles E. Mitchell

Charles E. Mitchell, Assistant-in-Research

Pier E. Tang

Pier Tang, Assistant-in-Research

James A. Newman

James A. Newman, Assistant-in-Research

R. M. Williams, Jr.

Richard M. Williams, Jr. NSF Fellow

Approved by:

L. Crocco

L. Crocco, Robert H. Goddard Professor
of Aerospace Propulsion

1 June 1966
Guggenheim Laboratories for the Aerospace Propulsion Sciences
PRINCETON UNIVERSITY
Princeton, New Jersey

TABLE OF CONTENTS

	Page
TITLE PAGE	1
TABLE OF CONTENTS	2
I. SUMMARY	3
II. INTRODUCTION	5
III. THEORETICAL STUDIES	
A. General	8
B. Longitudinal Shock Wave Combustion Instability	10
C. Nonlinear Dissipation in Acoustic Liners	31
IV. NONLINEAR COMBUSTION INSTABILITY MECHANISMS: EXPERIMENTAL	
A. Transverse Mode Nonlinear Rocket Motor Studies	41
B. Longitudinal Nonlinear Rocket Studies	44
C. Nonlinear Displacement Effects	47
D. Droplet Distribution Studies	53
E. Experimental Techniques for Investigating the Combustion Process	59
APPENDIX A: A LINEARIZED TREATMENT OF QUASI-STEADY DROPLET BURNING	68
APPENDIX B: DISCUSSION OF NONLINEAR QUASI-STEADY DROPLET VAPORIZATION	76
REFERENCES	78
FIGURES	
DISTRIBUTION LIST	

I. SUMMARY

An analysis of nonlinear, longitudinal mode oscillations in a rocket combustor with a combustion time-lag has been performed. The presence of a shock-wave is considered and in this first attempt the time-lag is chosen to be one-half of the period of oscillation in order to simplify the analysis. A new technique of ordering the terms in the perturbation analysis is employed. The waveforms have been predicted for certain values of the interaction index. (III-B)

The operation of acoustic liners has been analyzed from a fluid mechanical point of view. The nonlinear losses which were previously considered only in an empirical manner have now been shown to be related to the jet formation at the exit of the orifice connecting the combustion chamber and the resonator cavity. The theory indicates certain errors which have been made in scaling the empirical results. The comparison between theory and experiments is rather good. (III-C)

Certain preliminary tests have been performed on the transverse mode test stand to provide background data for design of the acoustic liner now in fabrication. Adjustable volume in the individual resonator cavities is the cornerstone of this design. Effects of L/D in the transverse mode tests as well as axial amplitude distribution of the spinning first tangential instability have been investigated prior to liner testing. (IV-A)

Interest in the quasi-steady model of droplet burning has been revived since Heidmann and Wieber^{9,11} predicted a combustion time-lag behavior on the basis of that model. In their linearized approach certain variable coefficients in differential equations were considered as constant. This has been corrected and the variability is shown to have an importance with respect to the vaporization rate response and the droplet lifetime. (Appendix A). Also further work is continuing which is intended to make the model somewhat more realistic and to extend the analysis to nonlinear order by means of a perturbation technique. (Appendix B)

A series of tests have been conducted on quarter-size square-motor hardware for the purpose of cross checking previous data. It appears that wall effects, especially prevalent in limited element designs, constitute a means of triggering spontaneous instability. (IV-B)

Tests in the pseudo-rocket motor to investigate the vapor displacement mechanism of transverse mode instability now utilize capillary tubes externally vibrated to produce uniform size droplet arrays. Tests on droplet size variations under conditions of rapid vaporization and tangential mode gas oscillations are currently in progress. (IV-C)

The relationship between intermediate frequency phenomena and variations in the droplet population density resulting from impinging jets has been shown in preliminary correlations. Increasing the pressure level has been shown to decrease the frequency of the droplet population oscillations. Current tests are seeking the quantitative relationship of fluid properties such as surface tension, viscosity and density. (IV-D)

Tests in the square-motor using the initial shock wave (generated by the nozzle-end pulse gun) as a tracer to determine the trends in local gas conditions, i.e., speed of sound and temperature, have revealed marked decreases in these parameters near the injector-end with distributed combustion designs. Shock wave amplitude variations and decay characteristics provide a measure of the energy addition and dissipation at key locations in the chamber. These data indicate differences between the initial shock wave passage and the subsequent instability. (IV-E)

II. INTRODUCTION

This is the sixth yearly report on the research at Princeton University on the problem of combustion instability in liquid-propellant rocket motors. These investigations have been sponsored by the National Aeronautics and Space Administration under NASA Contract NASr-217 and, in the past, under NASA Grant NsG-99-60. The nonlinear aspects of the problem have been emphasized in both the theoretical and experimental portions of the program. Presently, the theoretical research primarily involves studies of possible mechanisms or forcing functions of the instabilities, the nonlinear gasdynamic oscillations associated with instability in rocket motors, the effect of the exhaust nozzle on the stability, and the effect of damping devices on the stability. In conjunction with the theoretical program, an experimental program of an equally broad range is being conducted. This program includes basic experiments both with rocket motors and "cold" chambers which have been designed to study various combustion processes in order to provide understanding which would be useful in the construction of a theoretical model. It also includes studies of the effects of exhaust nozzles and damping devices upon the instability as well as controlled testing of liquid rocket motors with parametric variations intended to determine the factors which strongly influence the incidence of nonlinear combustion instability.

In the theoretical study of mechanisms of combustion instability, the greatest difficulty involves the construction of the model or models which contain the essential physical aspects of the phenomena. In this respect the basic experiments are extremely useful. The theoretical study of the nonlinear gasdynamic oscillations presents another type of difficulty. Generally, mathematical techniques for the treatment of nonlinear partial differential equations are not well-developed and, in most cases, they are undeveloped. Therefore, the theoretician must develop techniques as he works with the physical problem as will be exemplified later in the report. Often, linear mathematical approaches have proven extremely helpful in effecting a better understanding of the nature of the instability. Note that a most important result of past nonlinear analyses has been that a "continuity"

exists between linear theory and nonlinear theory. Therefore in this report linear treatments as well as nonlinear treatments are used to analyze the general problem.

As is the norm for any status report, a considerable amount of the material discussed herein is in the state of active investigation. Thus, only tentative conclusions or observations are sometimes possible. At least a mention of one example of each type of work being conducted has been made so that this report would prove to be of maximum benefit to those readers working in similar areas.

During the next year, the following publications will appear:

"Effect of the Transverse Velocity Component on the Nonlinear Behavior of Short Nozzles", L. Crocco and W. A. Sirignano (accepted for publication in the AIAA Journal).

"A Theoretical Study of Nonlinear Combustion Instability in Liquid Propellant Rocket Engines", B. T. Zinn (to be presented at the XVIIth International Astronautical Congress).

Also, an AGARD monograph authored by L. Crocco and W. A. Sirignano presenting the report of the work on oscillatory flow in nozzles will appear shortly.

The following papers and reports were published during the past year:

"Relevance of a Characteristic Time in Combustion Instability", L. Crocco, The Second ICRPG Combustion Conference, 1-5 November 1965, Aerospace Corp., Los Angeles, California, CPIA Publication No. 105, May 1966, pg. 115.

"Nonlinear Aspects of Combustion Instability in Liquid Propellant Rocket Motors", L. Crocco, D. T. Harrje and W. A. Sirignano, *ibid*, pg. 63.

"A Theoretical Study of Nonlinear Transverse Combustion Instability in Liquid Propellant Rocket Motors", B. T. Zinn, Department of Aerospace and Mechanical Sciences Report No. 732, May 1966.

"A Study of Injector Spray Characteristics in a Simulated Rocket Combustion Chamber Including Longitudinal Mode Pressure Oscillations", D. A. Gary, Department of Aerospace and Mechanical Sciences Report No. 730, June 1966.

Additional background and history of the research on combustion instability at Princeton University may be found in References 1-8, 12, 18, 21-23. In addition, Reference 20 represents one of an extensive series of reports on earlier work primarily concerned with the linear type of combustion instability.

It should be acknowledged that this work made use of computer facilities supported in part by National Science Foundation Grant NSF-GP579.

III. THEORETICAL STUDIES

A. GENERAL

The theoretical effort in combustion instability at Princeton has been directed into four areas: nonlinear stability, acoustic liner studies, oscillatory flow in nozzles, and unsteady droplet burning. Portions of that work are presented in this report.

Previous efforts on nonlinear stability by Sirignano and Crocco¹, Sirignano^{2,3} and Zinn⁴ at Princeton had dealt with the problems of longitudinal shock wave instability with no combustion time-lag and with very small time-lag, longitudinal instability with no shock waves and with a combustion time-lag, and transverse instability with no shock waves and with a time-lag. Presently, studies are being performed to determine the nature of oscillations where both shock waves and time-lags of the order of the period of oscillation occur. Both longitudinal oscillations and transverse oscillations (in thin annular chambers) are being considered. In Section B, a discussion of an analysis of the longitudinal mode by Mr. C. E. Mitchell is presented.

Since acoustic liners are topics of a large amount of current interest, theoretical programs (as well as experimental programs) have been initiated to develop an understanding of the fluid mechanical phenomena involved in their operation and of their effect upon combustion chamber oscillations. An analysis for the case of not-too-large pressure amplitudes is presented in Section C.

The results of the work on oscillatory flow in nozzles will be presented in a forthcoming AGARDograph by Crocco and Sirignano so that no discussion of that work will be presented here.

Earlier work by Strahle and Crocco⁵ had indicated that quasi-steady droplet burning could not produce a time-lag behavior. Later work by Strahle^{6,7,8} indicated that the time-lag behavior might be produced from the unsteady droplet burning (where time derivatives are not negligible).

Recently, however, Heidmann and Wieber⁹ have performed a numerical analysis of the frequency response characteristics of propellant vaporization in the presence of transverse oscillations. They found a peak in the response

in the region where the droplet lifetime approximately equals the cycle time. Their numerical results were shown to indicate a time-lag behavior which is different from the results of Strahle who found no such behavior with his quasi-steady model of vaporization.

The main physical difference between the model of Strahle and that of Heidmann and Wieber involves the behavior of the droplet temperature under oscillatory conditions. Strahle assumed the droplet temperature oscillated only in some small layer near the surface and while the surface temperature varied considerably, the variation of the average droplet temperature was negligible. Heidmann considered the temperature to be uniform throughout the droplet even under oscillatory conditions so that surface temperature and average temperature were essentially equivalent.

This means that at high frequencies, Heidmann obtains that the surface vapor pressure cannot vary resulting in a negative response. Strahle, however, allows the vapor pressure to vary at high frequencies and obtains a positive response in the high frequency range. It remains to be determined which model applies best to which situations. Clearly, this can only be determined by solving the unsteady equation in the droplet.

Heidmann and Wieber based their quasi-steady analysis upon the steady-state rocket propellant vaporization analysis by Priem and Heidmann¹⁰. More recently the same authors using the same equations as a base have performed a linearized analysis¹¹ resulting in closed-form solutions.

In the linear treatment, they assumed certain coefficients in their differential equations to be constant with time. Actually, these coefficients are not constant with time. The variation of these coefficients with time would actually produce certain significant changes such as: changes in the droplet lifetime under oscillatory conditions and changes in the value of the interaction index n . The variability of these coefficients are considered in the linearized treatment presented in Appendix A and the results are discussed there.

A nonlinear treatment is being developed by Mr. Pier Tang which hopefully will improve upon the work by Heidmann and Wieber. A discussion of that effort is presented in Appendix B.

B. LONGITUDINAL SHOCK WAVE COMBUSTION INSTABILITY

It is well known that in certain ranges of mixture ratio and for certain injector configurations a type of longitudinal combustion instability exhibiting shock waves may occur in liquid propellant rocket engines.

In order to understand this kind of instability the wave shape and the dependence of the amplitude of the shock wave on combustion parameters (such as mixture ratio, injector etc.) must be determined. In particular it is of interest to find the wave form and the relationship between the combustion parameters (in this work represented in a gross way by the interaction index n , and the time lag τ) and the amplitude of the wave when the shock wave is periodic because, for given combustion parameters, the amplitude of the shock will in general grow or decay to the value given by this relationship.

Sirignano² treated the case of gas rocket shock wave instability, where the effect of combustion was represented principally by a gain factor, w . When w was equal to unity a neutrally stable condition was found to exist to first order in the wave amplitude. The amplitude of the periodic shock wave, determined by the condition of periodicity to first order, was found to be proportional to the excess of w over unity. The decay in pressure after the shock was found through the use of a second order analysis to have an exponential form. Later Sirignano treated the case where a time lag was present but was of the same (small) order of magnitude as the amplitude of the wave.

In both developments the assumptions of short (zero length, constant Mach number) nozzle and concentrated combustion were employed. For a treatment of liquid rocket shock wave instability, on the other hand, it is necessary first of all to consider time lags which are of the same order as the wave travel time. Also, it is desirable to relax the concentrated combustion assumption and consider arbitrarily distributed combustion. A final, most difficult refinement should be the improvement of the nozzle boundary condition.

An analysis which considers time lags of order one and distributed combustion is being attempted at the present time. As a first step in this direction a rocket model incorporating the simplifications of concentrated combustion and short nozzle but considering time lags of the order of the wave travel time has been employed. The remainder of this section will be devoted to the presentation of a stability analysis of such a system.

As a first guess it might seem that an analysis exactly similar to Sirignano's should be applicable since the only change from his model is the appearance of a significant phasing effect in the combustion boundary condition. This, however, is not the case. Indeed, such an analysis leads to the unacceptable conclusion that any shock wave must be followed by an expansion shock. This will be shown in the development which follows.

If the equations (one dimensional) describing the conservation of mass and momentum in the combustion chamber are combined, using the further assumptions of a homentropic flow field and a thermally and calorically perfect gas, then the following two equations are obtained:

$$\frac{\partial}{\partial t} \left(\frac{u}{a_0} + \frac{2}{\gamma-1} \frac{a}{a_0} \right) + \left(\frac{u}{a_0} + \frac{a}{a_0} \right) a_0 \frac{\partial}{\partial x} \left(\frac{u}{u_0} + \frac{2}{\gamma-1} \frac{a}{a_0} \right) = 0 \quad (1)$$

$$\frac{\partial}{\partial t} \left(\frac{u}{a_0} - \frac{2}{\gamma-1} \frac{a}{a_0} \right) + \left(\frac{u}{a_0} - \frac{a}{a_0} \right) a_0 \frac{\partial}{\partial x} \left(\frac{u}{u_0} - \frac{2}{\gamma-1} \frac{a}{a_0} \right) = 0 \quad (2)$$

Where u and a are, respectively, the gas velocity and local sonic speed, and the subscript zero signifies steady-state quantities. (Note that u_0 and a_0 are constants in the present model.)

u and a are now expanded in a power series in ϵ , an amplitude parameter which is unspecified at present.

$$u = u_0 + u_1 + u_2 + \dots$$

$$a = a_0 + a_1 + a_2 + \dots$$

where u_1 is $O(\epsilon)$ u_2 is $O(\epsilon^2)$ etc.

If these expansions are substituted in Equations (1) and (2), then to first order those equations become

$$\frac{\partial}{\partial t} \left(\frac{u_1}{a_0} + \frac{2}{\gamma - 1} \frac{a_1}{a_0} \right) + a_0(1 + M) \frac{\partial}{\partial x} \left(\frac{u_1}{a_0} + \frac{2}{\gamma - 1} \frac{a_1}{a_0} \right) = 0 \quad (3)$$

$$\frac{\partial}{\partial t} \left(\frac{u_1}{a_0} - \frac{2}{\gamma - 1} \frac{a_1}{a_0} \right) + a_0(1 - M) \frac{\partial}{\partial x} \left(\frac{u_1}{a_0} - \frac{2}{\gamma - 1} \frac{a_1}{a_0} \right) = 0 \quad (4)$$

where $M = \frac{u_0}{a_0}$ is the Mach number at the nozzle entrance.

The solution of this linear system of first order partial differential equations is

$$\frac{u_1}{a_0} + \frac{2}{\gamma - 1} \frac{a_1}{a_0} = 2f_r \left(t - \frac{x}{a_0(1 + M)} \right) \quad (5)$$

$$\frac{u_1}{a_0} - \frac{2}{\gamma - 1} \frac{a_1}{a_0} = 2f_s \left(t - \frac{x}{a_0(M - 1)} \right) \quad (6)$$

f_r and f_s are arbitrary functions of their arguments and represent, respectively, disturbances propagating in the positive x and negative x directions with velocities $a_0(1 + M)$ and $a_0(M - 1)$.

The boundary condition at the nozzle end of the chamber $x = L$ is, due to the zero length nozzle, simply a constant Mach number condition:

$$\frac{u_1(x = L)}{a_0} = M \frac{a_1(x = L)}{a_0} \quad (7)$$

At the injector ($x = 0$) the boundary condition is dependent upon the combustion assumed to be concentrated there. Following earlier work by Crocco¹² the change in mass burning rate is related directly to the rate of change of the sensitive time lag:

$$\dot{m} = \dot{m}_i \left(1 - \frac{d\tau}{dt} \right)$$

If the injection rate is taken to be constant then

$$\dot{m} = \dot{m}_0 \left(1 - \frac{d\tau}{dt} \right)$$

or, equivalently,

$$\frac{\dot{m} - \dot{m}_0}{\dot{m}_0} = - \frac{d\tau}{dt}$$

In the same analysis Crocco developed the following expression for $\frac{d\tau}{dt}$:

$$\frac{d\tau}{dt} = - n \left[\frac{p_1(t) - p_1(t - \tau)}{p_0} \right]$$

This expression can be shown to be valid even when p_1 is discontinuous.

The relationship between the mass flow perturbation and pressure thus becomes (to first order)

$$\frac{\rho_0 u_1 + u_0 \rho_1}{\rho_0 u_0} - 1 = n \left[\frac{p_1(t) - p_1(t - \tau)}{p_0} \right]$$

If the substitutions $\frac{\rho}{\rho_0} = \left(\frac{a}{a_0} \right)^{\frac{2}{\gamma-1}}$, $\frac{p}{p_0} = \left(\frac{a}{a_0} \right)^{\frac{2\gamma}{\gamma-1}}$

are made, then the combustion boundary condition takes the following form:

$$\frac{u_1}{u_0} = M \frac{2}{\gamma-1} (\gamma n - 1) \left[\frac{a_1}{a_0} - \frac{\gamma n}{(\gamma n - 1)} \frac{a_1(t - \tau)}{a_0} \right] + o(\epsilon^2) \quad (8)$$

Using Equations (5) and (8) one finds

$$\frac{u_1}{a_0} = f_r \left(t - \frac{x}{a_0(1-M)} \right) + f_s \left(t - \frac{x}{a_0(M-1)} \right) \quad (9)$$

$$\frac{a_1}{a_0} = \frac{\gamma - 1}{2} \left[f_r \left(t - \frac{x}{a_0(1+M)} \right) - f_s \left(t - \frac{x}{a_0(M-1)} \right) \right] \quad (10)$$

Substituting these values for $\frac{u_1}{a_0}$ and $\frac{a_1}{a_0}$ into (7), the nozzle boundary condition, yields

$$(1 - \gamma) f_r \left(t - \frac{L}{a_0(1+M)} \right) = - (1 + \gamma) f_s \left(t - \frac{L}{a_0(M-1)} \right)$$

where $\gamma = \frac{\gamma - 1}{2} M$.

This is equivalent to

$$(1 - \gamma) f_r(t) = - (1 + \gamma) f_s(t + \tau_0) \quad (11)$$

where $\tau_0 = \frac{2L}{a_0(1-M^2)}$ represents the wave travel time to zeroth order.

If the definition $f(t) = (1 - \gamma) f_r(t)$ is made, and Equations (8), (9), (10) and (11) are combined one obtains the following expression for f :

$$\frac{f(t)}{(1 - \gamma)} - \frac{f(t - \tau_0)}{(1 + \gamma)} = \frac{2}{\gamma - 1} \gamma \left[(\gamma^n - 1) \left(\frac{f(t)}{(1 - \gamma)} + \frac{f(t - \tau_0)}{(1 + \gamma)} \right) - \gamma^n \left(\frac{f(t - \tau)}{(1 - \gamma)} + \frac{f(t - \tau_0 - \tau)}{(1 + \gamma)} \right) \right] \quad (12)$$

It is clear that if u_1 and a_1 are to be periodic, then f must also be periodic. The period of a travelling wave is the same as its wave travel time. The wave travel time is τ_0 . Hence to first order $f(t) = f(t + \tau_0)$.

Making this substitution in Equation (12) yields the following requirement for a periodic solution:

$$(2\gamma^n - \gamma - 1) f(t) = 2\gamma^n f(t - \tau)$$

or
$$f(t) = \frac{2\gamma^n}{(2\gamma^n - \gamma - 1)} f(t - \tau) \quad (13)$$

It is obvious that a contradiction occurs unless $\frac{2\delta n}{2\delta n - \delta - 1} = \pm 1$ for, were this not the case, then f at time t would be larger (or smaller) than f at time $t - \tau$ and growth (or decay) in time would be indicated.

The quantity $\frac{2\delta n}{2\delta n - \delta - 1}$ goes to unity only as n becomes infinitely large, which is physically unreasonable. Hence the only real possibility is $\frac{2\delta n}{2\delta n - \delta - 1} = -1$, which implies $n = \frac{\delta + 1}{4\delta}$.

Another requirement is that $\tau = \frac{T_0}{2}, \frac{T_0}{4}, \dots, \frac{T_0}{2k}$ (k an integer), otherwise the solution could not be periodic since it would only be true at best that $f(t) = |f(t - T_0)|$.

The important result of the preceding analysis is that for a periodic solution to exist:

$$f(t) = -f(t - \tau) \quad \tau = \frac{T_0}{2k}, \quad n = \frac{\delta + 1}{4\delta}$$

Under the above conditions, no discontinuity in f can be tolerated. This is because a positive jump in f at time t , corresponding to a shock wave, would be followed by an expansion shock at time $t + \tau$. Thus one finds himself in the uncomfortable position of predicting that no shock wave instability is possible in a rocket engine which has combustion exhibiting a reasonable phase lag, while knowing that such instability is indeed observed.

Here it should be pointed out that Sirignano found no such difficulty in the case of no phase lag or vanishingly small phase lags. The reason for this is that to first order, in his treatment, the boundary conditions were the same at $x = 0$ and $x = L$ if $(w - 1)\alpha \ll 1$. To first order, then, he found no requirements on f were necessary for periodicity, only that $\epsilon \propto (w - 1)$.

In the present case, the appearance of $f(t - \tau)$ in the combustion boundary condition makes it necessary to place restrictions on f and τ as well as n in order to have the boundary conditions the same at

$x = 0$ and $x = L$ and therefore to have a periodic solution. These restrictions do not destroy the possibility of some kind of nonlinear wave form; they only exclude discontinuous solutions.

In the preceding analysis as well as in Sirignano's work, the Mach number was treated simply as a parameter, large compared with ϵ , so that terms of $O(\epsilon \cdot M)$ were of the same order of magnitude as terms of order ϵ . This is clearly the correct assumption when one considers the application of an infinitesimal perturbation to a rocket chamber operating under steady conditions with the size of its mass flow characterized by the nozzle entrance Mach number.

If $n > \frac{\gamma + 1}{4}$ and $\tau = \frac{T_0}{2k}$, then, according to the above analysis the original perturbation will grow in amplitude. Since a traveling wave is being considered and ϵ is very small, the kind of growth will be oscillatory in nature with the oscillations having a characteristic time approximately equal to T_0 , the zeroth order wave travel time. Adhering to the results of the foregoing analysis, the waveform must be continuous at least in this regime of initial growth.

On the other hand, if $n = \frac{\gamma + 1}{4}$ and $\tau = \frac{T_0}{2k}$, then the first order analysis predicts no growth. This suggests that the amplitude of a periodic wave solution which has grown from an infinitesimal perturbation must in some way be dependent on n so that when n is equal to $\frac{\gamma + 1}{4}$ the amplitude is zero. In this connection it is to be noted that from the first order analysis above, the excess of energy input from combustion over energy loss at the nozzle is of order $M \cdot H(n)$, where $H(n)$ is some function of n vanishing when $n = \frac{\gamma + 1}{4}$. Because of this, it seems that a reasonable estimate of the amplitude of periodic solutions which have grown from the perturbation of a steady operating condition would be that their amplitude is of order $M \cdot H(n)$. If this is a good assumption then it is certainly justifiable to require that the amplitude parameter ϵ , unspecified to this point, be given by the expression $\epsilon = M \cdot H(n)$. $H(n)$ is an unknown and not necessarily simple function of n , whose most important characteristic is, as stated above, that it vanishes when $n = \frac{\gamma + 1}{4}$.

However, since the form of $H(n)$ is not known instead of taking $\epsilon = M \cdot H(n)$, the reasonable assumption is made that $H(n)$ is of order unity or less. This then implies an expression for ϵ that is less strict, namely that $\epsilon = O(M)$.

If this assumption, $\epsilon = O(M)$, is made, then, to first order in ϵ , one finds that the problem has the same boundary condition at both ends of the chamber, $u_1 = 0$. This, of course, ensures a periodic solution with no constraints on the form of the arbitrary (periodic) function f . Both $H(n)$ and the form of f are then to be found from a second order analysis. Thus the assumption $\epsilon = O(M)$ removes the difficulty encountered when ϵ was taken simply as an unknown amplitude parameter that was independent of M .

In effect, taking $\epsilon = O(M)$ converts the problem to first order into a wave propagation problem in a chamber closed at both ends with no mean flow, where the wave form and dependence of amplitude on n are to be determined from a nonlinear analysis which must take into account the combustion, the nozzle, the mean flow and nonlinear wave effects.

The following analysis uses the condition $\epsilon = O(M)$. Note that it should be valid for waves which have grown from small perturbations, if the above argument is valid, and in any event it should be valid if a rocket is triggered by a finite disturbance of $O(M)$.

Power series expansions for u and a are again employed.

$$u = u_0 + u_1 + u_2 + \dots$$

$$a = a_0 + a_1 + a_2 + \dots$$

u_1 is $O(\epsilon) = O(M)$ $u_2 = O(\epsilon^2) = O(M^2)$. These power series are substituted into Equations (1) and (2) and yield the following first order equations:

$$\frac{\partial}{\partial t} \left(\frac{u_1}{a_0} + \frac{2}{\gamma - 1} \frac{a_1}{a_0} \right) + a_0 \frac{\partial}{\partial x} \left(\frac{u_1}{a_0} + \frac{2}{\gamma - 1} \frac{a_1}{a_0} \right) = 0 + O(\epsilon^2) + O(M\epsilon) \quad (14)$$

$$\frac{\partial}{\partial t} \left(\frac{u_1}{a_0} + \frac{2}{\gamma-1} \frac{a_1}{a_0} \right) - a_0 \frac{\partial}{\partial x} \left(\frac{u_1}{a_0} - \frac{2}{\gamma-1} \frac{a_1}{a_0} \right) = 0 + 0(\epsilon^2) + 0(M\epsilon) \quad (15)$$

Where advantage has been taken of the fact that

$$\frac{a}{a_0} = 1 + 0(M^2)$$

The solutions of (14) and (15) are simply

$$\frac{u_1}{a_0} + \frac{2}{\gamma-1} \frac{a_1}{a_0} = 2f_r \left(t - \frac{x}{a_0} \right) \quad (16)$$

$$\frac{u_1}{a_0} - \frac{2}{\gamma-1} \frac{a_1}{a_0} = 2f_s \left(t + \frac{x}{a_0} \right) \quad (17)$$

where, again, f_r and f_s are arbitrary functions of their arguments representing disturbances propagating in the $+x$ and $-x$ directions respectively.

The first order boundary condition at $x = L$ is $\frac{u_1}{a_0} = 0$, which implies:

$$f_r \left(t - \frac{L}{a_0} \right) = -f_s \left(t + \frac{L}{a_0} \right) \quad (18)$$

The injector-end boundary condition $\frac{u_1}{a_0}(x=0) = 0$ yields

$$f_r(t) = -f_s(t) \quad (19)$$

Combining (18) and (19)

$$f(t) = f \left(t + \tau_0 \right) ; \tau_0 = \frac{2L}{a_0} \quad (20)$$

$$\frac{u_1}{a_0} = f \left(t - \frac{x}{a_0} \right) - f \left(t + \frac{x}{a_0} \right) \quad (21)$$

$$\frac{a_1}{a_0} = \frac{\gamma-1}{2} \left[f\left(t - \frac{x}{a_0}\right) + f\left(t + \frac{x}{a_0}\right) \right] \quad (22)$$

Thus to first order, one finds (as expected) that f is periodic and that no requirements on the wave form are imposed.

The second order equations are

$$\begin{aligned} \frac{\partial}{\partial t} \left(\frac{u_2}{a_0} + \frac{2}{\gamma-1} \frac{a_2}{a_0} \right) + a_0 \frac{\partial}{\partial x} \left(\frac{u_2}{a_0} + \frac{2}{\gamma-1} \frac{a_2}{a_0} \right) = \\ - a_0 \left(M + \frac{u_1}{a_0} + \frac{a_1}{a_0} \right) \frac{\partial}{\partial x} \left(\frac{u_1}{a_0} + \frac{2}{\gamma-1} \right) \end{aligned} \quad (23)$$

$$\begin{aligned} \frac{\partial}{\partial t} \left(\frac{u_2}{a_0} - \frac{2}{\gamma-1} \frac{a_2}{a_0} \right) - a_0 \frac{\partial}{\partial x} \left(\frac{u_2}{a_0} - \frac{2}{\gamma-1} \frac{a_2}{a_0} \right) = \\ - a_0 \left(M + \frac{u_1}{a_0} - \frac{a_1}{a_0} \right) \frac{\partial}{\partial x} \left(\frac{u_1}{a_0} - \frac{2}{\gamma-1} \frac{a_1}{a_0} \right) \end{aligned} \quad (24)$$

Using expressions (21) and (22) the right hand sides of (23) and (24) can be written:

$$\text{r.h.s. (23)} = 2 \left(\frac{\gamma+1}{2} f\left(t - \frac{x}{a_0}\right) + \frac{\gamma-3}{2} f\left(t + \frac{x}{a_0}\right) + M \right) f'\left(t - \frac{x}{a_0}\right)$$

$$\text{r.h.s. (24)} = 2 \left(\frac{\gamma-1}{2} f\left(t - \frac{x}{a_0}\right) - \frac{\gamma+1}{2} f\left(t + \frac{x}{a_0}\right) + M \right) f'\left(t + \frac{x}{a_0}\right)$$

The general solutions of Equations (23) and (24) are found by standard methods to be

$$\frac{u_2}{a_0} + \frac{2}{\gamma-1} \frac{a_2}{a_0} = 2F_r\left(t - \frac{x}{a_0}\right) + 2f'\left(t - \frac{x}{a_0}\right) \left[\frac{x}{a_0} \left(\frac{\gamma+1}{2} f\left(t - \frac{x}{a_0}\right) + \frac{\gamma-3}{4} f\left(t + \frac{x}{a_0}\right) \right) \right] \quad (25)$$

$$\frac{u_2}{a_0} - \frac{2}{\gamma-1} \frac{a_2}{a_0} = 2F_s(t + \frac{x}{a_0}) + 2f'(t + \frac{x}{a_0}) \left[\frac{x}{a_0} f(t + \frac{x}{a_0}) - M \right] + \frac{3-\gamma}{4} \mathcal{J}(t - \frac{x}{a_0}) \quad (26)$$

where $\mathcal{J}(t) = \int^t f(\eta) d\eta$

and F_r and F_s are arbitrary functions of their arguments.

The second order boundary condition at $x = L$ is

$$\frac{u_2}{a_0} = M \frac{u_1}{a_0} \quad (27)$$

If (25) and (26) are solved for $\frac{u_2}{a_0}$ and the result substituted in Equation (27) along with expression (22) the following relationship results:

$$F_r(t - \frac{L}{a_0}) + F_s(t + \frac{L}{a_0}) + f'(t - \frac{L}{a_0}) \left[\frac{(\gamma+1)L}{a_0} f(t - \frac{L}{a_0}) - \frac{3-\gamma}{4} \int_0^{2L/a_0} f(\eta) d\eta \right] = (\gamma-1) M f(t - \frac{L}{a_0}) \quad (28)$$

at $x = 0$ the following boundary condition is applied:

$$\frac{u_2}{a_0} = M \frac{2}{\gamma-1} \left[(\gamma n - 1) \frac{a_1}{a_0} - \gamma n \frac{a_1}{a_0} (t - \tau) \right]$$

This is to be recognized as the same boundary condition (with $\frac{u_1}{a_0}$ substituted for $\frac{u_2}{a_0}$) as was used in the analysis in which M was considered large compared with ϵ (i.e., Equation (8)).

Substitution of the expression for $\frac{u_2}{a_0}$ from Equations (25) and (26) yields

$$F_r(t) + F_s(t) = 2M \left[(\gamma n - 1) f(t) - \gamma n f(t - \tau) \right] \quad (29)$$

Using (28) in (29):

$$\begin{aligned} F_s(t) - F_s\left(t + \frac{2L}{a_0}\right) &= 2M \left[(\gamma n - 1) f(t) - \gamma n f(t - \tau) \right] \\ &+ f'(t) \left[\frac{(\gamma + 1)L}{a_0} f(t) - \frac{3 - \gamma}{4} \int_0^{\frac{2L}{a_0}} f(\eta) d\eta \right] \\ &- (\gamma - 1) M f(t) \end{aligned} \quad (30)$$

Recall that our purpose is to find periodic solutions. Thus we now require that the overall solution be periodic and attempt to determine what wave form and $H(n)$ results.

$$\left[\frac{u_1 + u_2}{a_0} - \frac{2}{\gamma - 1} \frac{a_2 + a_1}{a_0} \right]_{x=0} \equiv \int_{(x=0)} (t) = \int_{(x=0)} (t + \mathcal{T}) \quad (31)$$

where \mathcal{T} is the (unknown at present) period.

$$\int_{(x=0)} (t) = -2f(t) + 2f'(t) \left(\frac{3 - \gamma}{4} \right) \mathcal{F}(t) + 2F_s(t) \quad (32)$$

$$\int_{(x=0)} (t + \mathcal{T}) = -2f(t + \mathcal{T}) + 2f'(t + \mathcal{T}) \frac{3 - \gamma}{4} \mathcal{F}(t + \mathcal{T}) + 2F_s(t + \mathcal{T}) \quad (33)$$

Now we say that $\mathcal{T} = \mathcal{T}_0 + \mathcal{T}_1$ where \mathcal{T}_1 is $O(\epsilon)$ and represents the first order correction to the wave travel time. It is clear that

$$F_s(t + \mathcal{T}) = F_s(t + \mathcal{T}_0) + O(\epsilon^2 M) \quad (34)$$

Expression (31) then becomes with the aid of (32), (33) and (34) :

$$F_s(t) - F_s(t + T_0) = -f(t + T) + f(t) - f'(t) \frac{3-\delta}{4} \left[\mathcal{F}(t) - \mathcal{F}(t + T_0) \right] \quad (35)$$

Due to the periodicity of $f(t)$:

$$\mathcal{F}(t) - \mathcal{F}(t + T_0) = \int_0^{2L} f(\eta) d\eta .$$

Equation (35) may now be rewritten:

$$F_s(t) - F_s(t + T_0) = -f(t + T) + f(t) - f'(t) \frac{3-\delta}{4} \int_0^{2L} f(\eta) d\eta . \quad (36)$$

The assumption is now made, following Sirignano², that $f(t + T)$ can be expanded in a Taylor series around $f(t + T_0)$. If this is done, then

$$f(t + T) = f(t + T_0) + f'(t + T_0) T_1 + O(\epsilon^3) \quad (37)$$

T_1 is found, by following the method used by Sirignano to be

$$T_1 = \frac{3-\delta}{2} \int_0^{2L} f(\eta) d\eta + \frac{\delta-1}{2} \left[f(0) + f\left(\frac{2L}{a_0}\right) \right] \quad (38)$$

$f(0)$ and $f\left(\frac{2L}{a_0}\right)$ represent respectively the values of f immediately after and before the discontinuity.

Crocco has shown that in order to have a periodic solution it is necessary for $\left[f(0) + f\left(\frac{2L}{a_0}\right) \right] = 0$. Using this fact Equation (38) reduces to

$$T_1 = \frac{3-\delta}{2} \int_0^{2L} f(\eta) d\eta \quad (39)$$

Substituting (39) in (37) and (37) in (36) yields

$$F_s(t) - F_s(t + T_0) = -f'(t) \frac{3 - \gamma}{4} \int_0^{\frac{2L}{a_0}} f(\eta) d\eta \quad (40)$$

Finally, substituting Equation (40) into Equation (30) one obtains the following equation for $f(t)$:

$$\frac{(\gamma + 1)L}{a_0} \frac{df}{dt} = -M(\gamma(2n - 1) - 1) + M 2\gamma n \frac{f(t - \tau)}{f(t)} \quad (41)$$

or

$$\frac{df}{dt} = a + b \frac{f(t - \tau)}{f(t)} \quad a = \frac{a_0}{(\gamma + 1)L} M(\gamma 2n - (\gamma + 1)) \quad b = \frac{M a_0 2\gamma n}{(\gamma + 1)L} \quad (42)$$

This is a nonlinear first order differential equation with a retarded variable. In general there are no "ready-made" methods for solving this type of equation. However, when $\tau = \frac{1}{j} T_0$ where j is an integer, the above equation may be represented by a system of j first order nonlinear equations in a single variable. This is accomplished by breaking $f(t)$ up into $f_1(t)$, $f_2(t)$ $f_j(t)$, where $f_1(t)$ represents $f(t)$ between $t = 0$ and $t = \frac{T_0}{j}$, $f_2(t)$ represents $f(t)$ between $t = \frac{T_0}{j}$ and $2 \frac{T_0}{j}$, etc. If one pursues this course of action the j equations for the $j f_j$ quantities will contain a single independent variable, say θ , where θ will run from zero to $\frac{T_0}{j}$. The k^{th} equation will then be of the form:

$$\frac{df_k}{d\theta} = a + b \frac{f_{k-1}}{f_k} \quad 1 < k \leq j$$

The first equation will be:

$$\frac{df_1}{d\theta} = a + b \frac{f_j}{f_1}$$

When one attempts to solve the system of j equations for one of the j functions he will obtain a j^{th} order very nonlinear equation. This kind of equation inherently presents great, if not insuperable difficulties in finding the analytical solution.

At the present time only the case $j = 2$ has been treated to any extent and for this value of j , corresponding to $\tau = \pi/2$, an analytical solution has been found only for the case $a = -b$. Unfortunately, $a = -b$ occurs only in the limit of large n so that the solution can be considered of interest only as a limiting case. When $a = 0$, corresponding to $n = \frac{\gamma+1}{2}$, a somewhat simplified equation is obtained from which the essential features of the solution may be inferred.

Consider the following pair of equations:

$$\frac{dy}{d\theta} = a + b \frac{x}{y} \quad (43)$$

$$y = f_1(t)$$

$$x = f_2(t)$$

$$\frac{dx}{d\theta} = a + b \frac{y}{x} \quad (44)$$

We will treat the three cases; $a = b(n = \frac{\gamma+1}{4\delta})$, $a = -b(n \rightarrow \infty)$, $a = 0(n = \frac{\gamma+1}{2})$.

If $a = b$,

$$\frac{dy}{dx} = \frac{x}{y} \quad \text{and} \quad y^2 - x^2 = C_1$$

If $a = -b$

$$\frac{dy}{dx} = \frac{x}{y} \quad \text{and} \quad y^2 + x^2 = C_2^2$$

If $a = 0$

$$\frac{dy}{dx} = \frac{x^2}{y} \quad \text{and} \quad y^3 - x^3 = C_3$$

Take first the case $a = b$. If $y^2 - x^2 = C_1$ then

$y_0^2 - x_0^2 = C_1$ and $y_1^2 - x_1^2 = C_1$. The boundary condition for the

equation is $y_0 = x_1$. Application of this condition yields the following relations

$$x_1^2 - x_0^2 = y_1^2 - y_0^2 = C_1$$

$$2y_0^2 = x_0^2 + y_1^2$$

Combination of these two equations gives

$$y_1^2 - x_0^2 = 2C_1 \quad (45)$$

It is necessary to recall here that θ , the independent variable, coincides with time only for the function y . For the function x , it corresponds to $t + T_0/2$. This means that $y(\theta = 1)$ and $x(\theta = 0)$ are the values of the two functions at time $t = T_0/2$.

The governing equations when $a = b$ are:

$$\frac{dy}{d\theta} = a(1 + \frac{x}{y}) \quad (46)$$

$$\frac{dx}{d\theta} = a(1 + y/x) \quad (47)$$

In order to restrict the problem to the case where no expansion shocks occur, y_0 must be positive or zero. But inspection of (46) and (47) shows that unless x_0 is negative the slopes of y and x will always be positive. This would render the satisfaction of the boundary condition impossible, hence x_0 must be negative. Since x_0 is negative, y_1 must be negative and greater than or equal to x_0 in absolute value, otherwise an expansion shock would occur at $t = T_0/2$. Now from (45) it is clear that if $|y_1| \geq |x_0|$ then C_1 must be positive or zero accordingly. Since y at $\theta = 0$ is positive and is negative at $\theta = 1$, y must pass through zero at some θ between zero and one. At this point, since $y^2 - x^2 = C_1$, $x^2 = -C_1$. This implies that, when y passes through zero, x is imaginary. An imaginary x (recall that this corresponds to f in the time interval $(T_0/2 \leq t \leq 0)$) is unacceptable on physical grounds. Hence $C_1 > 0$ is ruled out and C_1 must be identically zero.

For $C_1 = 0$, $y^2 = x^2$ or $y = \pm x$. If $y = x$ then (46) and (47) predict always positive slopes, so that this alternative is not viable. The only remaining possibility is $y = -x$. From (46) and (47) this implies that $y = \text{constant}$, $x = \text{constant}$. The only constant that allows satisfaction of the boundary condition $y_0 = -x_1$ is, of course, zero. Thus for the case $a = b$, $n = \frac{\gamma+1}{4\gamma}$, it is found that the only possibility is a zero amplitude solution. This of course agrees with the earlier arguments presented which required that $H(n) = 0$ when $n = \frac{\gamma+1}{4\gamma}$. It is interesting to observe that the condition $y = -x$, for $\epsilon = 0$, $n = \frac{\gamma+1}{4\gamma}$, is the same result that was obtained in the first analysis considered here, where ϵ was taken to be infinitesimally small and independent of Mach number. Thus it seems that the present non-linear analysis gives indications of converging to the linear analysis at the stability limit.

Whenever $a = 0$, which corresponds to $n = \frac{\gamma+1}{2}$, the governing pair of equations is

$$\frac{dy}{d\theta} = b \frac{x}{y} \quad (48)$$

$$\frac{dx}{d\theta} = b \frac{y}{x} \quad (49)$$

$$(b > 0)$$

This set of equations was combined and solved above to yield

$$y^3 - x^3 = C_3 \quad (50)$$

It must be true then that

$$y_0^3 - x_0^3 = y_1^3 - x_1^3.$$

Using the boundary condition, $x_1 = -y_0$, then implies $x_0 = -y_1$. (Recall $x_0 = f_2(t = T_0/2)$, $y_1 = f_1(t = T_0/2)$). It is physically impossible for x_0 to be negative, for then the condition $x_0 = -y_1$ would imply an expansion shock at $t = T_0/2$.

The condition $x_0 = -y_1$ combined with Equation (50) yields

$$x_1^3 + x_0^3 = -C_3.$$

This substituted into the expression obtained by combining (49) and (50) gives

$$\frac{dx}{d\theta} = \frac{b^3 \sqrt{-x_1^3 - x_0^3 + x^3}}{x} \quad (51)$$

At $x = x_0$ then

$$\left(\frac{dx}{d\theta}\right)_{x=x_0} = -b \frac{x_1}{x_0}, \text{ and since } x_1 \text{ must be negative}$$

$\left(\frac{dx}{d\theta}\right)_{x=x_0}$ is positive. Inspection of (48) and (49) indicates that if

$\left(\frac{dx}{d\theta}\right)_{x=x_0}$ is positive, then $\frac{dx}{d\theta}$ is always positive. This would make it

impossible for x_1 to be non-positive, which it must be to exclude expansion shocks. Hence x_0 cannot be positive. The only alternative is to take $x_0 = -y_1 = 0$.

Inspection of (48) and (49) under the condition $x_0 = -y_1 = 0$ reveals that $f(t)$ must have an infinite slope at $t = T_0/2$ and pass through zero there. Also, from inspection, the slope of $f(t)$ is zero at $t = 0$ and $t = T_0$.

The substitution $\phi = \frac{x^2}{2}$ into Equation (51) at $x = 0$ yields

$$\frac{d\phi}{d\theta} = -b x_1$$

Integrating this it can be seen that x "starts out" from $\theta = 0$ like $x \sim -2\sqrt{-b x_1 \theta}$ (recall x_1 negative).

The final special case to be considered is $a = -b$. This corresponds to $n \rightarrow \infty$ for the present model. The three relevant equations are

$$\frac{dy}{d\theta} = a\left(1 - \frac{x}{y}\right) \quad (52)$$

$$\frac{dx}{d\theta} = a\left(1 - \frac{y}{x}\right) \quad (53)$$

$$a < 0$$

$$x^2 + y^2 = C_2^2 \quad (54)$$

Equation (54) says that the solution to (52) and (53) traces out a circle of radius C_2 in x, y space. Because of physical restrictions it is possible to rule out most of the circle as representing no real solution. First it is clear that the point x_0, y_0 may not occur in the half plane $y < 0$ because this would be an indication of an expansion shock at $t = 0$. Similar arguments rule out the possibility of x_0, y_0 being found in the first quadrant, $y \geq 0, x > 0$ and the second quadrant $y \geq 0, x < 0$, leaving as the only possibility that x_0, y_0 is to be found at $x = 0, y_0 = k$. As τ increases the circle is traced in a counter-clockwise direction to the point $x_1 = -k, y_1 = 0$.

After inspection of (52) and (53) it is seen again that the slope of $f(t)$ is infinite at $t = \tau_0/2$, where $f(t)$ passes through zero. For, $a = -b$, however the slope of $f(t)$ at zero and τ_0 is negative and equal to a , rather than zero. ($a \sim -2\gamma n, n \rightarrow \infty$).

An exact solution to the system of Equations (52) and (53) can be found. It is given below as an indication of the complication to be expected in solutions of equations of this type even for a special, simplified case

$$4a \bullet = 2y + k/2 \log \left[\left(\frac{y - k/2}{y + k/2} \right) \left(\frac{\sqrt{k^2 y^2 + \sqrt{3} k/2}}{y - k/2} - \frac{\sqrt{3}}{3} \right) \left(\frac{\sqrt{k^2 - y^2 + \sqrt{3} k/2}}{y + k/2} + \frac{\sqrt{3}}{3} \right) \right] \\ - 2\sqrt{k^2 - y^2} + k/2 \sin^{-1} \frac{2y}{\sqrt{2} k} - \frac{k}{2} \sin^{-1} \left(\frac{-y}{k} \right) + \bar{K}(k)$$

$\bar{K}(k)$ is the right hand side of the above equation with y replaced by k . $k = y_0 = -x_1$ must be determined by the conditions found above, namely that $x_0 = y_1 = 0$.

For general values of a and b , that is, for general values of n numerical techniques are presently being attempted. Here also difficulties are incurred because of the boundary condition $f(0) = -f(\frac{2L}{a_0})$ and the physical requirement of no expansion shocks.

It was a stated purpose of the present investigation to find the dependence of the amplitude of the wave on n . This will be possible only after several values of n have been tried for given M and γ . Hopefully then one will be able to plot a curve of ϵ vs. n and find eventually the $H(n)$ belonging in the equation $\epsilon = MH(n)$. In this connection note that Sirignano found for his model $\epsilon = \frac{\gamma-1}{2} M(w-1)$ where w corresponds in a general way to n . For the present work, due to the different approach used, there is no guarantee of a similar simple expression for $H(n)$.

In summation, this investigation has led so far to the following conclusions:

1) No shock wave instability seems possible when the n, γ combustion model is employed, as long as the combustion perturbation terms $O(M\epsilon)$ are of the same order as the wave amplitude. That is when ϵ is not dependent on Mach number.

2) When the amplitude of the wave phenomena can be considered large compared with the combustion and nozzle damping effects, (as may occur through growth of a small perturbation or through a triggered wave) then it appears that periodic shock wave solutions are possible using the n, γ combustion model.

NOMENCLATURE

a	speed of sound
b	parameter defined after Equation (42)
C_1, C_2, C_3	constants introduced after Equation (44)
f_r, f_s, f	arbitrary functions of their arguments which are solutions to Equations (3), (4) and (16), (17)
\mathcal{F}	quantity defined after Equation (26)
H	quantity defined in the text following Equation (13)
k	quantity defined after Equation (54)
\bar{K}	constant defined in text following Equation (54)
p	pressure
\int	quantity defined in Equation (31)
t	time
T	period
u	velocity
w	quantity defined in the first page of the text
x	dependent variable defined after Equation (43)
y	dependent variable after Equation (43)
ϵ	amplitude parameter
η	dummy variable of integration
θ	independent variable introduced in text after Equation (42)
ρ	density

Subscripts:

0	zero order steady-state quantity
1,2	first and second order quantities

Superscript:

primes	represent differentiation with respect to the functions argument
--------	--

C. NONLINEAR DISSIPATION IN ACOUSTIC LINERS

An important flow phenomenon with acoustic liners is the nonlinear dissipation or "loss" of energy. Even for very small amplitudes this dominates over the linear dissipation (which is related to the friction at the walls of the orifice). Therefore, this nonlinear dissipation effects the damping of oscillations in those combustors where liners have proved useful.

Prior to this presentation, investigators^{13,14} have determined this nonlinear loss by empirical means only. That method will be shown herein to be unsatisfactory since errors occur whenever the cold-air experimental results are scaled to actual motor operations.

Acoustic liners are in reality a combination of many Helmholtz resonators each of which consists of a small cavity connected to the combustion chamber by means of an orifice tube[#]. The fact that, in most practical designs, the cavities of all resonators are not separated does not add any essential complexity to the problem provided that the cavity dimensions are negligibly small compared to the wavelength of the oscillation of interest.

The resonator has a natural frequency which can be determined to a good approximation from the statement of conservation of energy¹⁵; i.e., the sum of kinetic energy plus potential energy in the system remains constant with time (with conditions in the combustion chamber considered to be stationary for the purpose of this calculation). With little loss of accuracy, it can be said that all of the kinetic energy in the system is associated with the flow within and very near to the orifice and all of the potential energy is associated with the compressible gas medium in the cavity. The natural or resonant frequency depends upon the orifice dimensions, the cavity volume and the gas properties. When conditions in the combustor are oscillatory, the flow in the resonator will oscillate at the same frequency as the chamber flow. As the chamber frequency approaches

This orifice tube usually has a circular cross-section in practice and will be considered so in the following discussion and analysis. However, the extension to general cross-section is trivial.

the natural frequency of the resonator the amplitude of the resonator oscillations increases. Since all losses are proportional to amplitude, it is desirable to design the resonator so that its natural frequency is very close to the frequency of the most common mode of oscillation in the chamber in order to achieve maximum damping.

The direction of the flow through the orifice and the pressure gradient there are oscillating with time since for half of the cycle the chamber[#] pressure is higher than the cavity pressure and for the other half cycle the cavity pressure is higher. For not-too-large velocity amplitudes the flow separates near the entrance^{##} of the orifice with reattachment^{###} a few diameters downstream. Then the flow separates at the exit again forming a jet. Typically, the per cent loss of kinetic energy due to separation at the entrance of the orifice tube is not very large. However, the exit loss is essentially equal to the total kinetic energy of the flow which is converted to turbulence in the jet breakup. It is this exit jet loss which is conjectured to be the primary nonlinear loss in acoustic liner operation.

Although previous papers^{13,14} make a vague connection between the occurrence of turbulence and nonlinear losses, they give neither a physical description of the actual phenomenon nor an analysis of the situation but rather only certain empirical correlations which are misleading. In this presentation the flow in and near the resonator is analyzed with proper account of the primary nonlinear losses taken.

The analysis is based upon the following simplifying assumptions.

1) The loss due to separation at the orifice tube entrance is neglected while the exit loss is set equal to the kinetic energy of the flow in the jet.

[#] Here we mean the pressure in the chamber near the orifice. The cavity dimensions are assumed small compared to the wavelength so that pressure in the cavity may be considered to be uniform.

^{##} Note that the entrance and exit locations are interchanged every half cycle as the flow direction changes.

^{###} Here we are considering orifices with not-too-small length to diameter ratios.

- 2) There is no mean flow through the orifice.
- 3) One-dimensionality may be assumed for the flow through the orifice with shear in the boundary layer averaged over the cross-section.
- 4) The unsteady boundary layer is small compared to the diameter of the orifice so that flat-plate results may be used to calculate the friction on the orifice wall.
- 5) The length-to-diameter ratio of the orifice is sufficiently high to consider the flow just outside the orifice (at both the entrance and the exit) to be quasi-steady.
- 6) The amplitude of the velocity oscillations is sufficiently higher than the critical velocity for separation and jet formation so that the portion of time in the cycle when potential flow occurs as the velocity goes through zero is negligible compared to the period of the cycle. Therefore, it is reasonable to consider that the flow is always separated.
- 7) The orifice length as well as the cavity dimensions are considered very small as compared to the wavelength of the oscillation.
- 8) The entropy and mean temperature of the cavity gas remains constant with time even though dissipation in the jet occurs. This is reasonable if the chamber volume is much larger than the product of some mean flow rate (say an RMS value) and a characteristic observation time of interest (say a damping time). Also, of course, the portion of heat transferred to the walls due to the oscillations must be negligible. If these assumptions about entropy and mean temperature can be made for the cavity gas, they should also be reasonable for the gas in the much larger combustion chamber.
- 9) Only the oscillating pressure in the chamber is considered. This analysis can only be considered as a first step since oscillating velocity in the chamber is not considered. Neither is the effect of a mean flow in the chamber past the orifice considered.
- 10) The amplitude of the oscillations are not so large as to cause choking of the flow through the orifice at any instant of time.

Consider subscripts 1 and 2 to denote conditions at the chamber-end and cavity-end of the orifice, respectively. Also subscripts I and II denote

stagnation conditions several diameters from the orifice in the chamber and cavity, respectively.

Whenever the flow is positive in direction which (by definition) means from the chamber to the cavity we have through assumption 5 that

$$P_I = P_1 \left(1 + \frac{\gamma - 1}{2} M_1^2\right)^{\frac{\gamma}{\gamma - 1}} ; \quad P_{II} = P_2 \quad (1a)$$

and when the flow is negative in direction which means from the cavity to the chamber we have

$$P_I = P_1 ; \quad P_{II} = P_2 \left(1 + \frac{\gamma - 1}{2} M_2^2\right)^{\frac{\gamma}{\gamma - 1}} \quad (1b)$$

Employing the concept of conservation of momentum developed for a control volume which includes only the fluid in the orifice, one finds that

$$\frac{d}{dt} \int_0^l \rho u dx = P_1 - P_2 + \frac{\tau}{A} + \rho_1 u_1^2 - \rho_2 u_2^2 \quad (2)$$

where l is the orifice length, A is the orifice cross-sectional area and τ is the total force due to friction on the orifice walls.

Relating the pressure in the cavity to the mass in the cavity and further relating that to the mass flux through the orifice we find that under assumption (8)

$$\rho_2 u_2 A = \frac{d}{dt} (\rho_{II} V) = \bar{\rho} V \frac{d}{dt} \left(\frac{P_{II}}{\bar{p}} \right)^{\frac{1}{\gamma}} \quad (3)$$

where bar superscripts denote steady-state quantities and V is the volume of the cavity.

It is convenient to obtain the solution by a method of successive approximations. The first approximation would be correct to $O(\epsilon)$ where ϵ is an amplitude parameter, the second approximation would be correct to $O(\epsilon^2)$,

and so forth. The parameter ϵ is determined by the amplitude of the chamber oscillations by setting $p_I = \epsilon \cos \omega t$. Note that here p_I is only the perturbation in chamber pressure. Since the linear damping due to the friction will actually be smaller than the nonlinear damping effects, γ will be considered with the second order terms. The order of the approximation for a quantity will be denoted by the numeral in the superscript.

Combination of Equations (1), (2), and (3) yields the following to first order

$$\bar{p} \frac{d}{dt} \int_0^l u^{(1)} dx = p_I - p_{II}^{(1)} = \epsilon \cos \omega t - p_{II}^{(1)} \quad (4)$$

$$\frac{u_2^{(1)} A \gamma}{V} = \frac{d}{dt} \frac{p_{II}^{(1)}}{\bar{p}}$$

These relations hold for both positive and negative flow direction.

One can show by means of the linear wave equation applied to a tube which is much shorter than the wavelength of the oscillation that the density gradient, the pressure gradient and the velocity are constant over the length of the tube at any instant of time. This means that Equations (4) immediately become the following

$$\frac{V l}{Ac^2} \frac{d^2}{dt^2} p_{II}^{(1)} + p_{II}^{(1)} = \epsilon \cos \omega t \quad (5)$$

$$u^{(1)} = \frac{V}{\gamma A \bar{p}} \frac{dp_{II}^{(1)}}{dt}$$

where \bar{c} is the steady-state speed of sound.

Note that Equations (4) and (5) would have resulted to all orders, not just linear order, if the incompressible assumption were made since those equations do not assume anything about the continuity of mass. It is there-

fore quite fortuitous that previous investigators^{1,2,3} have obtained the correct linear approximation by incorrectly assuming incompressibility. Actually at each instant of time there is a linear variation in density through the tube.

For similar reasons one can use the incompressible results for the friction force and be accurate[#] to linear order for a compressible gas. So we have

$$\tau/A = \sqrt{8\mu\bar{\rho}\omega} (\ell/d) u^{(1)} \quad (6)$$

where μ is the dynamic viscosity, ω is the angular frequency, and d is the orifice diameter.

To second order, we have for positive flow direction

$$\bar{\rho} \frac{d}{dt} \int_0^{\ell} u^{(2)} dx = -\frac{\gamma\bar{p}}{2} \left(\frac{u^{(1)}}{\bar{c}}\right)^2 + P_I - P_{II}^{(2)} + \tau/A - \frac{d}{dt} \int_0^{\ell} \rho^{(1)} u^{(1)} dx \quad (7a)$$

$$\frac{d}{dt} \frac{P_{II}^{(2)}}{\bar{p}} = \frac{\gamma A}{V} \left\{ u_2^{(2)} + \frac{P_{II}^{(1)}}{\bar{p}} u_2^{(1)} \right\} \quad (8)$$

While for negative flow direction we have

$$\bar{\rho} \frac{d}{dt} \int_0^{\ell} u^{(2)} dx = P_I - P_{II}^{(2)} + \frac{\gamma\bar{p}}{2} \left(\frac{u^{(1)}}{\bar{c}}\right)^2 + \tau/A - \frac{d}{dt} \int_0^{\ell} \rho^{(1)} u^{(1)} dx \quad (7b)$$

Equation (8) holds for negative flow as well.

The solutions of Equations (7) and (8) for $P_{II}^{(2)}$ and $u^{(2)}$ contain particular solutions of two types: those due to the last inhomogeneous terms on the right-hand sides of Equation (7) and Equation (8) and those related to the dissipative effects represented by the friction term τ/A and the exit loss $\pm (\gamma\bar{p}/2) (u^{(1)}/\bar{c})^2$ in Equations (7). The particular

This is true only in a case such as ours where the mean flow is zero.

solutions[#] of the first type merely modify the solution by producing harmonics or constants other than the harmonic obtained in the linear solution so that they are unessential and disregarded for our purposes here. The particular solutions of the second type do modify the harmonic obtained from the linear solution and are most important. The solutions which exclude the higher harmonics are denoted as $\tilde{u}^{(2)}$ and $\tilde{p}_{II}^{(2)}$. Note that since the inhomogeneous terms of the second type are independent of position in the tube, $\tilde{u}^{(2)}$ is a function of time only. Now from Equations (7) and (8) we see that

$$\frac{Vl}{Ac^2} \frac{d^2}{dt^2} \tilde{p}_{II}^{(2)} + \tilde{p}_{II}^{(2)} = \pm \frac{\delta \bar{p}}{2} \left(\frac{u^{(1)}}{\bar{c}} \right)^2 + \frac{\bar{I}}{A} + \epsilon \cos \omega t \quad (9)$$

$$u^{(2)} = \frac{V}{A\bar{p}} \frac{dp_{II}^{(2)}}{dt}$$

where the plus sign is used for $u^{(1)} < 0$ and the negative sign is used for $u^{(1)} > 0$.

Equations (5) have the solution

$$u^{(1)} = \alpha^{(1)} \sin \omega t$$

$$p_{II}^{(1)} = -\alpha^{(1)} \frac{\delta A\bar{p}}{V\omega} \cos \omega t$$

where

$$\alpha^{(1)} = \frac{\omega_0^2}{\omega^2 - \omega_0^2} \frac{V\omega}{\delta A\bar{p}} \epsilon$$

$$\omega_0^2 = Ac^2 / lV$$

These results may be used to calculate the inhomogeneous part of Equation (9).

In order to actually obtain these solutions, the continuity equation must be employed.

One finds by Fourier expansion[#] that

$$\pm \frac{\gamma \bar{p}}{2c^2} (u^{(1)})^2 = - \frac{4}{3\pi} \bar{p} (\alpha^{(1)})^2 \sin \omega t \quad (10)$$

plus terms containing higher harmonics which are neglected here for our purposes. Also substituting into Equation (6), one obtains

$$\tau/A = - \sqrt{8\mu\bar{p}\omega} \left(\ell/d \right) \alpha^{(1)} \sin \omega t \quad (11)$$

Now by substituting (10) and (11) into (9), $\tilde{p}_{II}^{(2)}$ and $\tilde{u}^{(2)}$ may be determined. Doing so, one obtains

$$\tilde{u}^{(2)} = \alpha^{(2)} \sin(\omega t + \phi^{(2)}) \quad (12)$$

$$\tilde{p}_{II}^{(2)} = - \frac{\gamma A \bar{p}}{V \omega} \alpha^{(2)} \cos(\omega t + \phi^{(2)})$$

where $\alpha^{(2)}$ and $\phi^{(2)}$ are determined from the relationship

$$- \frac{\gamma A \bar{p}}{V \omega} \left(1 - \frac{\omega^2}{\omega_0^2} \right) \alpha^{(2)} \cos(\omega t + \phi^{(2)}) = \epsilon \cos \omega t - \alpha^{(2)} \sqrt{8\mu\bar{p}\omega} \sin(\omega t + \phi^{(2)}) \left[\frac{\ell}{d} + \frac{\Delta n \ell}{d} \right]$$

The definition

$$\frac{\Delta n \ell}{d} = \left(\frac{\alpha^{(2)}}{3\pi} \right) \left(\sqrt{2/\omega\nu} \right)$$

has been employed in order to denote the nonlinear damping effect. ν is the kinematic viscosity. Note that $\alpha^{(2)}$ replaced $\alpha^{(1)}$ and $\phi^{(2)}$ replaced $\phi^{(1)} = 0$ with no loss of accuracy when Equations (10) and (11) were used to substitute for the inhomogeneous terms in Equation (9).

Of course, as already noted, the plus sign is used whenever $u^{(1)} < 0$ and the negative sign is used whenever $u^{(1)} > 0$.

The above equation is readily solved to yield

$$\alpha^{(2)} = \frac{\epsilon}{\bar{p} \sqrt{\left[l\omega \left(1 - \frac{\omega_0^2}{\omega^2} \right) \right]^2 + 8\omega r \left[\frac{l}{d} + \frac{\Delta_{nl}}{d} \right]^2}}$$

$$\phi^{(2)} = \arctan \frac{\left[\frac{l}{d} + \frac{\Delta_{nl}}{d} \right] \sqrt{8\omega r}}{l\omega \left[1 - \frac{\omega_0^2}{\omega^2} \right]} \quad (13)$$

This equation for $\alpha^{(2)}$ is actually a fourth order polynomial since $\alpha^{(2)}$ appears in Δ_{nl} . However, since the coefficient of the highest degree term is smaller than the others, it is quite accurate to solve for $\alpha^{(2)}$ by an iterative technique employing the above form.

Actually the nonlinear exit loss does not depend upon viscosity and frequency but the defined quantity Δ_{nl} will depend upon viscosity and frequency. This means that the value of Δ_{nl} determined experimentally in one gas medium at one frequency must be scaled by the square root of the product of the frequency ratio and the kinematic viscosity ratio in order to have the value of Δ_{nl} in another gas medium at another frequency. Since Reference 2 does not scale in this manner, their approach is in serious error.

The predicted dependence of Δ_{nl}/d upon the velocity agrees with experimental results⁽¹⁾ as shown in Figure 1. In that case, experiments were performed in air at a frequency of oscillation of 234 cycles per second. On the basis of the agreement between theory and experiment, one may conclude that the exit loss is the most important phenomenon in the nonlinear operation of resonators and the nonlinear loss may accurately be predicted by the theory outlined above.

In order to have a complete theory of acoustic liner operation, it still remains to determine the effect of flow past the orifices in the chamber and the integrated effect of many resonators in the wall of the chamber.

NOMENCLATURE

A	orifice cross-sectional area
C	speed-of-sound
d	orifice diameter
l	orifice length
M	Mach Number
p	pressure
t	time
u	gas velocity in orifice
V	volume of cavity
x	axial position in orifice
α	velocity amplitude
γ	ratio of specific heats
Δ_{nl}	effective length correction for nonlinear loss
E	pressure amplitude
μ	dynamic viscosity
ν	kinematic viscosity
ρ	density
τ	friction force
ϕ	phase angle
ω	angular velocity

Subscripts:

1	conditions at chamber end of orifice
2	conditions at cavity end of orifice
I	conditions in chamber
II	conditions in cavity

Superscripts:

bar	indicates steady-state quantity
1,2	indicates order of approximation

IV. NONLINEAR COMBUSTION INSTABILITY MECHANISMS: EXPERIMENTAL

A. TRANSVERSE MODE NONLINEAR ROCKET MOTOR STUDIES

In preparation for the testing with the acoustic liner, the theoretical liner studies having been described in Section III-C, a number of tests were performed on the transverse mode hardware. Certain of these tests were attempts to ascertain the environment within a prototype resonator cavity when both stable and unstable conditions existed within the combustion chamber. Temperature measurements for speed of sound estimates were made with .005 inch diameter bare wire thermocouples placed near the far end of the acoustic resonator cavity while others were placed in or near the connecting orifices from the chamber. These measurements revealed temperatures of approximately 900°F during steady-state operation. Upon the initiation of first tangential mode combustion instability an instantaneous rise to approximately 1800°F was exhibited followed by a rapid[#] decline toward an asymptotic value of roughly 1200°F. The latter description applied to the thermocouple at the orifice-end whereas the temperature excursions further back in the resonator cavity were less pronounced.

Such temperature data, together with the modified acoustic liner theory (III-C), provide the design background for the acoustic liner now in fabrication. The design consists of 56 individual resonator cavities (60 nominal, but placement of the pulse gun, transducers, TEAL jets, etc., necessitated the elimination of four) and allows for individual resonator volume adjustments. Each resonator cavity has six connecting orifices to the chamber so spaced as to minimize interaction between each other or with the cavity walls. The resonator cavity is internally threaded so that the movable plug may be moved in or out appropriately to accurately size the chamber and hence its characteristic frequency. Initially, the resonator lengths will be based upon the temperature data just discussed, assumed gas composition, and the knowledge of the fundamental mode within the combustion chamber. However, realizing the difficulty of precise tuning, variations about the mean will be tried in the early tests using flush-mounted Kistler transducers at the far end of several resonators to determine which resonator cavity best

[#] Order of 1 second.

achieves the proper resonant condition (registering maximum pressure oscillation amplitude). In addition, further temperature measurements are contemplated. The screw-type plug design also allows blockage of the resonator cavity by moving the plug to the orifice-end. Thus, the number of "open" resonator cavities can be regulated. This capability will allow investigations into the most effective locations for the open resonators, e.g., it might be possible to achieve similar stability benefits with certain circumferential groupings of open resonators, much like baffle placement. Axial placement has already been investigated at Pratt and Whitney¹⁶.

To catalog the axial variation in amplitude of the first transverse mode, another important factor to consider in resonator cavity placement, a number of variable-length tangential tests were run. The standard cylindrical length was 4 inches (effective length 6 inches) or a L/D of approximately .7 (with the standard 9-inch diameter hardware) while the maximum length tests was 10 inches (effective length 12 inches) and the L/D was \sim 1.3. The tests were made with the 16-spud injector and included tests with the sodium seeding jet (see Section IV-C).

In the L/D tests, variations in the pk-pk pressure amplitude at the 3-inch axial location were compared as shown in Figure 2. The amplitude is seen to reach a minimum in the vicinity of an L/D of 1 (7-inch cylindrical length or a 9 inch equivalent length when the reflecting point in the nozzle is taken into account). This same effect was noted by Osborn and Bonnell¹⁷ in transverse mode tests with gas rockets and was attributed to interaction between the longitudinal and transverse modes. No evidence of either combined mode tendencies or phase changes were observed in the current tests. Measurements closer to the injector face are necessary before final conclusions, which must be based on axial phase comparisons near L/D values of 1, can be drawn.

The values of the amplitudes recorded at 4 axial stations for the 10-inch cylindrical chamber are shown in Figure 3. The average pk-pk pressure amplitude values at 3, 5, 7 and 9 inches from the injector are 204 ± 17 , 179 ± 0 , 151 ± 12 and 131 ± 6 psi. The best linear fit is shown. A steady falloff in amplitude is indicated as the nozzle is approached.

Still higher amplitudes have been observed in past tests at the 1-inch axial location.

Phase comparisons were made for the 10-inch hardware and variations of only a few degrees existed between upstream and downstream transducers. In certain tests at Princeton in the past¹⁸ a noticeable phase lag ($\sim 45^\circ$) was shown when the pressure records from the downstream transducers were compared to those upstream. On the other hand, Clayton and Rogero¹⁹ reported a 49° phase lead. The early Princeton data was based on testing with LOX-on-Ethanol doublets, which exhibited rapid completion of combustion (within 3 inches from the face²⁰), the present test series uses like-on-like injector designs which spread the combustion further from the injector face²¹ and finally the JPL study; although using corporal propellants with direct impingement, the orifice sizes were much larger (.0986" and 0.173" versus .059") and the longer chamber length and lower contraction ratio would also tend to indicate an axially distributed combustion situation. Such factors may well be responsible for the phase differences exhibited. The JPL data did show a similar loss in pk-pk pressure amplitude as the nozzle was approached. Because of the shock-type nature of the waves observed the actual magnitudes must remain somewhat in question in the JPL tests.

Another study which is directly related to previous transverse test results should be mentioned here. These previous data (Figures IV-1 and IV-2 of Reference 1) indicated opposite spin direction tendencies for LOX/ALC versus LOX/RP-1 with identical injector configurations. The current investigation concerns early combustion phenomena with emphasis on chemical kinetic factors. Using the low pressure chemical kinetics device developed by Glassman and Sawyer³³, alcohol and kerosene-type fuels are being tested. Preliminary results indicate that a slow chemical kinetic reaction is immediately initiated in the case of alcohol, while for the kerosene-types a sizable delay is observed followed by a more rapid reaction rate. Further work in this area will be continued this fall when undergraduate help is available.

B. LONGITUDINAL NONLINEAR ROCKET STUDIES

In the comparisons of square-motor stability behavior previously reported^{3,21,22} certain differences exhibited by the 2 x 2[#] type injectors compared to the 4 x 4 types were difficult to understand. To briefly review the situation: the coarse 2 x 2 pattern (2 like-on-like fuel elements and 2 similar oxidizer elements placed 1.34 inches apart) was spontaneously unstable above certain lengths; while the 4 x 4 type employing 4 times as many elements (8 fuel, 8 oxidizer with 1/2 the spacing, .67 inches, and 1/2 the orifice diameter, .059 inch) required pulsing to drive it unstable under identical operating conditions. Still finer patterns (the 6 x 6 for example) in general followed the 4 x 4 behavior.

As mentioned in the last yearly report,²¹ the role played by the chamber wall in the combustion instability phenomena was a prime question that needed to be answered. An approach was outlined which involved the use of any of the typical injector elements (pairs of 0.040, 0.050 or 0.120 inch diameter orifices) with spacing held constant in the 4, 16 and 36 number arrays. Such tests would involve square-motor hardware of different cross-sectional areas to cross check the previously obtained stability data. All four elements in the 2 x 2 case have contact with chamber walls on two sides, contrasted to the 4 x 4 design where 4 have two-wall contact, 8 have one-wall contact and 4 have no wall contact whatsoever. The 6 x 6 design stands 4, 16, and 16.

It was decided that the tests would proceed based on a quarter-size chamber and injector design. Thus, a quarter-size 4 x 4 injector was used which retained 2 elements of each propellant and resembled a scaled down 2 x 2 type. The spacing between elements remained at 0.67 (the 4 x 4 standard). Chamber and nozzle sections were cast in copper with appropriate transducer pulse gun and ignitor ports.

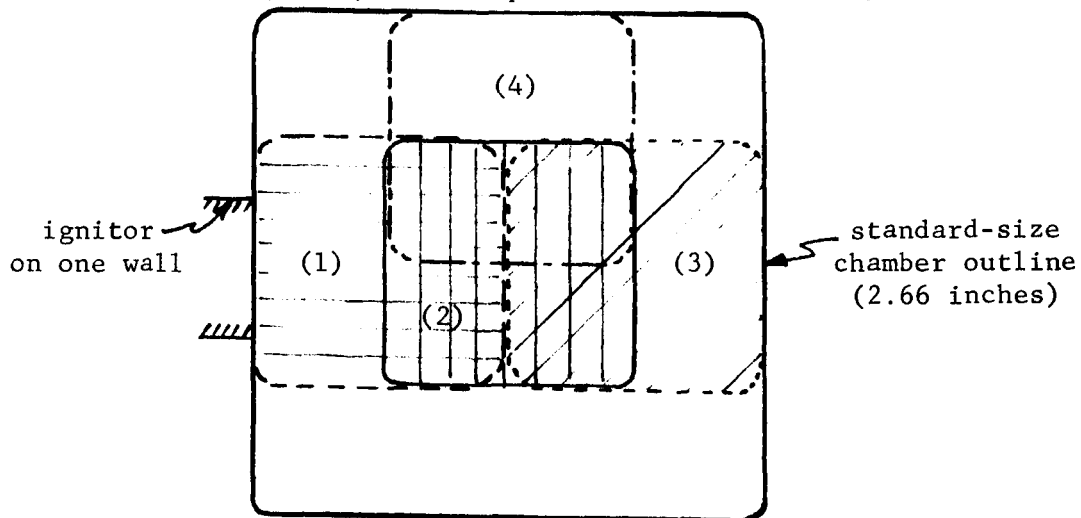
The test data resulting from the first series of tests are illustrated in Figure 4. For reference purposes, representative data from 2 x 2, 4 x 4 and 6 x 6 tests using standard size chambers are also plotted against mixture ratio in the same figure. Failing to follow the previous 4 x 4

[#] Figures illustrating the injector designs are found in References 3, 21 or 22.

(or 6 x 6) results, the quarter-size tests were spontaneously[#] unstable in much the same fashion as the previous 2 x 2 tests. The spontaneous instability characteristically occurred 100 millisecc. or so after ignition.

The quarter-size injector was then placed in the standard-size chamber hardware (retaining the same nozzle-end arrangement) and promptly responded with a return to the pulsed-type instability characteristic of 4 x 4 and 6 x 6. Pulsing was supplied by bursting a 15,000 lb. disk with 15 grains of pistol powder. The pulse gun was located near the nozzle.

This same test is replotted in Figure 5 as a reference for the additional tests in the investigation into the influence of the placement of the propellants near the chamber wall as a triggering mechanism for combustion instability. Because the gaseous ignition system (a spark plug with gaseous hydrogen and oxygen) is present in the first square-motor chamber section, effects were rechecked on the opposite wall as well. The quarter-size injector was moved so that the fuel orifices were in the same relative position to the wall as in the conditions present in the 4 x 4 full-size hardware or the 1/4 (4 x 4) in the quarter-size hardware (see sketch below).



(1) thru (4) represent four positions of the quarter-size injector

The central position, away from the walls, is shown as (2) and has a vertical cross-hatch. The near-wall positions are shown as (1), horizontal-hatch, and (3), diagonal-hatch. Both fuel and oxidizer jets are moved toward the wall in position (4).

[#] Maximum amplitude was reached in a few cycles similar to Figure 31, Ref. 22.

In Figure 5 the data with the fuel orifices moved to the ignitor wall or opposite wall ((1) or (3)) show the same lower stability-limit as in the central location (based on mixture ratio) with more stable operation at higher mixture ratios. The LOX orifice tests also improved stability over the central location with instability occurring at high mixture ratios when the LOX orifices were placed adjacent to the ignitor wall. Two spontaneous instability blips did occur at lower mixture ratios as well as a very slow damp in another test.

When both fuel and LOX orifices were moved adjacent to the wall (position (4)), the full range of pulsed instability associated with the central position returned although at a lower amplitude (75 psi vs. 123 psi). Also present was one spontaneously unstable test. It is difficult to generalize from such limited data that enhanced triggering is shown in this case. However, when two walls are exposed to the propellant sprays from the LOX and fuel orifices, as in the quarter-size chamber tests and in the full-size 2 x 2 testing one would expect additional wall-effects. The mixed propellant case appears to represent an addition of the instability zones determined from wall tests with the individual propellants.

In summary, wall-effects seem to play a definite role in spontaneous instability initiation based on the tests just described. To fairly evaluate stability behavior of an injector design care must be taken so that such effects will not overshadow the test objective. Tests on fuel and oxidizer orifices located near baffle surfaces have also been shown to play a role in the damping rates²¹ of tangential mode instability. Of interest in the tests described is that pulsing the spontaneous instability in the quarter-size hardware in a number of instances stabilized the motor. However, within 100 millisecc or so retriggering occurred. This triggering is believed to be due to the proximity of the wall and the effect on the local combustion process - with a local "pop" reinitiating instability.

C. NONLINEAR DISPLACEMENT EFFECTS

The purpose of this study is to attempt to understand more fully the effects of oscillatory gas motion on the displacement of liquid and vapor from an evaporating fluid in a pseudo rocket motor. The results of this study would hopefully lead to a better understanding of parametric relationships involved in droplet and jet breakup, droplet evaporation and the displacement of vapor of the injected propellants in an actual rocket motor, under conditions of transverse combustion instability.

In the past²³ the injected fluid, Freon 114, was steadily introduced through a cylindrical tube into the chamber resulting in a turbulent jet of size comparable to that of a typical shower head injector (orifice diameter $\approx .120$ "). The jet was disturbed by a tangentially directed pulse of nitrogen gas. Under these conditions the displacement of the liquid core and vaporized Freon could be observed using a spark shadowgraph technique. Little in the way of quantitative data, however, could be gained from these tests. Oscillatory conditions persisted only for a few milliseconds which severely limited any experimental observations. Due to the nature of the experiment, reproducibility was a problem particularly as far as the velocity fluctuations were concerned. Perhaps more important is the fact that one could not readily distinguish between the effects of the acoustic field and those of the externally introduced nitrogen gas pulse. In this regard the system was redesigned as follows.

In place of the nitrogen pulse gun a 60 watt Universal horn driver unit was installed. An oscillatory signal is supplied to the driver from a Knight audio generator via a Bogen 100 watt amplifier. Acoustic field intensities of up to 165 db are attainable with this apparatus. Velocity fluctuations of up to 100 feet per second have been measured. The pressure oscillations are measured with a Barium Titanate probe which was calibrated with a General Radio sound level indicator. Unfortunately limited range of the calibration instrument (135 db) necessitates extrapolation to the higher field intensities. Attempts are underway to improve the calibration through the use of a Giannini pressure transducer, the time response of which is well-known. Velocity measurements are made with a Thermo Systems,

constant-temperature hot wire anemometer system. Again, limited facilities do not permit accurate calibration over the full-range required for this experiment. Corrections had to be made for measurements at the variety of chamber pressures under consideration. This correction was performed using a simple Reynold's number correlation and incorporating the change into the mathematical description of the rate of heat transfer from a fine wire (based on King's law). The use of the above system enables one to subject the chamber and the injected fluid to a variety of imposed steady and oscillatory pressures.

The technique by which the fluid is introduced into the system has also been drastically altered. Based on the method suggested by Nicholls et al²⁴, a droplet generator was designed. This is shown in Figure 6. The device allows a maximum of four fine liquid streams to be injected simultaneously into the pseudo rocket. Currently, however, only one such stream is being observed because of photographic clarity considerations. The generator is attached to the voice coil of a 20 watt speaker. Through the use of another audio oscillator and a 20 watt amplifier the generator can be made to vibrate at any desired frequency. Like all vibrating capillary devices for producing a stream of uniform liquid drops, the operation of this generator is based on Rayleigh's analysis of the instability of capillary jets.²⁵ By considering a cylindrical liquid jet whose surface is perturbed, Rayleigh has shown, by calculating the change in potential and kinetic energy from the unperturbed condition, that the frequency of maximum instability of the jet is

$$f_c = \frac{u_j}{4.508 d_j} \quad (1)$$

where u_j is the jet velocity and d_j the jet diameter. When the jet is mechanically disturbed at such a frequency, droplets of uniform size are formed. However, it has been observed by this writer that a range of frequencies can result in uniform drop sizes. This fortunate situation allows the production of a variety of droplet sizes and spacings without changing

the injector needle diameter or the injection velocity. The droplet size will of course depend upon the driving frequency and, as can be shown from conservation of volume, the initial drop size D (ignoring the vaporization prior to the droplet formation) is related to the initial jet diameter by:

$$\frac{D}{d_j} = \left(\frac{3 \Delta}{2 d_j} \right)^{1/3} \quad (2)$$

The selection of drop diameter D is not as flexible, however, as is indicated by the above. Schneider²⁶ has shown that in order to produce a smooth capillary jet a minimum pressure head exists. Below this value the liquid forms a small drop which is attached to the exit surface by the action of surface tension. The drop grows and when it reaches a size such that its weight can overcome the surface tension, it detaches from the surface and falls. Droplets formed in this way are usually very large. If the liquid head is increased above this limiting value a smooth liquid jet of diameter equal to the tube diameter is formed. The minimum velocity of a smooth jet exiting from a capillary tube is dependent on the surface tension, the density of the fluid and the tube diameter. Schneider's analysis shows that

$$u_m^{-2} > \frac{8\sigma}{d_j \rho} \quad (3)$$

therefore jet velocities below this value cannot be attained. Consequently the driving frequency (Equation 1) is limited which in turn restricts the droplet size (Equation 2).

Another consideration with regard to the droplet generator is the terminal velocity of the droplets formed. By equating buoyancy and gravity forces this terminal velocity, when the droplet is falling through a quiescent atmosphere, may be expressed by:

$$v_T = \frac{g D^2 (\rho_f - \rho_a)}{18 \eta_a} \quad (4)$$

where the drag coefficient has been chosen equal to $\frac{24}{Re}$ for laminar flow. Therefore, in order to produce droplets of uniform spacing the initial droplet velocity must be equal to the terminal velocity. If the initial velocity is less than this value (but higher than that specified by Equation 3) the droplet spacing will increase as the drops proceed through the chamber. If the initial velocity is higher than the terminal velocity coalescence of the droplets will occur. The curves of Figure 7, which represent the terminal and minimum velocities as a function of tube diameter, shows that a minimum tube diameter exists below which the droplet generator cannot function. The tube size currently being used is .012" in diameter. This unfortunately produces relatively large droplets; (at the critical driving frequency it can be shown that the droplet diameter, $D = 1.89 d_j$, equals 576 microns for this case). However, the droplets are not so large that accurate experimental observations cannot be made. A photograph of a typical stream of droplets produced by this generator is shown in Figure 8. This picture and those that follow were taken with the existing spark system modified somewhat for conventional photography (versus the previous shadowgraph arrangement).

When the generator is stationary and the chamber is not resonated the jet appears as is shown in Figure 9a. Breakup is observed to take place some distance from the injector unit. This behavior is well known and in the absence of any externally applied disturbance is due to surface tension forces causing localized necking and subsequent breakup of the liquid jet. When the chamber is resonated (using the horn driver unit), however, the time to breakup and the size and shape of resultant ligaments is altered considerably. These details are seen in Figure 9b. Breakup distance as a function of acoustic field strength has been measured but the results are not yet finalized due to the previously discussed calibration inaccuracies. Generally, the breakup time (distance) decreases with increasing field intensity. Again this result is not unexpected since the jet breakup is enhanced by the transverse flow of gas. This effect has been investigated by Clark²⁷ for the case when the transverse gas flow is steady.

Perhaps more interesting is the trend toward more regularity in droplet (ligament) size and spacing when the chamber is resonated. The

effect may be seen in Figure 9b which can be compared to Figure 9a . This effect has been observed in the past by Miesse²⁸ in 1955 and Reba and Brosilow²⁹ in 1960. Whether such droplet grouping can be directly related to high frequency combustion instability, longitudinal or transverse (as contrasted to droplet population effects related to buzz phenomenon as covered in Section IV-D) is unknown at this time. The principle interest here is the use of this breakup mechanism in the study of transverse vapor displacement effects.

When the flow of liquid is disturbed by either or both of the above mentioned mechanisms the droplets that are formed permit a detailed examination of the way the droplets move, are distorted and the rate at which they evaporate. Since the droplets are moving at a known velocity (their terminal velocity) the distance from the injector exit is directly proportional to the time that the droplets have been evaporating. Hence when the chamber is resonated the distance from the injector is indicative of the number of acoustic cycles the droplets have been subjected to. This will permit the determination of droplet size as a function of the number of the number of acoustic cycles and thence the evaporation rate under oscillatory conditions. With this technique it should be possible to examine the applicability of the quasi-steady evaporation rate theory under violently non-steady conditions.

By utilizing a shadowgraph technique in which pictures are taken at distinct intervals during an acoustic cycle it is possible to observe the direction of vapor and liquid displacement (Figure 10) and hence to evaluate the importance of any gas motion, either cyclic or unidirectional, which may be present. Also the manner by which the vapor production influences jet breakup may be examined. This effect has already been observed to a limited extent. For example when the liquid is injected into the chamber and the chamber pressure is below the vapor pressure of the fluid at its injection temperature, as is often the case in an actual rocket motor, jet breakup is very rapid and the resulting array of droplets, ligaments and vapor is widely dispersed. This is illustrated in Figure 11 . The predominant mechanism for this type of disintegration is that the large quantities of vapor being produced throughout the jet as the liquid boils causes a

violent eruption of the liquid core.

As a corollary to the cold flow studies, attempts have been made recently to observe via high speed photography the processes occurring near the injector face of the 9" diameter transverse rocket hardware. The purpose of such tests is to examine to what degree there exists, if any, bulk tangential gas motion in the region of the injected propellants. To date, emphasis has been on developing the technique to an extent whereby these observations can be made with some assuredness. Current practice is to inject a tracer stream of fuel which has been seeded with a sodium salt. The intense sodium D line radiation accompanying the combustion of this tracer stream permits the photography of the stream and the subsequent observation of the flow of combustion gases. The recent use of color film, as opposed to black and white, has lead to a distinct improvement over earlier pictures where lack of contrast was the prime difficulty. Before accurate data can be given in this phase of the overall study additional testing is necessary. These tests will hopefully provide higher amplitude spinning tangential mode oscillations, while improved timing, aperture setting and filters will further improve photographic clarity. These tests are now in progress and the results are expected shortly.

NOMENCLATURE

- d_j - jet diameter
- D - droplet diameter
- f_c - critical driving force
- g - acceleration due to gravity
- u_m - minimum fluid velocity
- u_j - jet velocity
- v_T - droplet terminal velocity
- η_a - viscosity of atmosphere
- ρ_a - atmospheric density
- ρ_f - fluid density
- λ - wavelength of driving force
- σ - surface tension

D. DROPLET DISTRIBUTION STUDIES

In last year's progress report²¹ under the subject of "Droplet Distribution Studies" it was pointed out that variations in droplet population densities were observed in both streak and still photography. These tests were performed using like-on-like doublet injectors in the cylindrical-shaped resonating chamber apparatus. The streak photographs at that time had been taken at only the standard test condition (i.e., $P_c = 100$ psig in the nitrogen-filled chamber - a gas density roughly corresponding to a 1500 psi LOX/RP-1 hot firing). The frequency of the droplet population changes was approximately 100 cps[#] or 1/5 the first longitudinal natural frequency based on the chamber length then in use. In addition, the still photographs, which provided data for droplet size distribution counts, indicated 2 and 3 to 1 variations in the count depending on whether the photos were taken in the high or low population regions.

Further studies of these effects have been undertaken with a goal of explaining the mechanisms responsible for the experimentally observed data. Historically, such droplet population variations have been observed by a number of investigators, e.g., Heidmann, Priem and Humphrey³⁰ noted a grouping frequency of about 2000 cps under atmospheric conditions with similar type impinging liquid jets. Riebling and Powell³¹ recently reported similar variations using sheets formed by liquid jets on curved surfaces.

Since an order of magnitude increase in pressure apparently decreased the observed frequency an approximately similar amount, it was felt that any systematic testing should initially involve pressure as the variable.

Prior to the initiation of these tests several modifications of the experimental apparatus have been introduced. The chamber itself has been lengthened to 20 inches with two more widows added at downstream locations. The longer length places the natural acoustic frequencies in a range that could easily be duplicated by the observed frequencies under appropriate chamber conditions in order to check "resonance" effects. The

These data were generally based on only three cycles and thus were considered preliminary.

additional windows provide the necessary access to droplets resulting from ligament as well as initial impingement type breakup. Also the siren assembly has been modified slightly to facilitate keeping the nitrogen flow circumferentially uniform (a problem in the past due to a small number of exit orifices). After the preliminary data (as reported in Reference 21) was taken using a 30-inch, continuous film loop, streak camera it was decided that a longer loop (and hence larger camera) was necessary to improve the accuracy of the frequency data. A new camera was designed and built, employing an 80-inch continuous loop of 35 mm film (Royal X-Pan Recording film was used). Thus the observation time was approximately tripled with a sufficient number of cycles recorded on each film. A mercury arc light source is being used in conjunction with the same lens system as employed in taking still pictures. This system provides a magnification of 5.2. With these modifications completed, a systematic survey of the phenomenon was undertaken.

The primary variables to be examined were the frequency, chamber pressure, injector velocity (ΔP), injector diameter (drop size), and fluid properties such as surface tension, viscosity and density. Also important would be the gas viscosity but at present there seems to be no feasible means of varying this parameter.[#] Also examined was the ratio of the number of droplets in the wave maximum to that in the minimum, specifically to check for the existence and magnitude of any possible resonance effect.

Initial tests were conducted with water using a spud with a .040 inch, 90° impinging jet injector. Both ΔP and chamber pressure were varied to get preliminary data on the shape of the frequency-chamber pressure curve. Figure (12) illustrates this power law curve (solid line) for 50 psi ΔP . For the same range of chamber pressures a somewhat higher frequency, though similarly shaped curve, was found for 150 psi ΔP (dashed line). Next a .059 inch, 90° injector was used and again provided similar data with lower frequencies evident.

Then the fluid properties were varied, with a mixture consisting of 50% methyl alcohol and 50% water being used to vary the surface tension,

[#] N_2 , Air and He differ in viscosity by only about 10% within the temperature ranges normally encountered in the apparatus.

viscosity and density.[#] Data for each of these tests can be seen in Figure 12 as represented by a square symbol (double-dashed line). It might be noted that if the data from Reference 30 were also plotted in this figure it would fit in well with the points discussed. In the future, additional tests are planned to further separate the effects of the physical properties. A surface tension reducing agent is being employed for this purpose in one test series, thus changing the surface tension while maintaining the viscosity and density.

After obtaining these data it was decided to formulate an empirical relation, through the use of nondimensional analysis, in order to fit the observed points. The approach was as follows:

assuming that frequency = $f = f(D_0, \rho_l, v, \sigma_l, \mu_l, P_c)$

$$\text{or } f = AD_0^a \rho_l^b v^c \sigma_l^d \mu_l^e P_c^f$$

considering dimensions $1/T = L^a \frac{M^b}{L^{3b}} \frac{L^c}{T^c} \frac{M^d}{T^{2d}} \frac{M^e}{L^e T^e} \frac{M^f}{L^f T^{2f}}$

balancing dimensions

$$M : 0 = b + d + e + f$$

$$L : 0 = a - 3b + c - e - f$$

$$T : -1 = -c - 2d - e - 2f$$

$$\text{or } a = -(1 + d + e)$$

$$b = -(d + e + f)$$

$$c = 1 - 2d - e - 2f$$

$$\text{thus } f = A \frac{v}{D_0} \left(\frac{\sigma_l}{\mu_l v} \right)^{c_1} \left(\frac{\rho_l v^2}{P_c} \right)^{c_2}$$

$$\text{or } \frac{f D_0}{v} = A \left(\frac{\sigma_l}{\mu_l v} \right)^{c_1} \left(\frac{\rho_l v^2}{P_c} \right)^{c_2}$$

This decreased surface tension by 50%, viscosity increased by 30% and density decreased by 6%.

Now using the test data to get c_1 and c_2 , one first plots logarithmically those data points where $\sigma_e / \mu_e V$ were constant. Doing this one obtains $c_2 = .84$ as seen in Figure 13. Similarly, one determines $c_1 \approx 2.5$ as seen in Figure 14. However, in Figure 14 it must be noted that there are three separate and distinct curves each with slope c_1 , one for water, a second for the alcohol-water solution and a third for alcohol as used in the hot firings (this third group will be discussed later). Thus each curve has a different proportionality constant which seems to depend on the physical properties of the liquid. The basis for the separation of curves should be clarified when the physical properties are individually varied, specifically the surface tension in the next test series. Prior to that determination, the preliminary empirical solutions are:

$$\text{water: } \frac{fD_0}{V} = .071 \left(\frac{\sigma_e}{\mu_e V} \right)^{2.5} \left(\frac{\rho_e V^2}{P_c} \right)^{.84}$$

and

$$\text{water-alcohol: } \frac{fD_0}{V} = .85 \left(\frac{\sigma_e}{\mu_e V} \right)^{2.5} \left(\frac{\rho_e V^2}{P_c} \right)^{.84}$$

The third curve in Figure 14 resulted from an analysis of intermediate frequency data as observed in the transverse rocket tests^{3,21,22}. It can be seen that these data result in a curve which has a slope of about 2.5 and it's position falls at the location one would expect for 100% alcohol. This fact seems to lend some evidence to the postulate that the droplet grouping can be a cause of combustion instability in the intermediate frequency range. Future cold flow tests will be made with 100% alcohol to confirm the location of this curve based on test stand results.

Before leaving the subject of combustion instability, as it is involved in this particular study, the subject of longitudinal resonance should be discussed. With the 20-inch long cylindrical chamber the first longitudinal mode is approximately 340 cps. In the tests previously described the siren was not utilized but rather the droplet variations were

self-generated by the liquid jets. Using the siren and properly adjusting the chamber pressure based on the individual curves as shown in Figure 12 resonance could be achieved in the chamber in concert with the natural breakup phenomena. However, such testing failed to indicate noticeable improvement in the ratio of droplets in the high versus the low population regions and hence one would conclude that such oscillations are not generated by the acoustic modes or acoustic environment. Another point to consider, however, is whether or not the phasing of the intermediate frequency oscillations might not be influenced by such acoustic factors. That is, phasing in the sense that all jets would have a common time base. Looking to the Visicorder traces from the test firings, a typical example is shown in Figure 15, definite phase relationships are found between the two circumferential locations for the intermediate frequency. In this case no explanation is apparent since acoustic propagation should be found for any pressure variation whether generated by factors related to the sensitive time lag (i.e., times small compared to the acoustic wave periods) or factors based on lower frequency mass fluctuations (the effective mechanism in the case of droplet population variations). Returning to considerations in the longitudinal case and the cold flow study, the ability to observe phasing effects, which might be viewed as a weak interaction phenomenon, will be enhanced through the use of photo conductive cells (discussed in the following paragraph) rather than streak film records. This is based on a necessity for observing simultaneously the fluctuations of pressure (generated by the siren) and the droplet population fluctuations (a function of the impinging jets) over a number of cycles rather than ten or-so cycles as would be evident from film data.

Returning to the discussion of additional tests to separate variables and probe phase dependencies, etc., the use of photoconductive cells as the primary measurement technique becomes increasingly desirable. The bulk of the data reduction time is currently spent in developing and analyzing the streak film loops. Furthermore, direct phase comparisons (as previously discussed) could result from the success of such a system. Preliminary results using this technique, which employs the 1620 IBM computer for data interpretation, offers some encouragement. The principle problem

remaining involves the sensor response. Should this problem prove insurmountable a return to the more tedious methods will be necessary to complete the study. However, if the desired goals were attained, this technique could provide droplet size data as well as the droplet density data currently sought.

NOMENCLATURE

- a - f - exponents
- D_0 - diameter of orifice
- f - frequency
- L - length units
- M - mass units
- P_c - chamber pressure
- ΔP - pressure drop across orifice
- T - time units
- V - velocity
- μ_l - viscosity of liquid
- ρ_l - density of liquid
- σ_l - surface tension of liquid

E. EXPERIMENTAL TECHNIQUES FOR INVESTIGATING THE COMBUSTION PROCESS

To study the nature of the environment within a liquid rocket motor, with special reference to the distributed combustion designs (the like-on-like injector approach, for example) certain probing studies were initially attempted. Passing a 1/8 inch diameter tube through the walls of a square-motor³ chamber section, and thereby crossing the center of the stream of flowing combustion gases, allowed certain qualitative measurements of heat transfer nonuniformities to be made. This was possible because the thermocouple measurements within the water-cooled tube were made over a rather short portion of the exposed length (see Figure 16). The heat transfer variations were indicative of the transverse mixture ratio variations associated with the injector. These preliminary measurements were scheduled to be followed by gas samples along the same transverse line. The design of the sampling probe is such that this feature can be added using an internal tube.

In the process of considering other methods of attacking the problem of rocket combustion property measurements, it was felt that direct measurements of the speed of sound might be attained. Rather than using ultrasonic measurements across the flow at different axial locations, an approach followed by Hersh³², an attempt was made to follow a shockwave as it moved axially through the combustion region. The shock front, generated near the nozzle, moves toward the injector and thus surveys the speed of sound axially. In addition, data is supplied based on the local wave-shape, a point which will be discussed later. Since the shock wave has a finite amplitude, the speed of sound is always less than the shock velocity.

Using this method it was felt that undisturbed combustion and flow processes would be surveyed by the initial wave. Subsequent waves would constitute longitudinal mode combustion instability, which normally would result from the initial disturbance, and would provide data on combustion conditions existing under an instability environment.

Again using the square-motor hardware, and the chamber sections which provide for transducer insertion, it was possible to spread the Dynisco transducers at roughly three-inch intervals starting near the injector face.

The axial locations of the transducers for the initial series of tests were 1, 4, 7, 11, 13 1/2, and 16 1/2 inches in a 70 inch nominal length[#] chamber. In later tests points 14 1/2, 19 1/2, 25 1/2, 33 1/2, 45, 55 and 65 inches have been examined. The long chamber, with the pulse gun located 64.6 inches from the injector, provided a more than adequate distance for the shock to become planar - disregarding boundary layer interaction effects which would be present in any case.

Experimentally, the problem focused on the ability of both the instrumentation and recording system to provide measurements in error less than ± 5 microseconds (since the speed of sound is roughly 3500 ft/sec in the rocket motor, and the distances between transducers is ≈ 3 inches, the elapsed time is therefore ≈ 70 microseconds, where 5 microseconds represents a 7% error). To ascertain the capability of the experimental arrangement, tests were performed with the chamber filled with helium which closely approximates the sound speed^{##} associated with the hot firings. Several factors were evident from these helium tests and associated system checkouts. The seven-channel tape recorder exhibited tape skew in a random fashion such that the 5 microsecond criterion could not be met from that source of error alone. The variations between head stacks and variations between a.c. amplifiers, necessary on each transducer output, introduced significant errors.

To improve the time resolution between channels a 10 KC sinusoidal^{###} oscillation was superimposed on the recorded transducer data. The amplitude was such that the peaks were clearly evident in the presence of combustion or electronically originated noise. With this 100 μ second time reference, further time breakdown was possible through superposition of a 5 KC sine wave during data playback. This later time reference was not an integral part of the original recorded data and thus the phase varied from channel to channel between the 100 μ second time reference and these 10 μ second oscillations (the 10 μ second period resulted from 5 KC oscillations superimposed during

Actually the length to the nozzle entrance is 68.6 - reflection occurring in the subsonic portion of the nozzle adds another inch or so.

The chamber pressure was adjusted to duplicate the density associated with the hot firings as well.

A sharply peaked wave shape would have been more appropriate but this was not possible because of the flat frequency response limitation of 10 KC on the tape recorder.

a 20/1 time expansion playback). What the 5 KC did accomplish was the limiting of the error through the pinpointing of shock wave arrival to a portion of the 10μ second time interval.

The next problem involved the response of the transducers themselves. Although each of these strain gauge-type design instruments was of similar construction, the maximum pressure ratings were 1000, 1500 and 2000 psi with two transducers in each pressure category. For evaluation, the transducers were placed in groups of three in a special test section and, with a helium-filled chamber, were subjected to a standard pulse. All recorded the shock passage within 5μ seconds of one another. Next these same transducers were used in the locations where "hot" data would be gathered (1, 4, 7, 11, 13 1/2 and 16 1/2 inches). Based on a constant speed of sound in the helium, calculations were also made of the time intervals expected. The actual data, because of the rise rate considerations,[#] had to be corrected slightly depending on where in the 100μ second reference time interval the shock wave actually occurred. The extent of the correction is seen in Figure 17.

Turning our attention to the actual rocket motor firings, the choice of LOX and ethyl alcohol was made based on previous testing experience. The 4 x 4 like-on-like type injector design was used with the mixture ratio close to stoichiometric on the majority of the tests. This allowed stable operation at 70 inches with the possibility of pulse initiation of longitudinal mode combustion instability. Following the procedures previously described (time references, corrections, etc.) the resulting data on shock wave velocities is presented in Figure 18. The data from three tests are shown

[#] The negative slope following each sine wave peak, which initiates the time reference interval, is in opposition to the pressure rise indicative of the passing shock. Prior to the sine wave peak there is a positive slope which aids the pressure rise. Thus, detection of the wave passage tends to be delayed slightly in some regions (former case) while detection is aided in others (later case). The toe on the wave front shape is a significant factor in these measurements since the slope on the time reference sine wave, based on the necessity of maintaining reasonable amplitudes, is roughly half that of the maximum rise rate based on the tape recorder limitations.

together with error bars. Clearly, the velocity of the injector-bound shock wave (incident wave) is shown to decrease as the region of early combustion is approached. Based on the gas velocities generated by the combustion process (order of 170 ft/sec for these 900 psi chamber pressure tests with $A_c/A_t \approx 12.2$) the shock velocity would be expected to increase approaching the injector if uniform temperature gases existed throughout the chamber. Since the velocity is found to decrease, the indications are that temperatures are depressed considerably near the injector face. This could result from limited gas recirculation associated with the closely spaced injector grid pattern tested (fuel and oxygen elements .67 inches apart). The lack of noticeable recirculation of the hot combustion products in the case of the 4 x 4 grid versus that of 2 x 2 pattern was evident from static pressure surveys as well.²¹ It should be noted that the spacing between fuel and oxidizer pairs for the 4 x 4 design is quite representative of the dimensions associated with conventional ring-type designs that emphasize relatively high mass flow per unit cross-sectional area of the injector.

Another item of some importance results from these interpretations of the data. In the transverse mode case again the region of maximum energy release occurs characteristically within a few inches of the injector face. Thus, the speed of sound data in this location would provide a better means of accurately calculating mode frequencies and one would expect the resultant frequency to also be depressed. Such effects have been observed on high thrust rocket hardware with complicating features such as baffles which are also a factor in frequency depression. Based on the transverse mode studies at Princeton, as the amplitude is increased (resulting in an acceleration of the combustion process) the first tangential mode frequency has been found to increase in value from a low of 2500 cps to a maximum of 3100 cps in the 9-inch diameter hardware. Such data have been obtained from individual tests (i.e., increasing amplitude and frequency with time) as well as compilations of rocket test data.

In the longitudinal mode case, velocity decreases near the injector end often go unnoticed when averaged with increased velocity due to the finite amplitude of the shock waves encountered as well as uncertainties in

the speed of sound.

The effect of finite amplitude waves on the shock wave velocity as well as the effect of the local gas velocities is clearly brought out in Figure 19. In these tests the mass flow has been kept constant with changes being made at the nozzle-end. The chart below illustrates the ranges covered for these three variables:

Pressure (Psia)	Contraction Ratio (A_c/A_t) [#]	Nozzle Entrance Velocity (ft/sec)
150	2.02	1095
300	4.13	507
900	12.2	168

Looking at the incident waves for the three test series shown in Figure 19, the effect of the gas velocity is most evident in the 150 psia test. Here the measured velocity (local slope at 33.3 inch station) was 2780 ft/sec versus a calculated value of 2900 ft/sec. The 300 and 900 psia tests fall on a common line with a slope of 3470 ft/sec (calculated value 3520 ft/sec). The higher pressure ratio across the shock and resultant shock velocity increase in the 300 psia case (as compared to the 900 psia case) was such as to compensate for the higher gas velocities encountered.

Taking into account the reflected wave at the injector-end provides an additional basis for the conclusions previously drawn concerning the depressed shock wave velocity and hence reduced sound speed and temperature near the injector-end. The measured slope in the first two inches from the injector is approximately 2500 ft/sec compared to a sound speed of approximately 3500 ft/sec.

In the reflected wave regime, separation of the three curves is somewhat less than would be expected even though the final slopes represent the calculated spread in velocities. The 150 psia test is hampered in that the shockwave amplitude is steadily decreasing (complete damping occurs in

[#] Measured values after testing.

5 to 10 cycles). Also, as pointed out later, the maximum waveshape amplitudes on the reflected waves are reached only after 10 or so inches have been traversed. Improved early rates of steady-state combustion at the higher pressure would also tend to merge the three curves.

Besides the measurements of the velocity near the injector-end of the rocket, it is of interest to observe the differences between the waveshapes encountered at the various axial locations for helium and LOX/ALC tests. Figure 20 makes such a comparison where the incident wave amplitudes have been equalized for convenience of waveshape comparisons. These are not the first waves but rather the second incident waves in both cases since the nozzle reflection from the triggering pulse (4 inches to the nozzle plus 4 inches return, or a wave more than 8 inches behind the incident wave initially with the spacing narrowing with time) has coalesced by the second wave.

It should be noted that, in Figure 20, the characteristic exponential falloff behind the incident and reflected waves with helium is only found on the reflected wave in the hot firing. The LOX/ALC data initially follows the helium traces after the passage of incident wave and then the pressure is seen to increase prior to the arrival of the reflected wave. Possible causes for these waveform differences will be discussed next.

To present these pressure waveform data more graphically, the amplitude ratio is plotted versus axial position in Figures 21 and 22. The amplitude ratio is defined as the shock wave amplitude of the reflected wave compared to that of the incident wave. Based on the data collected on incident wave amplitude pressure variations along the chamber, this comparison amplitude is assumed constant[#] (arrowed line at ratio 1). Also in the graphs shown is the base of the reflected wave which is also plotted as an amplitude ratio.

The first point to note in Figure 21 is the characteristic form of the helium run data. The sequence of events depicted is as follows: the incident wave travels toward the injector-end with a uniform amplitude (actually a very slight decrease occurs with time because of frictional

[#] Near the injector face, at the 1" station, this point is difficult to document because the reflected and incident wave amplitudes merge as one because of insufficient time separation.

losses - even with the more energy consuming reflection losses, 20 waves or so occur before complete damping takes place); then, at the injector-end, the amplitude approximately doubles with reflection; moving back toward the nozzle we find that at each station at the instant of reflected wave arrival evidence of the incident wave remains in the form of an exponentially decaying local pressure, this pressure is noted as the "base of the reflected wave"; and finally the peak of the reflected wave, for the helium case, remains roughly one unit amplitude above the base, i.e., the shock wave is riding on top of a changing pressure base, a base that would disappear at the midlength or sooner. #

Looking now at the LOX/Ethanol case, having a better idea of the cold flow solution, several differences are evident. First, the base of the reflected wave rises at the 4 and 7-inch stations while falling more rapidly than the helium case at the stations to follow. This point was previously pointed out in reference to Figure 20 . The current figure under discussion points out that the maximum change from this source occurs approximately 6 inches from the injector face. One explanation is that additional combustion (i.e. a rate increase) takes place following the short time delay after the passage of the shock. This might be interpreted as direct evidence of the existence of the sensitive time-lag as related to the nonlinear case.

The reflected wave peak also departs markedly from the helium data. At the 4-inch station the points are coincident. Beyond that point the peak climbs to a maximum near the 11-inch station. Looking at the "hot" reflected shock wave amplitude, one notes that near the 4-inch station only one quarter amplitude is present and this value continues to increase until at 16 1/2 inches the full amplitude is evident. One interpretation of this series of events is that, unlike the helium case, considerable energy (and hence shock amplitude) is lost in the first few inches of the chamber because of the presence of droplets and ligaments and the lack of a perfect reflecting surface. The regaining of the amplitude could indicate energy transfer to the shock wave in the prime combustion region. No delayed combustion, as in the incident wave, would appear to be present since the

If the wave shape decays rapidly to a constant pressure prior to the following wave, then the "base" of zero could be reached prior to the midlength of the rocket.

back side of the shock shows the characteristic exponential falloff.

One interpretation of this portion of the wave travel is that the previously disturbed combustion process is now capable of adding energy instantaneously. This would follow the "no time-lag case" which theoretically described the phenomenon associated with combustion instability in the gas rocket.^{1,2} The late peaking (11 inches) might well be associated with later phases of the combustion process, i.e., primarily the gaseous phase. This energy addition does not indicate the presence of a detonation type phenomenon based on the velocities observed in the reflected waves of Figure 19 (the experimental velocities were within a few percent of the values calculated based on pressure ratio across the shock, speed of sound, and the gas velocities present).

A comparison between Figure 21 and Figure 22, second wave to fiftieth wave, would tend to indicate that once the longitudinal mode instability has been fully-established the primary change noted is the higher "peak" values in the prime combustion zone. The "base" values recorded in Figures 21 and 22 are approximately the same. If we interpret the higher peak as a more rapid restoration of energy, then one would conclude that this energy balance has been noticeably changed in the presence of combustion instability. Three tests are shown in Figure 22 and agreement is good near the peak. No explanation is currently available for the spread in the amplitude ratio values approaching the midlength.

In the hot firings (Figures 21 and 22) the "base" curve is not asymptotic to 0 at the midlength nor is the "peak" curve asymptotic to 1. The reason is the nozzle loss which, due to its magnitude, necessitates the reflected wave to have "extra" energy. This was not true in the helium case where the nozzle-end loss was simulated by a flat plug which extended to a point 1/3 of the subsonic length downstream of the nozzle entrance. Unlike the flowing case, no substantial loss resulted.

To evaluate the meaning of changes to the shock wave amplitude as a measure of the energy addition or subtraction to the system, tests are currently in progress emphasizing the nozzle-end. Using the same techniques, but armed with an exact theory of nozzle losses due to finite amplitude waves

(the theory applies to the "short" nozzle¹²), some of these vital points should be clarified.

Until these tests are completed, together with certain associated theoretical studies, energy relationships as interpreted from shock amplitude variations can only be considered tentative. It is hoped that this technique will shed considerable light on the processes taking place in rocket combustors before and after the onset of combustion instability.

APPENDIX A

A LINEARIZED TREATMENT OF QUASI-STEADY DROPLET BURNING

The problem of quasi-steady droplet burning in a convective flow field has been treated by a linearized method.¹¹ Certain general comments about that work may be found in Section III-A and in Appendix B. In this appendix, the same problem will be treated employing the same basic assumptions except that the actual time-dependent droplet size will be considered in the formulation rather than some time-wise mean size.

If M is the droplet mass and w is the mass vaporization rate, we have

$$w = - \frac{dM}{dt}$$

and if superscript bars denote mean-flow quantities and primes denote perturbation quantities, the following results

$$\frac{\bar{w}'}{\bar{w}} = - \frac{\bar{M}}{\bar{w}} \frac{d}{dt} \left(\frac{M'}{\bar{M}} \right) + \frac{M'}{\bar{M}} \tag{A-1}$$

The last term in the above equation was omitted in Ref. 11. Also \bar{M}/\bar{w} was considered as constant there.

The vaporization rate is given by

$$w = 2\pi\rho D r \text{Nu}_m \ln \frac{p_c}{p_c - p_L}$$

where the Nusselt number for mass transfer is given by

$$\text{Nu}_m = 2 + 0.6 (\text{Sc})^{1/3} (\text{Re})^{1/2}$$

For Reynolds number sufficiently greater than unity and assuming negligible[#] variation in the relative velocity between gas and droplet, we may approximate the Nusselt number as being proportional to the square root of pressure

[#] This is not true actually and the variation of the velocity should be considered in a complete analysis.

times droplet radius. So considering ρD equal to a constant and noting that droplet radius is proportional to droplet mass to the one-third power, we have following Heidmann

$$\frac{\bar{w}'}{\bar{w}} = \frac{1}{2} \frac{\bar{M}'}{\bar{M}} + \beta \frac{\bar{P}_L'}{\bar{P}_L} - (\beta - \frac{1}{2}) \frac{\bar{P}_c'}{\bar{P}_c} \quad (A-2)$$

where

$$\beta = \frac{\frac{\bar{P}_L}{\bar{P}_c - \bar{P}_L}}{\ln \frac{\bar{P}_c}{\bar{P}_c - \bar{P}_L}}$$

As shown by Heidmann, the vapor pressure may be written as

$$\frac{\bar{P}_L'}{\bar{P}_L} = b \frac{\bar{T}_L'}{\bar{T}_L} \quad (A-3)$$

where b is a constant.

The droplet temperature is given by

$$\frac{d\bar{T}_L}{dt} = \frac{1}{c_p \bar{M}} [2 k \pi Nu_h r (\bar{T}_g - \bar{T}_L) Z - \lambda w]$$

where the Nusselt number for heat transfer is given by

$$Nu_h = 2 + 0.6 (Pr)^{1/3} (Re)^{1/2}$$

Considering the temperature difference $(\bar{T}_g - \bar{T}_L)$ and the correction factor for simultaneous heat and mass transfer Z to be constant, we may obtain the following equation

$$\frac{\bar{c}_p \bar{T}_L'}{\bar{\lambda}} - \frac{\bar{M}}{\bar{w}} \frac{d}{dt} \left(\frac{\bar{T}_L'}{\bar{T}_L} \right) - \beta b \left(\frac{\bar{T}_L'}{\bar{T}_L} \right) = (1 - \beta) \frac{\bar{P}_c'}{\bar{P}_c} \quad (A-4)$$

Now, Heidmann and Wieber solved the system of equations (A-1) through (A-4) assuming \bar{M}/\bar{w} was time independent. Therefore, they had only to solve a simple system of linear differential equations with constant coefficients and since p_c' was sinusoidal, trigonometric functions were obtained as solutions. Actually, since \bar{M}/\bar{w} is time-dependent, the solutions are not merely trigonometric functions but are slightly more complex.

Under the assumption that $Nu_m = k_1 \sqrt{rp_c}$ with k_1 a constant, one can show that

$$\bar{w} = kr^{3/2} \tag{A-5}$$

where

$$k = 2 \pi \bar{\rho} \bar{D} \sqrt{\bar{p}_c} \left(\ln \frac{\bar{p}_c}{\bar{p}_c - \bar{p}_L} \right) k_1$$

Noting that

$$\bar{M} = (4/3) \pi \bar{\rho}_L r^3$$

and

$$\bar{w} = - \frac{d\bar{M}}{dt}$$

one can show further that

$$r^{3/2} = r_o^{3/2} - (3k/8 \pi \bar{\rho}_L) t \tag{A-6}$$

and

$$\bar{M}/\bar{w} = (a - t) / 2 \tag{A-7}$$

where $a = 8 \pi \bar{\rho}_L r_o^{3/2} / 3k$ and the subscript zero denotes conditions at the initial time.

Equations (A-1) through (A-4) and (A-7) may be combined to give the following equations

$$\frac{d}{dt} [(a - t) \frac{M'}{M}] = (2\beta - 1) \frac{p_c'}{\bar{p}_c} - 2\beta b \frac{T_L'}{\bar{T}_L}$$

and

$$(a - t) \frac{d}{dt} \left(\frac{T_L'}{\bar{T}_L} \right) - \frac{2\bar{\lambda}}{c_p \bar{T}_L} \beta b \left(\frac{T_L'}{\bar{T}_L} \right) = \frac{2\bar{\lambda}}{c_p \bar{T}_L} (1 - \beta) \frac{p_c'}{\bar{p}_c}$$

With $p_c' / \bar{p}_c = \cos(\omega t + \phi)$ the above equations may be integrated to obtain

$$\frac{M'}{M} = \left(\frac{2\beta - 1}{\omega} \right) \frac{\sin(\omega t + \phi)}{a - t} - \frac{2\beta b}{a - t} \int \frac{T_L'}{\bar{T}_L} dt' \quad (A-8)$$

$$\frac{T_L'}{\bar{T}_L} = \frac{2\bar{\lambda}}{c_p \bar{T}_L} (1 - \beta) (a - t)^{-B} \int \frac{\cos(\omega t' + \phi)}{(a - t')^{1-B}} dt' \quad (A-9)$$

where $B = 2\bar{\lambda}\beta b / c_p \bar{T}_L$. So now it remains to evaluate the integrals appearing above.

In Eq. (A-9) the denominator of the integrand and the factor before the integral are expanded as a power series in t . Then integration by parts yields

$$\frac{T_L'}{\bar{T}_L} = \frac{2\bar{\lambda}}{c_p \bar{T}_L} (1 - \beta) \left\{ \sin(\omega t + \phi) \left[\mu_0 + \mu_1 \left(\frac{t}{a}\right) + \mu_2 \left(\frac{t}{a}\right)^2 + \dots \right] + \cos(\omega t + \phi) \left[\nu_0 + \nu_1 \left(\frac{t}{a}\right) + \nu_2 \left(\frac{t}{a}\right)^2 + \dots \right] \right\} \quad (A-10)$$

where

$$\mu_0 = \frac{1}{\omega a} - \frac{2c_2}{(\omega a)^2} + \frac{4 \cdot 3 \cdot 2}{(\omega a)^3} c_4 + \dots$$

$$\mu_1 = B\mu_0 + \frac{c_1}{(\omega a)} - \frac{3 \cdot 2 c_3}{(\omega a)^2} + \frac{5 \cdot 4 \cdot 3 \cdot 2 c_5}{(\omega a)^3} + \dots$$

$$\mu_2 = \frac{B(B+1)}{2!} \mu_0 + B(\mu_1 - \mu_0) + \frac{c_2}{\omega a} - \frac{4 \cdot 3 \cdot c_4}{(\omega a)^2} + \frac{6 \cdot 5 \cdot 4 \cdot 3 c_6}{(\omega a)^3} + \dots$$

$$v_0 = \frac{c_1}{(\omega a)^2} - \frac{3 \cdot 2 c_3}{(\omega a)^3} + \frac{5 \cdot 4 \cdot 3 \cdot 2 c_5}{(\omega a)^5} + \dots$$

$$v_1 = B v_0 + \frac{2 c_2}{(\omega a)^2} - \frac{4 \cdot 3 \cdot 2 c_4}{(\omega a)^3} + \frac{6 \cdot 5 \cdot 4 \cdot 3 c_6}{(\omega a)^4} + \dots$$

$$v_2 = \frac{B(B+1)}{2!} \mu_0 + B(v_1 - B v_0) + \frac{3 c_3}{(\omega a)^2} - \frac{5 \cdot 4 \cdot 3 c_5}{(\omega a)^3} + \frac{7 \cdot 6 \cdot 5 \cdot 4 c_7}{(\omega a)^4} + \dots$$

with $c_n = (1-B)(2-B)\dots(n-B)/n!$. Of course, the series converges most rapidly for large ωa ; that is, whenever the droplet lifetime is significantly longer than the period of oscillation.

Integrating (A-10) by parts and substituting into (A-8) we find that

$$\begin{aligned} \frac{M'}{\bar{M}} = & \frac{2\beta - 1}{\omega} \frac{\sin(\omega t + \phi)}{a - t} \\ & + \frac{4\beta b^-}{\bar{c}_p \bar{T}_L} (\beta - 1) \left\{ \left(\frac{v_0}{\omega} + \frac{\mu_1}{a\omega^2} - \frac{2v_2}{a^2\omega^3} \right) \right. \\ & + \left. \left(\frac{v_1}{\omega} + \frac{2\mu_2}{a\omega^2} \right) \frac{t}{a} + \frac{2v_2}{\omega} \left(\frac{t}{a} \right)^2 + o\left(\frac{t}{a} \right)^3 \right\} \frac{\sin(\omega t + \phi)}{a - t} \\ & + \frac{4\beta b^-}{\bar{c}_p \bar{T}_L} (\beta - 1) \left\{ \left(\frac{v_1}{a\omega^2} - \frac{\mu_0}{\omega} + \frac{2\mu_2}{a^2\omega^2} \right) \right. \\ & + \left. \left(\frac{2v_2}{a\omega^2} - \frac{\mu_1}{\omega} \right) \frac{t}{a} - \frac{2\mu_2}{\omega} \left(\frac{t}{a} \right)^2 + o\left(\frac{t}{a} \right)^3 \right\} \frac{\cos(\omega t + \phi)}{a - t} \end{aligned} \tag{A-11}$$

Now combining (A-1), (A-5), (A-6), and (A-11), the perturbation in the vaporization rate is found to be the following

$$\begin{aligned}
 w' = & \frac{3k^2}{8\pi\bar{\rho}_e} \left[(\beta - \frac{1}{2}) \left\{ \frac{\sin(\omega t + \phi)}{\omega} - (a-t) \cos(\omega t + \phi) \right\} \right. \\
 & + \frac{2\beta b \bar{\lambda}}{c_p \bar{T}_L} (\beta - 1) \left\{ \left(\frac{v_0}{\omega} + \frac{\mu_1}{a\omega^2} - \frac{2v_2}{a^2\omega^3} - a\mu_0 \right) \right. \\
 & + \left(\frac{v_1}{\omega} + \frac{2\mu_2}{a\omega^2} + a(\mu_0 - \mu_1) \frac{t}{a} + \left(\frac{2v_2}{\omega} + (\mu_1 - \mu_2) a \right) \left(\frac{t}{a} \right)^2 \right. \\
 & \left. \left. + 0 \left(\frac{t}{a} \right)^3 \right\} \sin(\omega t + \phi) + \frac{2\beta b \bar{\lambda}}{c_p \bar{T}_L} (\beta - 1) \left\{ \left(\frac{v_1}{a\omega^2} - \frac{\mu_0}{\omega} \right) \right. \right. \\
 & + \frac{2\mu_2}{a^2\omega^2} - a v_0 \left. \left. + \left(\frac{2v_2}{a\omega^2} - \frac{\mu_1}{\omega} + (v_0 - v_1) a \right) \frac{t}{a} - \left(\frac{2\mu_2}{\omega} \right) \right. \right. \\
 & \left. \left. + (v_2 - v_1) a \left(\frac{t}{a} \right)^2 + 0 \left(\frac{t}{a} \right)^3 \right\} \cos(\omega t + \phi) \right] \tag{A-12}
 \end{aligned}$$

So (A-12) shows that the vaporization rate perturbation is not periodic even though the pressure and temperature in the ambient gas are periodic. This implies that the droplet lifetime changes under oscillatory conditions. Equations (A-3) and (A-10) indicate that droplet temperature and vapor pressure are not periodic either. In order to include all members in an array of droplets we must allow the phase ϕ to vary[#] between 0 and 2π . Therefore, integration over the ϕ - dimension shows that the average droplet lifetime for an array should not change under oscillatory conditions.

A quantity of interest for combustion stability studies is the response factor defined for a single droplet as follows:

$$N_1 = \frac{\int_0^T w' \frac{p_c'}{p_c} dt}{\int_0^T \left(\frac{p_c'}{p_c} \right)^2 dt}$$

[#] At the instant $t=0$ when the droplet of radius r_0 is introduced, the pressure oscillation could be at any phase.

where T is the period of the oscillation. In order to obtain an average for the droplet over the array; N_1 must be integrated over ϕ and divided by 2π . Furthermore, to obtain the nondimensional quantity which is useful in combustion stability analyses, the last result should be divided by the average burning rate of a droplet over its lifetime (for non-oscillatory conditions). Therefore we have

$$N = \frac{\frac{1}{2\pi} \int_0^{2\pi} N_1 d\phi}{\int_0^a \frac{\bar{w}}{a} dt}$$

which by use of Eq. (A-12) results in the following

$$\begin{aligned} N = & (1-2\beta) \left(1 - \frac{T}{2a}\right) + \frac{4\beta b \bar{\lambda}}{\bar{c}_p \bar{T}_L} (\beta-1) \left\{ \left(\frac{v_1}{(a\omega)^2} - \frac{\mu_0}{a\omega}\right) \right. \\ & + \frac{2\mu_2}{a^3\omega^2} - v_0 \left. \right\} + \left(\frac{2v_2}{(a\omega)^2} - \frac{\mu_1}{a\omega} + v_0 - v_1\right) \frac{T}{2a} \\ & + \left(\frac{2\mu_2}{a\omega} - v_1 + v_2\right) (1/3) \left(\frac{T}{a}\right)^2 + 0\left(\frac{T}{a}\right)^3 \left. \right\} \end{aligned}$$

This last result is substantially different from that obtained by Heidmann so it is seen that the variability of the coefficients in the differential equation should not be neglected.

NOMENCLATURE

a	droplet lifetime
b	proportionality constant defined in Equation (A-3)
B	constant defined after Equation (A-9)
c_n	constants defined after Equation (A-10)
c_p	specific heat at constant pressure
D	molecular diffusion coefficient
k	constant defined after Equation (A-5)
k_1	constant defined before Equation (A-5)
M	droplet mass
N	response factor defined in equations
N_1	response factor defined in equations
Nu_h	Nusselt number for heat transfer
Nu_m	Nusselt number for mass transfer
p	pressure
Pr	Prandtl number
r	droplet radius
r_o	initial droplet radius
Re	Reynolds number
Sc	Schmidt number
t	time
T	temperature
T	period of oscillation
w	mass vaporization rate
Z	correction factor for heat transfer
β	quantity defined after Equation (A-2)
λ	latent heat of vaporization
μ, ν	constants defined after Equation (A-10)
ρ	gas density
ρ_L	liquid density

Subscripts:

- c combustion chamber conditions
- L liquid condition

Superscripts:

- bar denotes mean-flow quantity
- prime indicates perturbation quantity

APPENDIX B

DISCUSSION OF NONLINEAR QUASI-STEADY DROPLET VAPORIZATION ANALYSIS

A theory for describing the rocket combustion process has been derived by Priem and Heidmann¹⁰. In that theory, the evaporation of the propellant drop is assumed to be the rate-controlling combustion process. The histories of the droplet, i.e., the variations of drop size, drop temperature, drop velocity and combustor gas velocity, are considered. By using this model, Heidmann and Wieber^{9,11} calculate drop vaporization in a rocket combustor with superimposed acoustic oscillations.

In their analysis, the acoustic field contains pressure, temperature and velocity perturbations and affects the drop dynamics, heat and mass transfer processes. Under certain conditions, the assumed rate-controlling process exhibits dynamic behavior which may cause instability in the combustor. Detailed discussions on frequency response and boundary conditions are presented in their works.

However, a more strict analytical study of this problem is necessary. In the linear analysis by Heidmann and Wieber, the validity of several assumptions is questionable. For instance, Nu_m and Nu_h are assumed proportional to $(r P_c)^{1/2}$ with no variability due to velocity where Nu_m and Nu_h are the Nusselt numbers of mass transfer and of heat transfer respectively, r is the drop radius and P_c is the chamber pressure. This is acceptable if the Reynolds number is large compared to unity and if the relative velocity between gas and drop is constant. Furthermore, the temperature difference between gas and droplet $(T_g - T_L)$ and the correction factor for simultaneous heat and mass transfer Z are assumed constant but actually do vary. By making use of the vaporization model of Priem and Heidmann a quasi-steady linear analysis of a single drop vaporization is underway at Princeton. All equations derived for the steady case are assumed to be valid in the unsteady case and a set of linear equations for perturbations in the vaporization process is developed. It is noticed that all perturbation quantities are not equally important; comparison of order of magnitude of each term would hopefully simplify the equations and effort is being made to form analytical expressions.

Two different cases will be studied in the linear analysis:

1) Transverse mode: With the assumption of small perturbations, no velocity effect appears in the first order analysis and only pressure perturbation affects the evaporation rate. Because all perturbed terms appear in ratios with the steady-state quantities, it should be noted that the velocity perturbation terms cannot be neglected in comparison with other terms in the region where the difference between the mean drop and gas velocities is small. Nevertheless, if the region is small and contributes very little to the whole process the assumption remains reasonable. 2) Longitudinal mode: Both pressure and velocity perturbations enter into the problem and a more complicated analysis is expected. Proper assumptions should be made as in the transverse analysis.

Further, a nonlinear analysis will be conducted. In the work of Heidmann and Wieber^{9,11} droplet evaporation was considered in the presence of acoustic oscillations of the combustion gas. The validity of using such a first order acoustic field is questionable for the nonlinear case. The reason is that whenever higher order equations are being studied, the associated higher order boundary conditions should be considered too. In this problem, the oscillation of the gas in the chamber is thought to provide a boundary condition for the infinity of the droplet field. So a more correct analytical study up to second order will be developed.

Two points will be clarified by this study. The first point concerns the initial temperature of the droplet. As reported in Reference 11, heating of the drop from an initial temperature apparently introduces an effect that results in the increase of the peak value of the response factor. Second, the importance of the double-frequency component as shown in Figure 3 of Reference 11 will be determined. Higher order evaporation rate affects the pressure and velocity perturbations and also gives higher order effects for the transverse case.

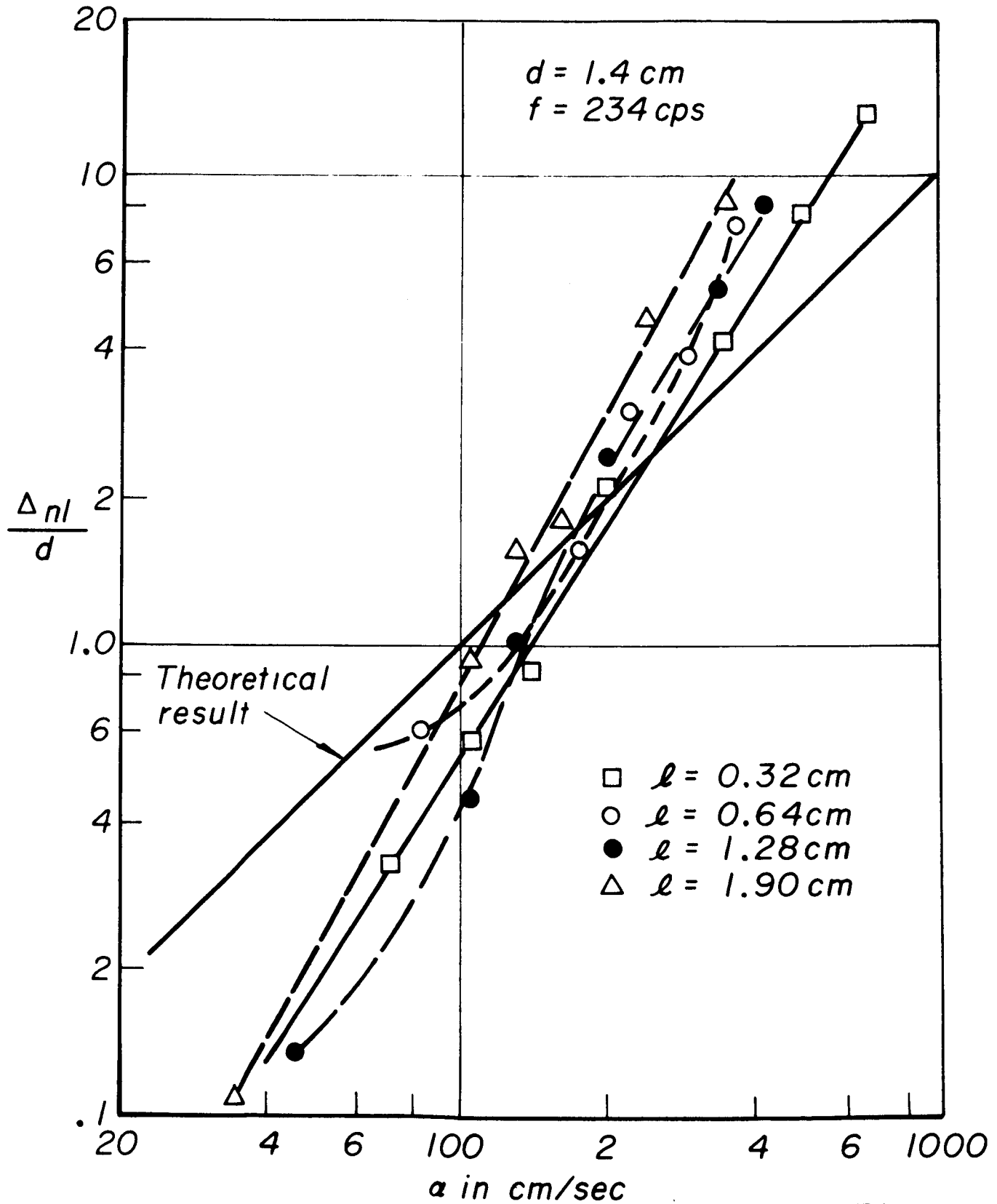
REFERENCES

1. Sirignano, W. A. and Crocco, L., "A Shock Wave Model of Unstable Rocket Combustors", AIAA Journal, Vol. 2, No. 7, July 1964, Pg. 1285.
2. Sirignano, W. A., "A Theoretical Study of Nonlinear Combustion Instability: Longitudinal Mode", Technical Report No. 677, Department of Aerospace and Mechanical Sciences, Princeton University, March 1964, (Ph.D. Thesis).
3. Crocco, L., Harrje, D. T., Sirignano, W. A., et al, "Nonlinear Aspects of Combustion Instability in Liquid Propellant Rocket Motors", (Fourth Yearly Progress Report), Department of Aerospace and Mechanical Sciences Report 553d, June 1, 1964.
4. Zinn, B. T., "A Theoretical Study of Nonlinear Transverse Combustion Instability in Liquid Propellant Rocket Motors", Technical Report No. 732, Department of Aerospace and Mechanical Sciences, Princeton University, May 1966 (Ph.D. Thesis).
5. Strahle, W. C., and Crocco, L., "Analytical Investigation of Several Mechanisms of Combustion Instability", (Bulletin of the Fifth Liquid Propulsion Symposium, 13-15, November, 1963), Chemical Propulsion Information Agency.
6. Strahle, W. C., "A Theoretical Study of Unsteady Droplet Burning: Transients and Periodic Solutions", Princeton University Aeronautical Engineering Laboratory Report No. 671, December 1963. (Ph.D. Thesis).
7. Strahle, W. C., "Periodic Solution to a Convective Droplet Burning Problem: The Stagnation Point", 10th Symposium, (International) on Combustion, Combustion Institute, Pittsburgh, Penn., June 1965, pg. 1315.
8. Strahle, W. C., "Unsteady Laminar Jet Flame at Large Frequencies of Oscillation", AIAA Journal, Vol. 3, No. 5, May 1965, pg. 957.
9. Heidmann, M. F. and Wieber, P. R.; "Analysis of n-Heptane Vaporization in Unstable Combustor with Traveling Transverse Oscillations", NASA TND-3424, 1966.
10. Priem, R. J. and Heidmann, M. F.; "Propellant Vaporization as a Design Criterion for Rocket-Engine Combustion Chambers", NASA TR R-67, 1960.
11. Heidmann, M. F. and Wieber, P. R.; "Analysis of Frequency Response Characteristics of Propellant Vaporization", NASA TM X-5219J, 1966.

12. Crocco, L., and Cheng, S. I., Theory of Combustion Instability in Liquid Propellant Rocket Motors, AGARD Monograph No. 8, Butterworths Scientific Pub., Ltd., London, 1956.
13. Ingard, U., "On the Theory and Design of Acoustic Resonators", J. Acoustical Soc. Amer., Vol. 25, No. 6, Nov. 1953, pp. 1037-1061.
14. Blackman, A. W., "Effect of Nonlinear Losses on the Design of Absorbers for Combustion Instabilities", ARS Journal, Vol. 30, No. 11, Nov. 1960, pp. 1022-1028.
15. Rayleigh, J. W. S., The Theory of Sound, Vol. II, Dover Publications, p. 172.
16. "A Study of the Suppression of Combustion Oscillations with Mechanical Damping Devices" Report #PWA (Pratt and Whitney) - FR-1330, 28 Nov. 1964
17. Osborn, J. R. and Bonnell, J. M., "Effect of Fuel Composition on High Frequency Oscillations in Rocket Motors Burning Premixed Hydrocarbon Gases and Air", ARS Journal, Vol. 31, No. 10, October 1961, pp. 1397-1401.
18. Reardon, F. H., "An Investigation of Transverse Mode Combustion Instability in Liquid Propellant Rocket Motors", Princeton University Aeronautical Engineering Report No. 550, 1 June 1961 (Ph. D. Thesis)
19. Clayton, R. M. and Rogero, R. S., "Experimental Measurements on a Rotating Detonation-Like Wave Observed During Liquid Rocket Resonant Combustion", Jet Propulsion Laboratory Technical Report No. 32-788, 15 August 1965.
20. Crocco, L., and Harrje, D. T., "Combustion Instability in Liquid Propellant Rocket Motors", (Twenty-Sixth Quarterly Progress Report) - Princeton University Aeronautical Engineering Report No. 216 - Z, 23 February 1959.
21. Crocco, L., Harrje, D. T., Sirignano, W. A. et al, "Nonlinear Aspects of Combustion Instability in Liquid Propellant Rocket Motors", (Fifth Yearly Progress Report), Princeton University Department of Aerospace and Mechanical Sciences Report No. 553e, 1 June 1965.
22. Crocco, L., Harrje, D. T., Lee, D. H., Strahle, W. C., Sirignano, W. A., Bredfeldt, H. R., and Seebaugh, W. R., "Nonlinear Aspects of Combustion Instability in Liquid Rocket Motors", (Third Yearly Progress Report), Princeton University Aeronautical Engineering Report 553c, June 1, 1963.

23. Gartner, E. M., "An Investigation of Vapor Displacement Effects Under Simulated Rocket Chamber Conditions", M.S.E. Thesis, Princeton University, July 1965.
24. Nicholls, J. A., Dabora, E. K., and Ragland, K. W. "A Study of Two Phase Detonation as it Relates to Rocket Motor Combustion Instability" NASA Contractor Report #272, August 1965.
25. Rayleigh, J. W. S., "Instability of Jets", Proc. London Math. Soc., 1878, Vol. 10, pg. 4-13.
26. Schneider, J. M., "The Stability of Electrified Liquid Surfaces", Report #CPRL-2-64, Charged Particle Research Lab., University of Illinois, Mar. 1964.
27. Clark, B. J., "Breakup of a Liquid Jet in a Transverse Flow of Gas", NASA TN D-2424, August 1964.
28. Miesse, C. C., "The Effect of Ambient Pressure Oscillations on the Disintegration and Dispersion of a Liquid Jet", Jet Prop. Vol. 25, #10, pg. 525, October 1955.
29. Reba, I. and Brosilow, C., "Combustion Instability: Liquid Stream and Droplet Behavior; Part III. The Response of Liquid Jets to Large Amplitude Sonic Oscillations". Aero Research Lab. WADC Technical Report 59-720, Sept., 1960.
30. Heidmann, M. F., Priem, R. J., and Humphrey, J. C., "A Study of Sprays Formed by Two Impinging Jets", NACA Technical Note 3835, March 1957.
31. Riebling, R. W., and Powell, W. B., "The Properties of Flowing Sheets Formed by Impingement of Liquid Jets on Curved Surfaces", AIAA preprint 66-610, Presented at the Second Propulsion Joint Specialists Conference, Colorado Springs, Colo., June 13-17, 1966.
32. Hersh, M., "Determinations of Local and Instantaneous Combustion Conditions From Acoustic Measurements in a Rocket Combustor and Comparison with Overall Performance", NASA Technical Note D-1192, March 1962.
33. Sawyer, R. F., "The Homogeneous Gas Phase Kinetics of Reactions in the Hydrazine - Nitrogen Tetroxide Propellant System", Princeton University Department of Aerospace and Mechanical Sciences Technical Report No. 761, 1965, (Ph. D. Thesis)

Theoretical vs experimental results



JP21-24019-66

Figure 1

Tangential mode pk-pk amplitude for various chamber lengths
as measured at the 3-inch station, LOX/ALC, 1x16 injector,
 $P_c = 150$ psi, $F = 1334$ lb., $D = 9$ inches

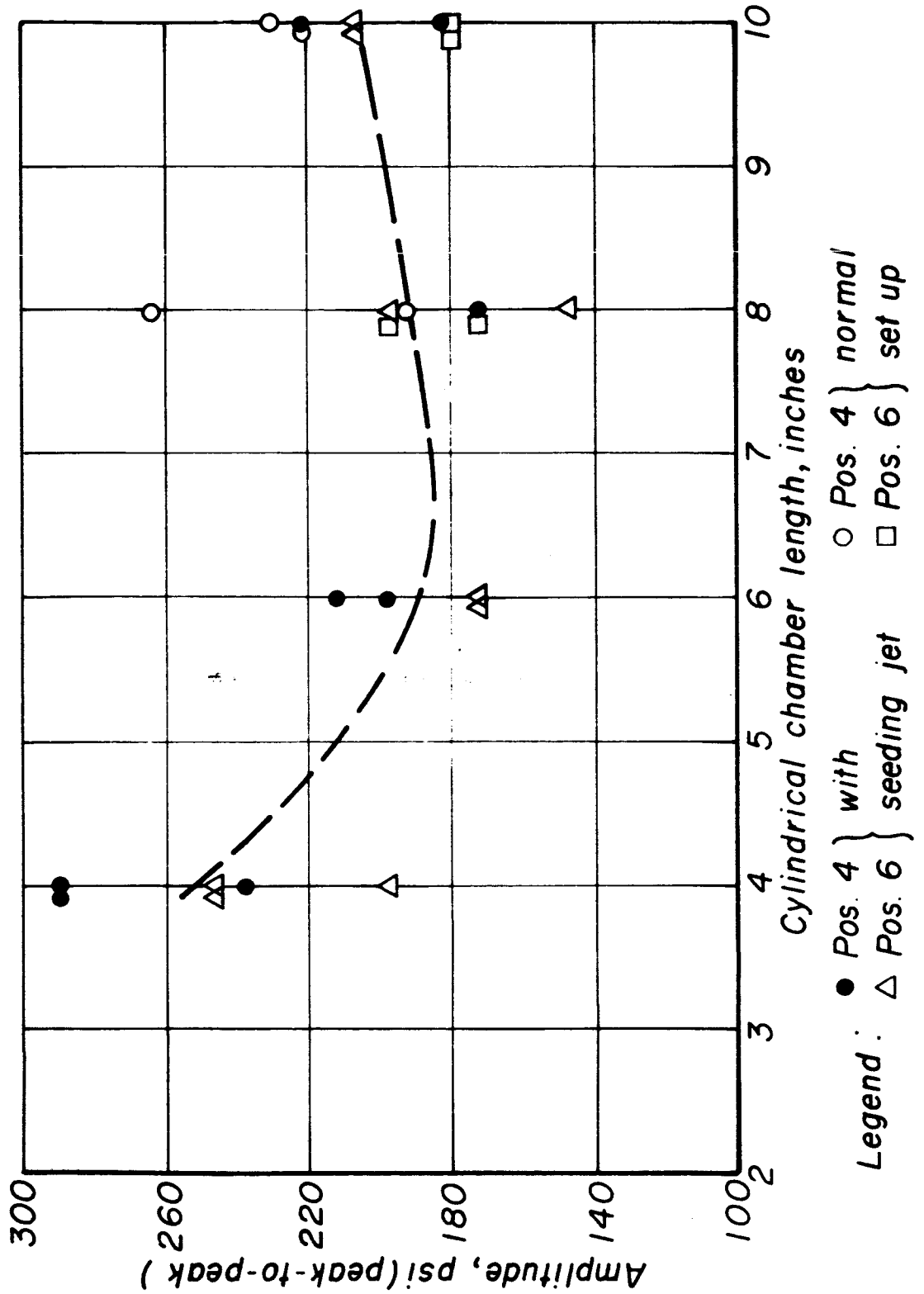


Figure 2

Tangential mode tests on 10 inch length, 9 inch diameter motor showing pk-pk amplitude vs axial position
LOX/ALC, 1x16 injector, $P_c = 150$, $F = 1334$ lb

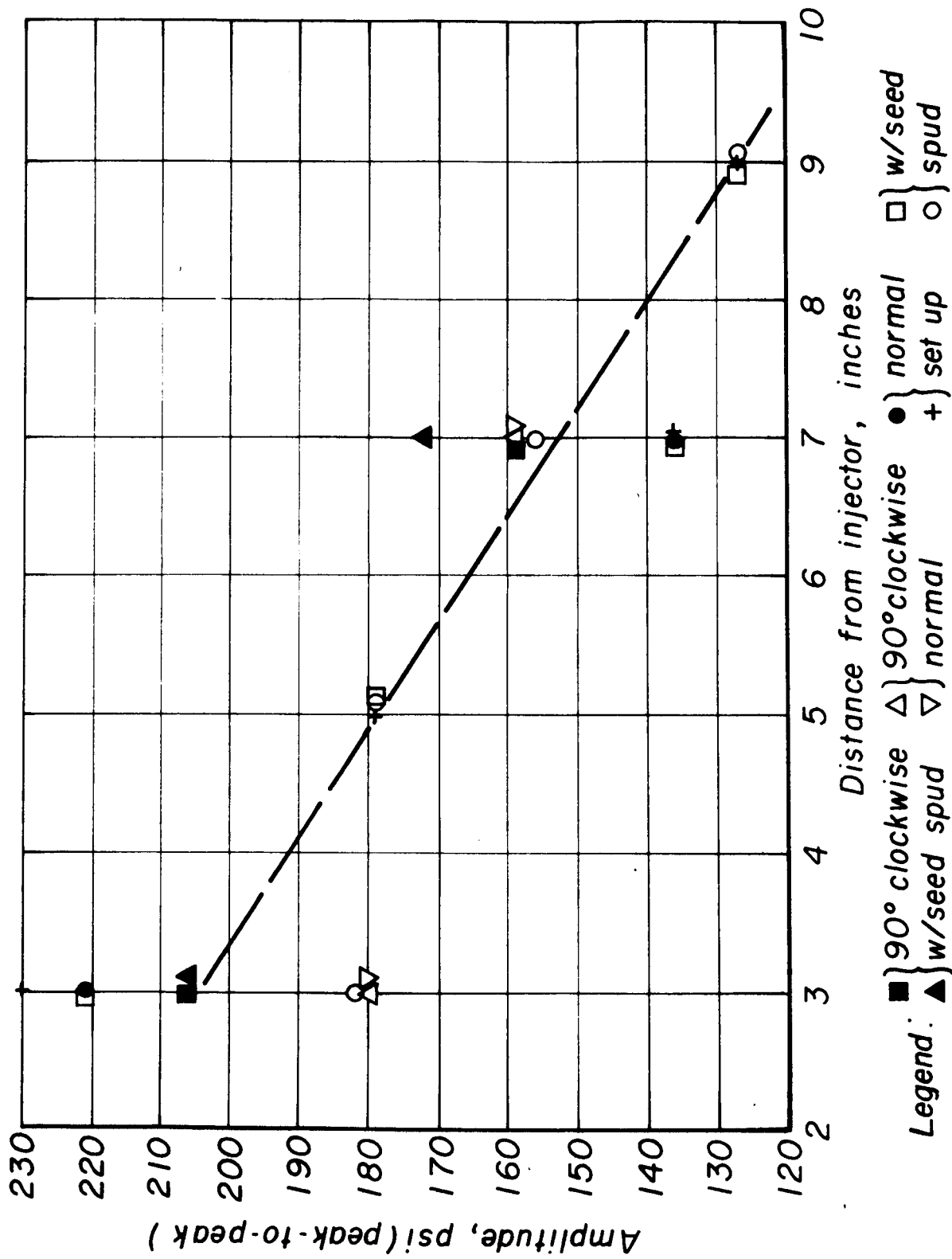
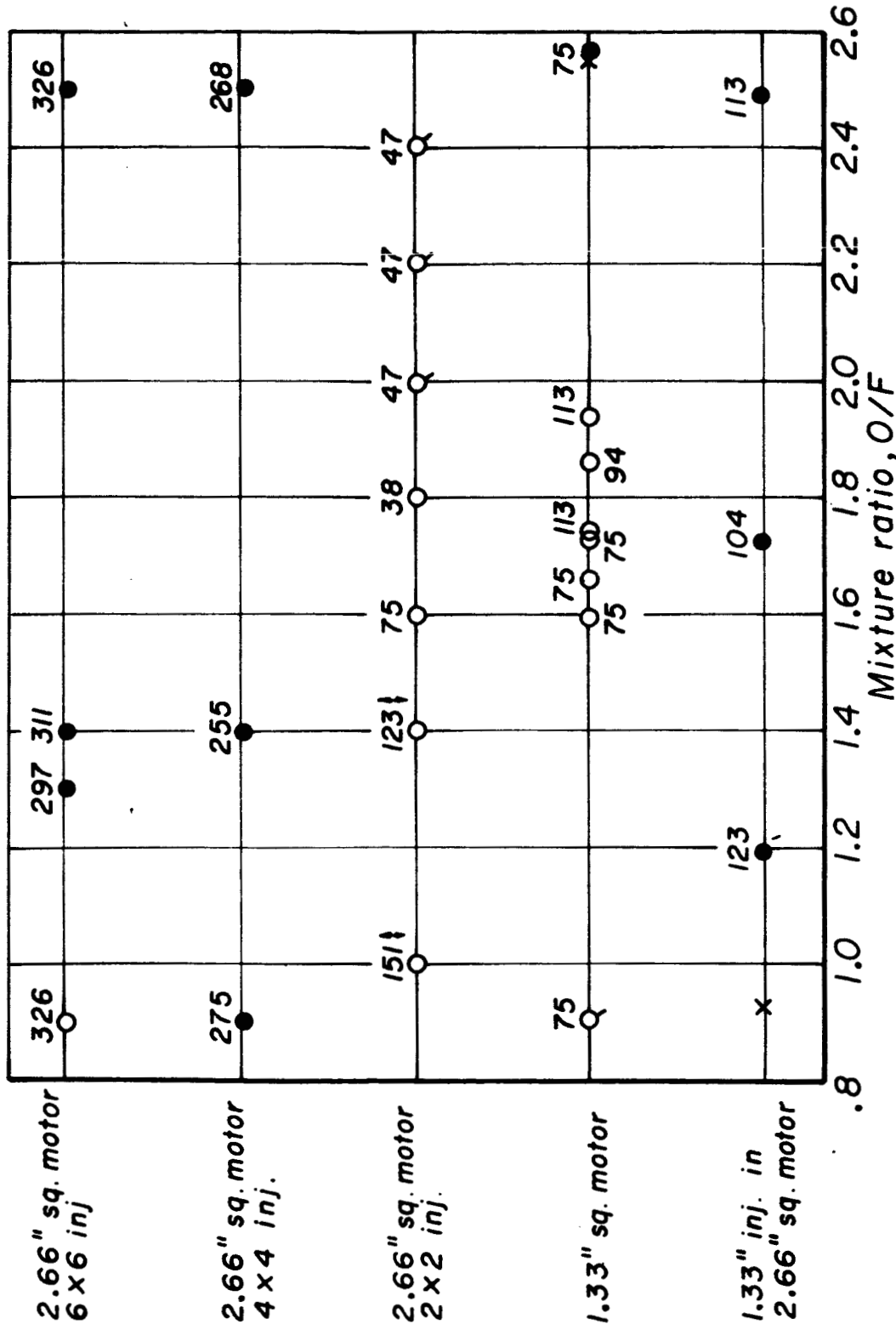


Figure 3

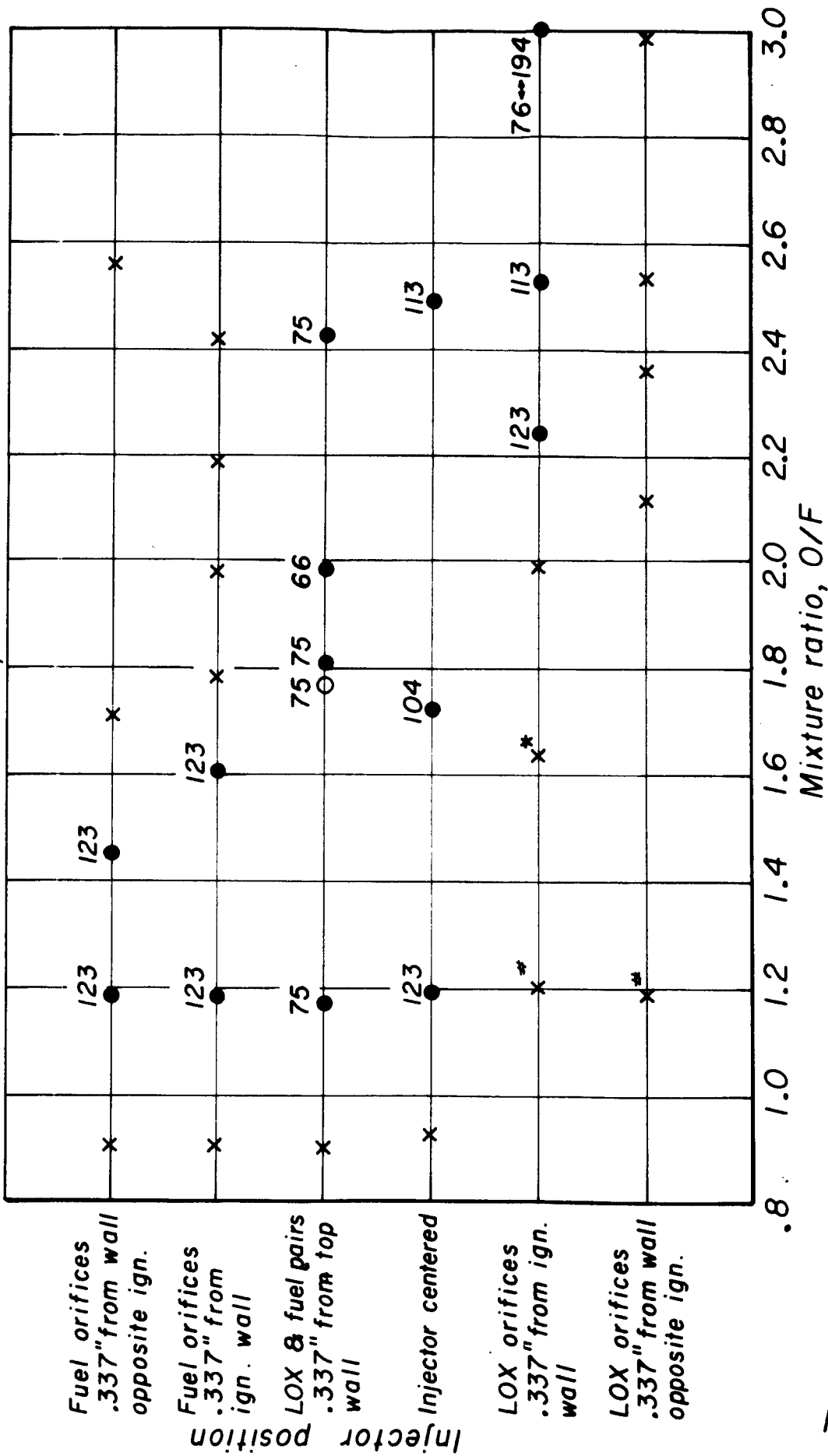
Longitudinal stability limits tests using various type IV injectors.
 Pulsed 15-5K nozzle end, L=24.5", P_c=300psia



Key x = Stable, ● = IL, ○ = Spontaneous IL,
 Q = In & out spontaneous IL

Figure 4

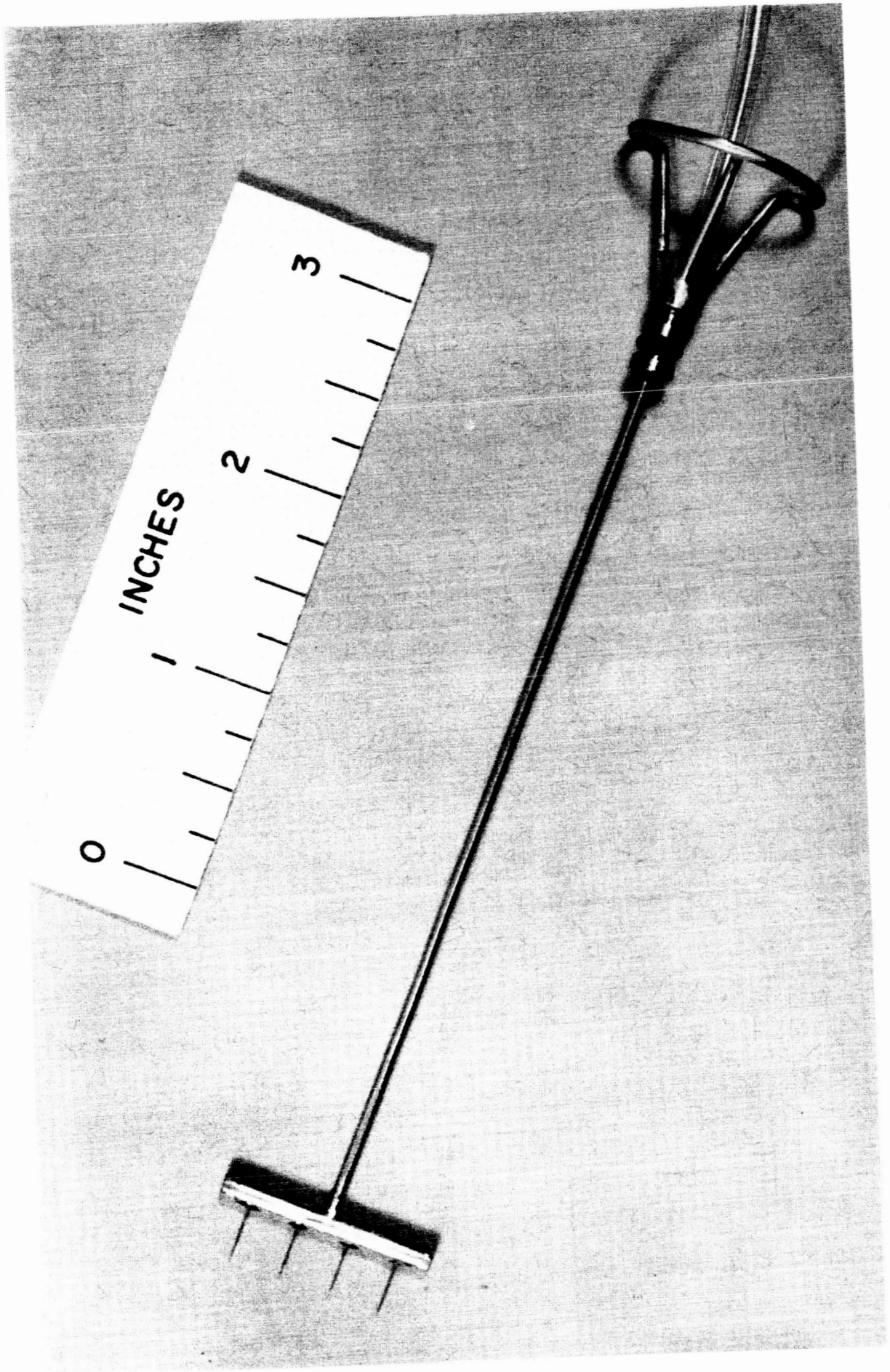
Longitudinal stability limits tests using 1.33" square injector (type IV) on 2.66" square-motor. $P_c = 300$ psia, thrust=200, Pulsed 15-5K at nozzle end, $L = 24.5$



Key x = Stable, ● = IL, ○ = Spontaneous IL
 *Damps ≈ 700 m/sec, # Spontaneous "blip" to ≈ 70psi pk-pk

Figure 5

JP21-P31-66



Droplet generator

Figure 6

Terminal and minimum velocities for Freon 114
and H₂O in nitrogen atmosphere

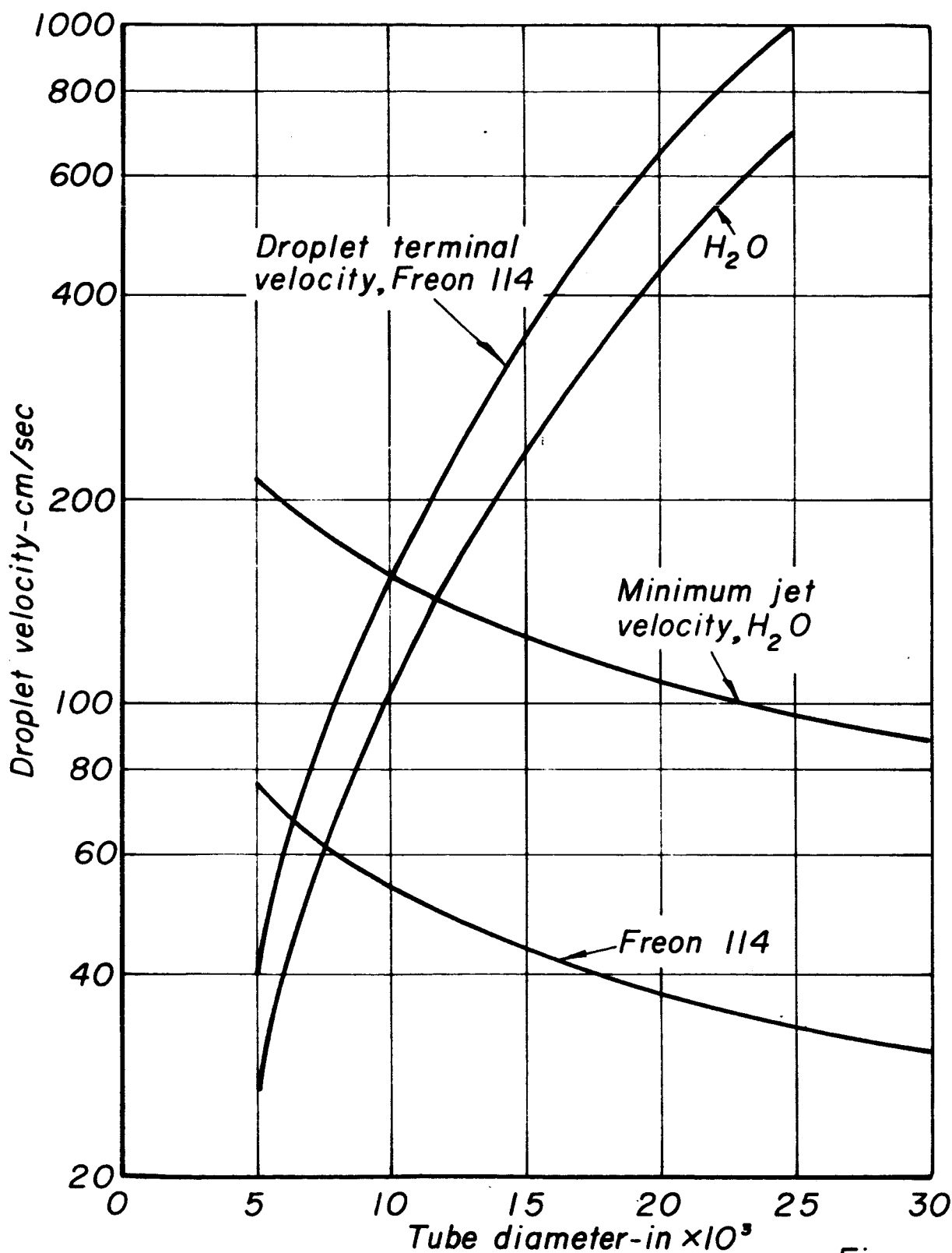
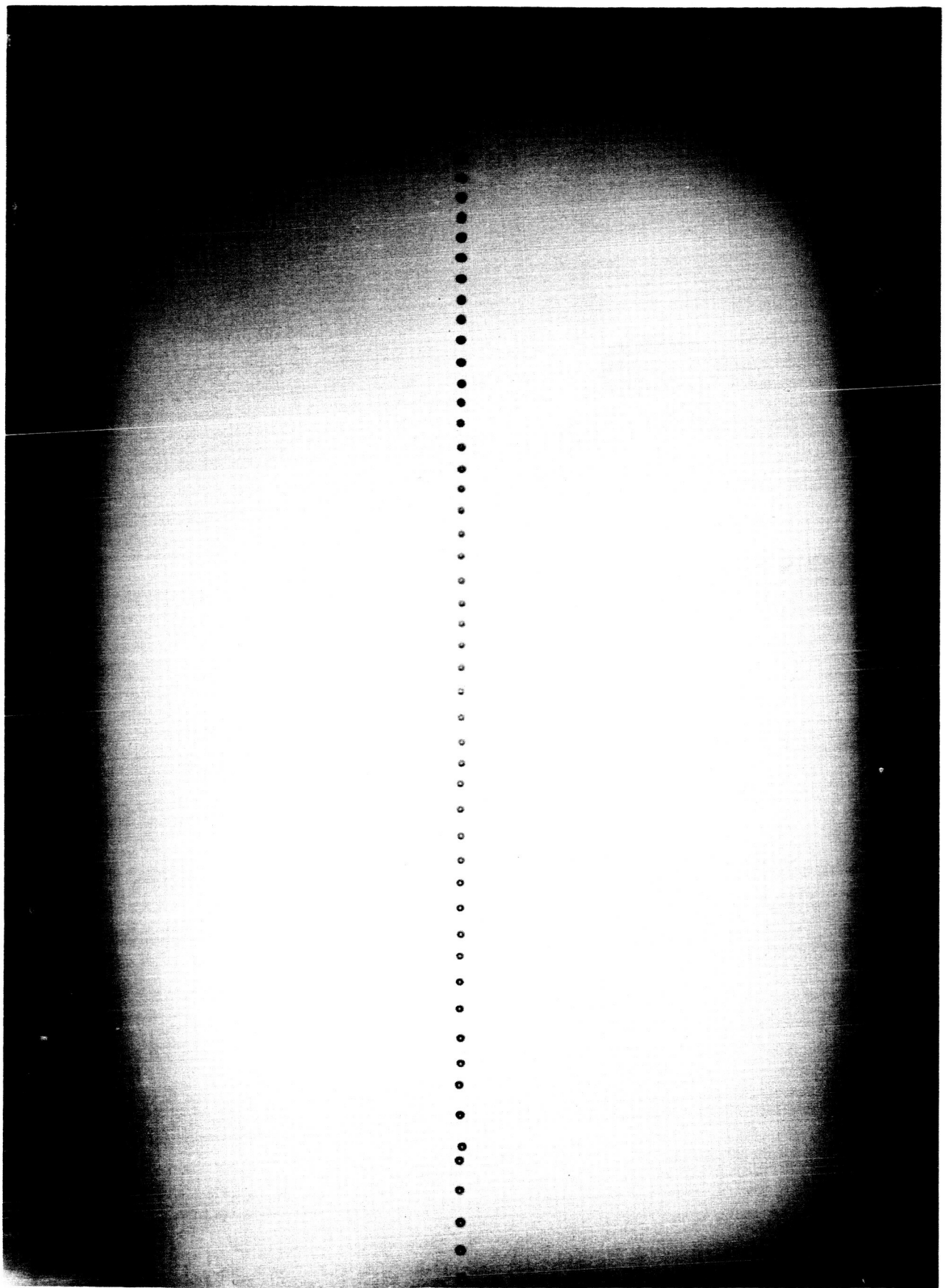


Figure 7

JP21-4117-66

VP21-P30-66



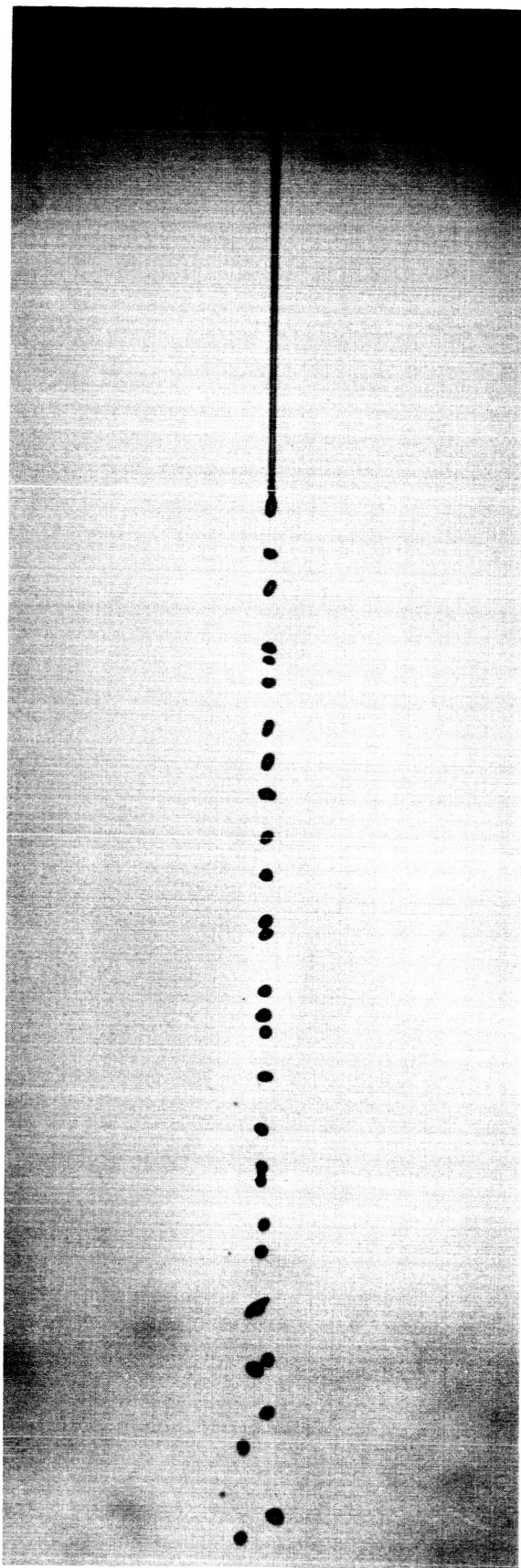
Water

$$f_c = 980 \text{ cps}$$

$$V_{inj} \cong 230 \text{ cm/sec}$$

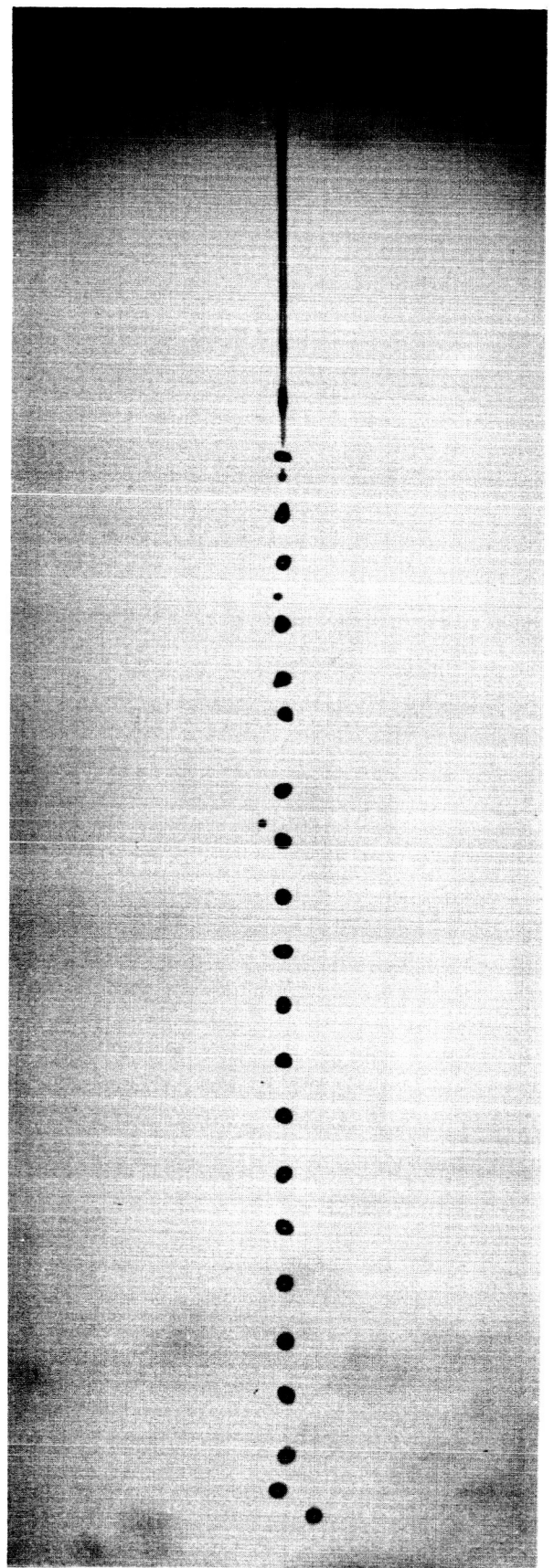
Figure 8

JP21-P28-66



a

Quiescent chamber



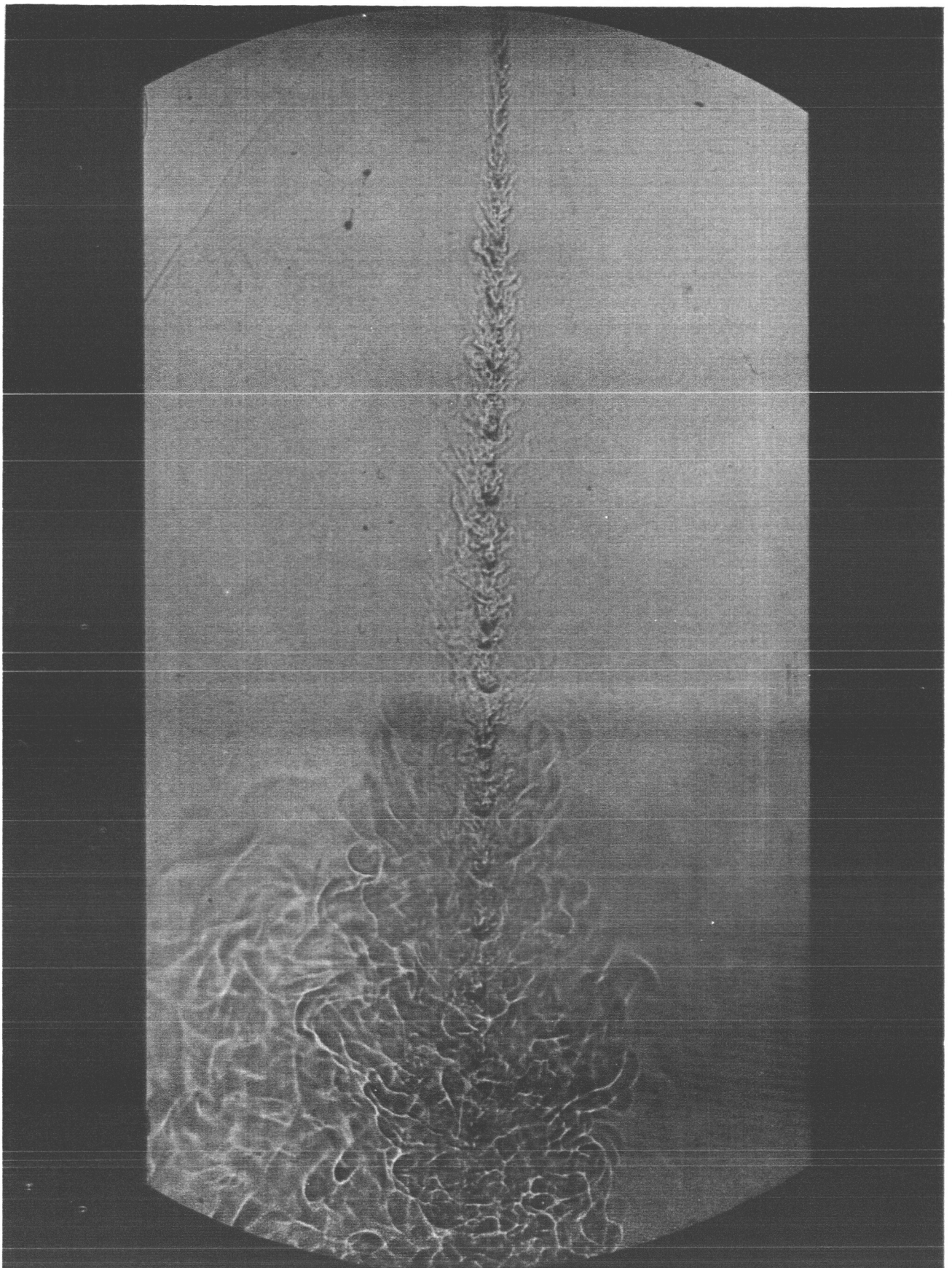
b

Chamber resonated at
890 cps

$V_{inj} \cong 400 \text{ cm/sec}$

Figure 9

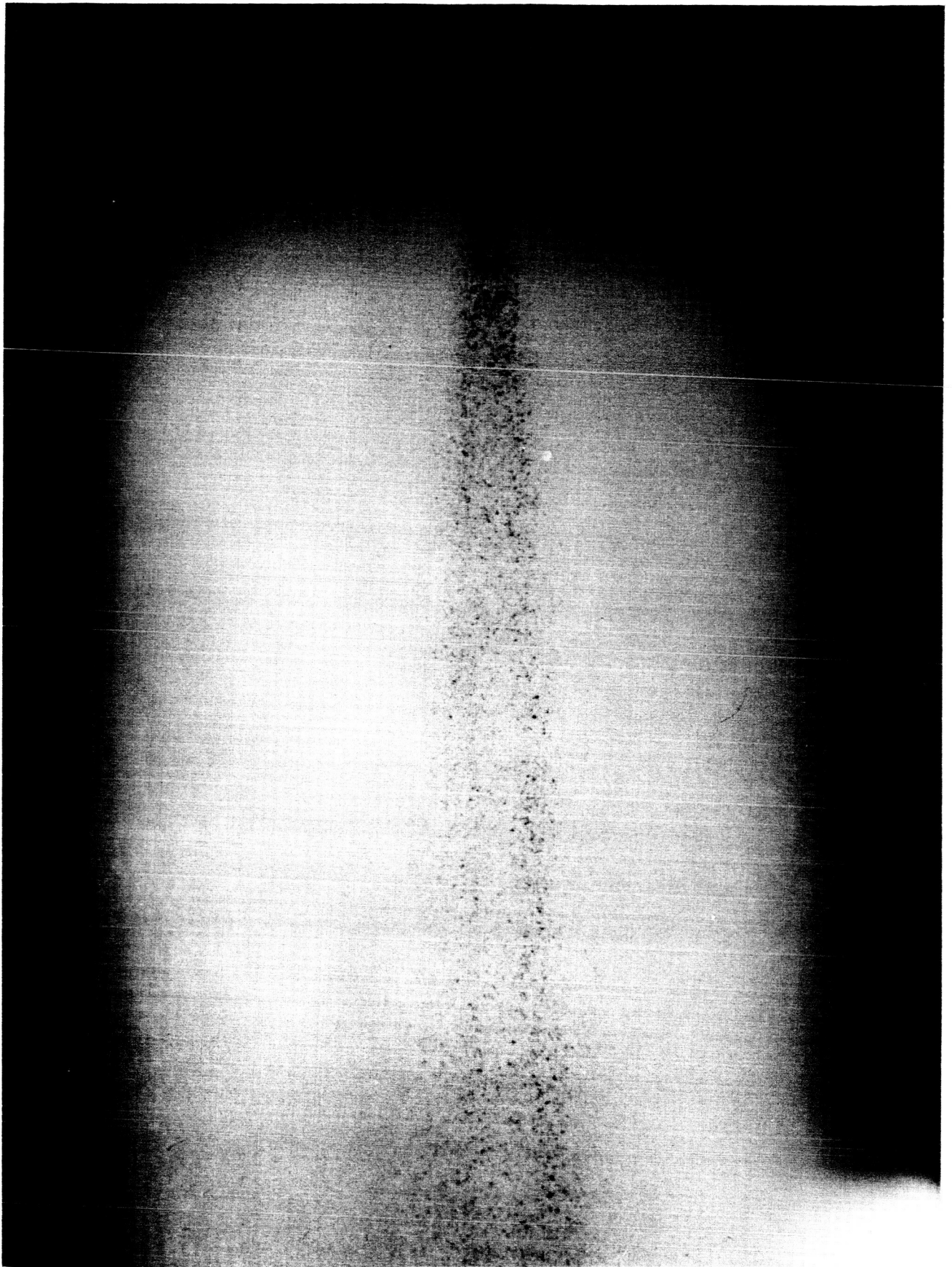
JP21-P27-66



Shadowgraph-vaporizing
Freon 114

Figure 10

JP21-P29-66



Spark photograph
Freon 114, $P_c = 10$ psig

Figure 11

JP21-4106-66

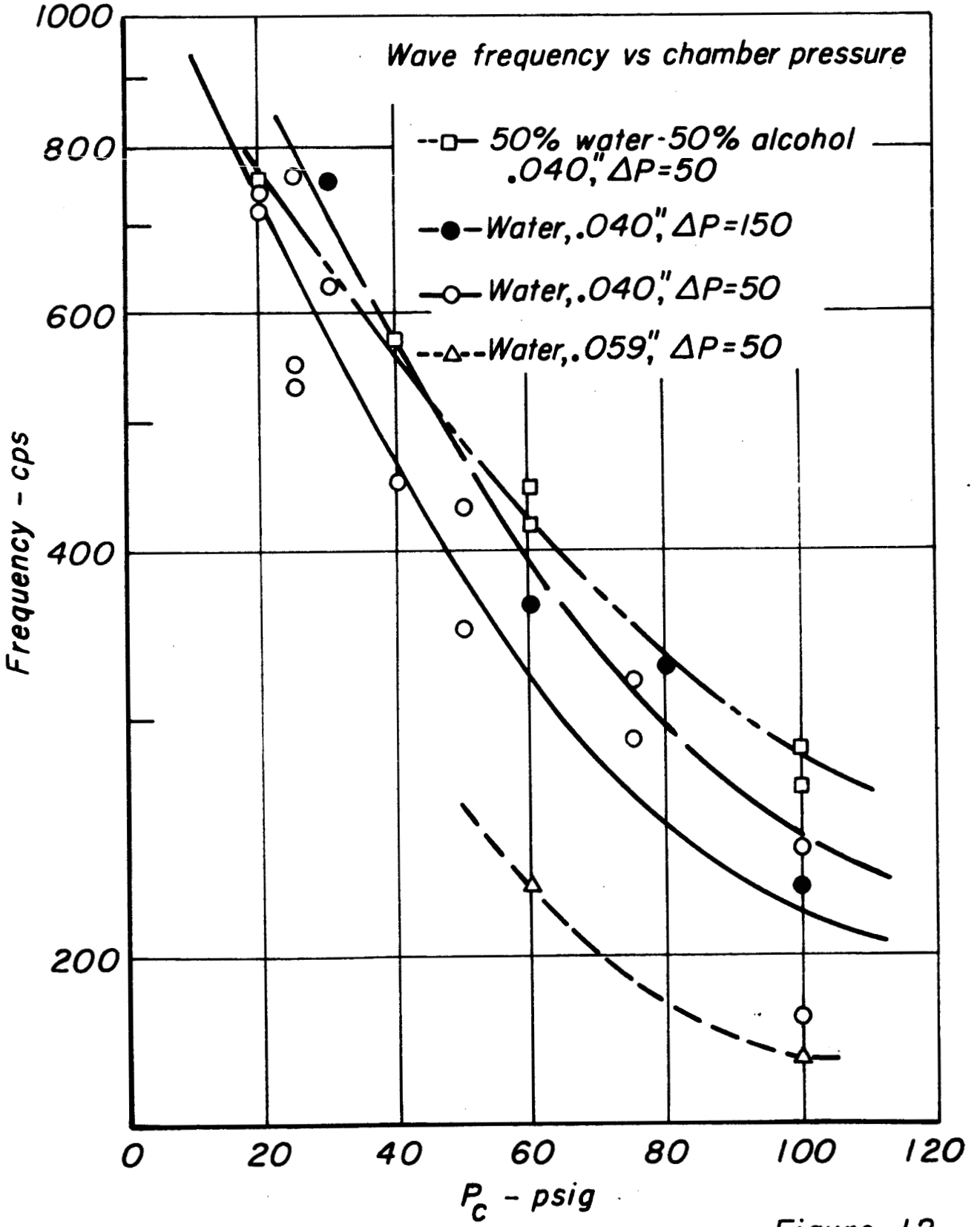


Figure 12

JP21-4107-66

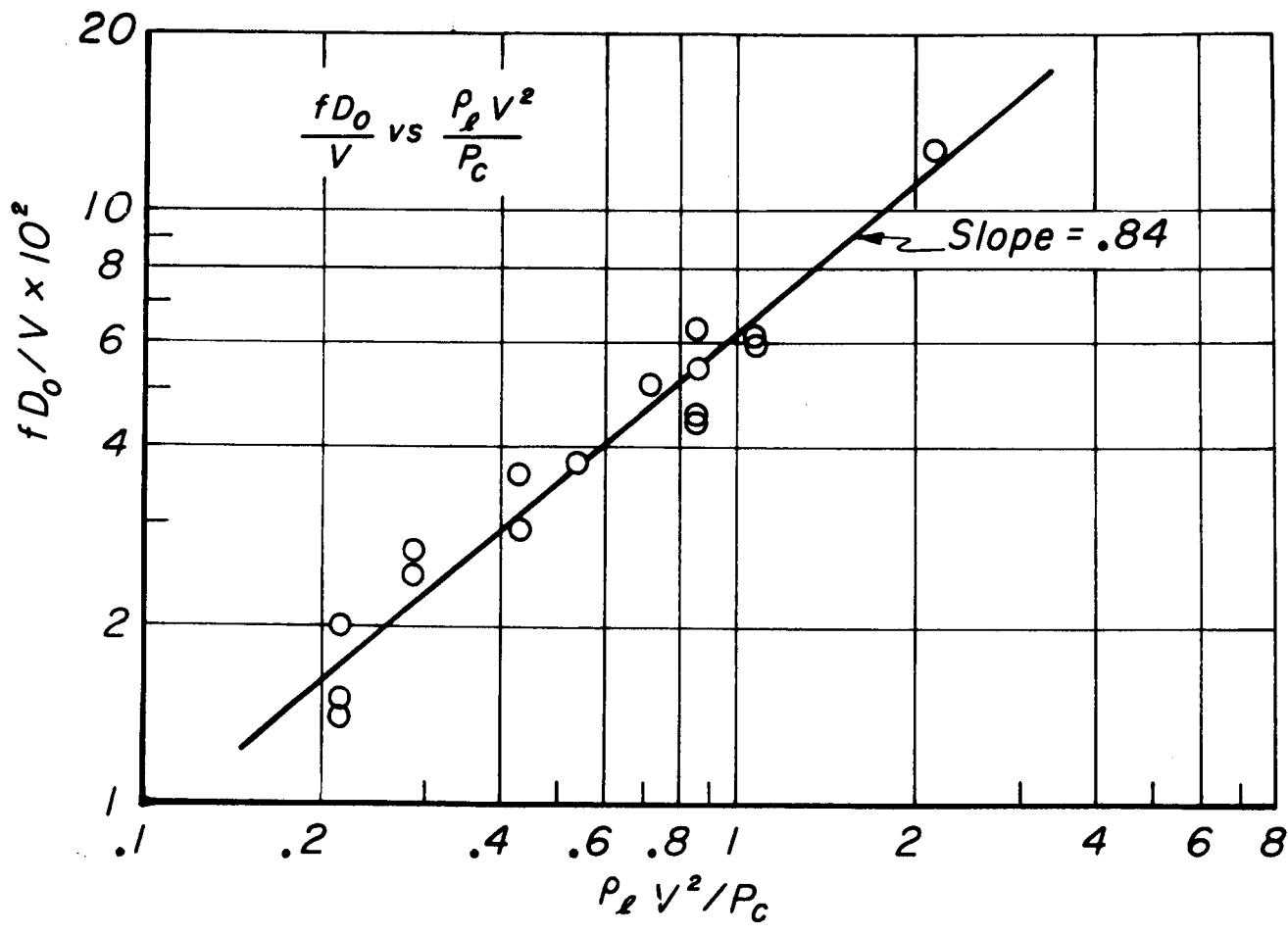


Figure 13

JP21-4108-66

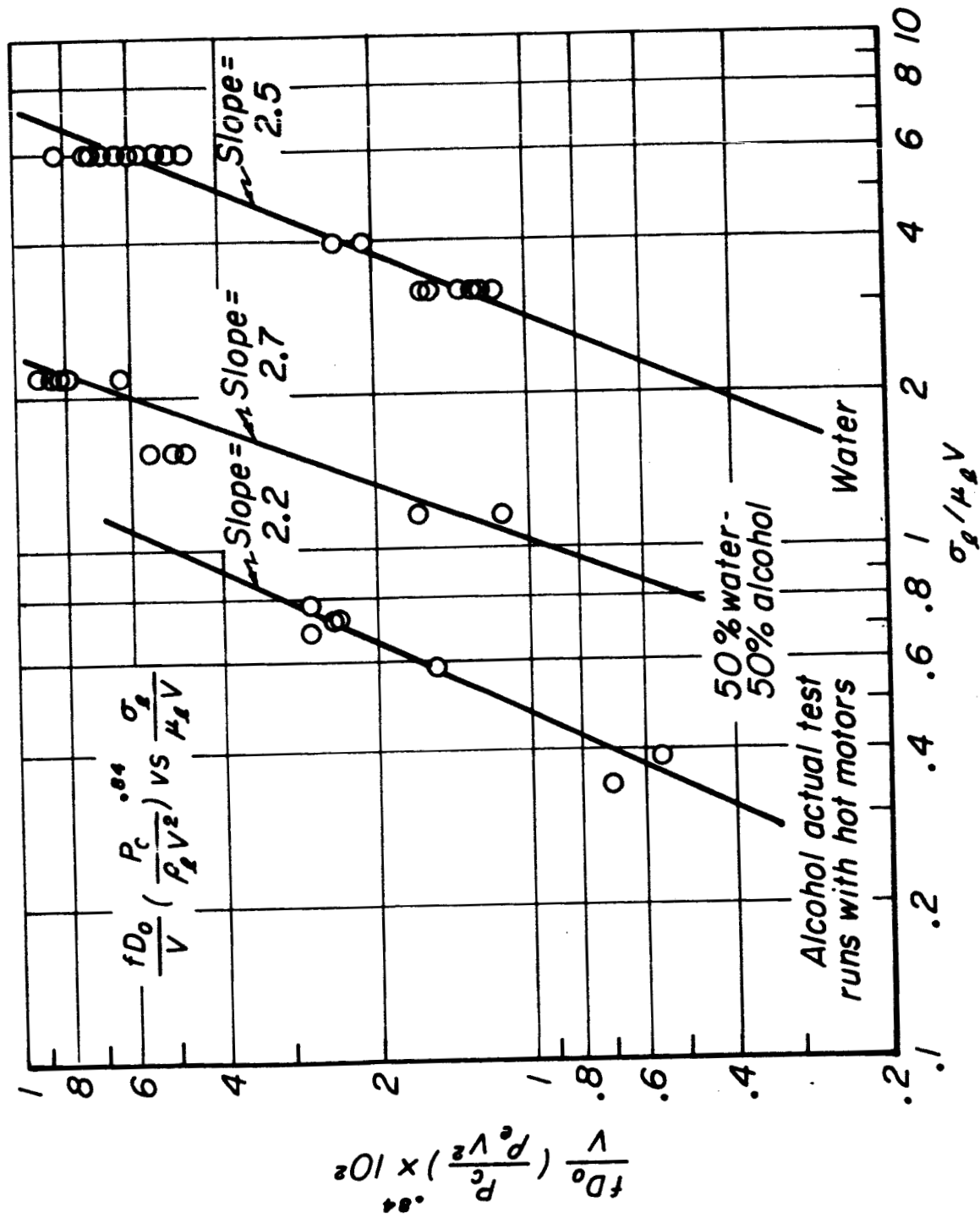


Figure 14

Test firing on transverse stand showing intermediate frequency incidence, $P_c = 134$ psia, $D_c = 9$ ins., $r = 1.95$, 12 spud injector

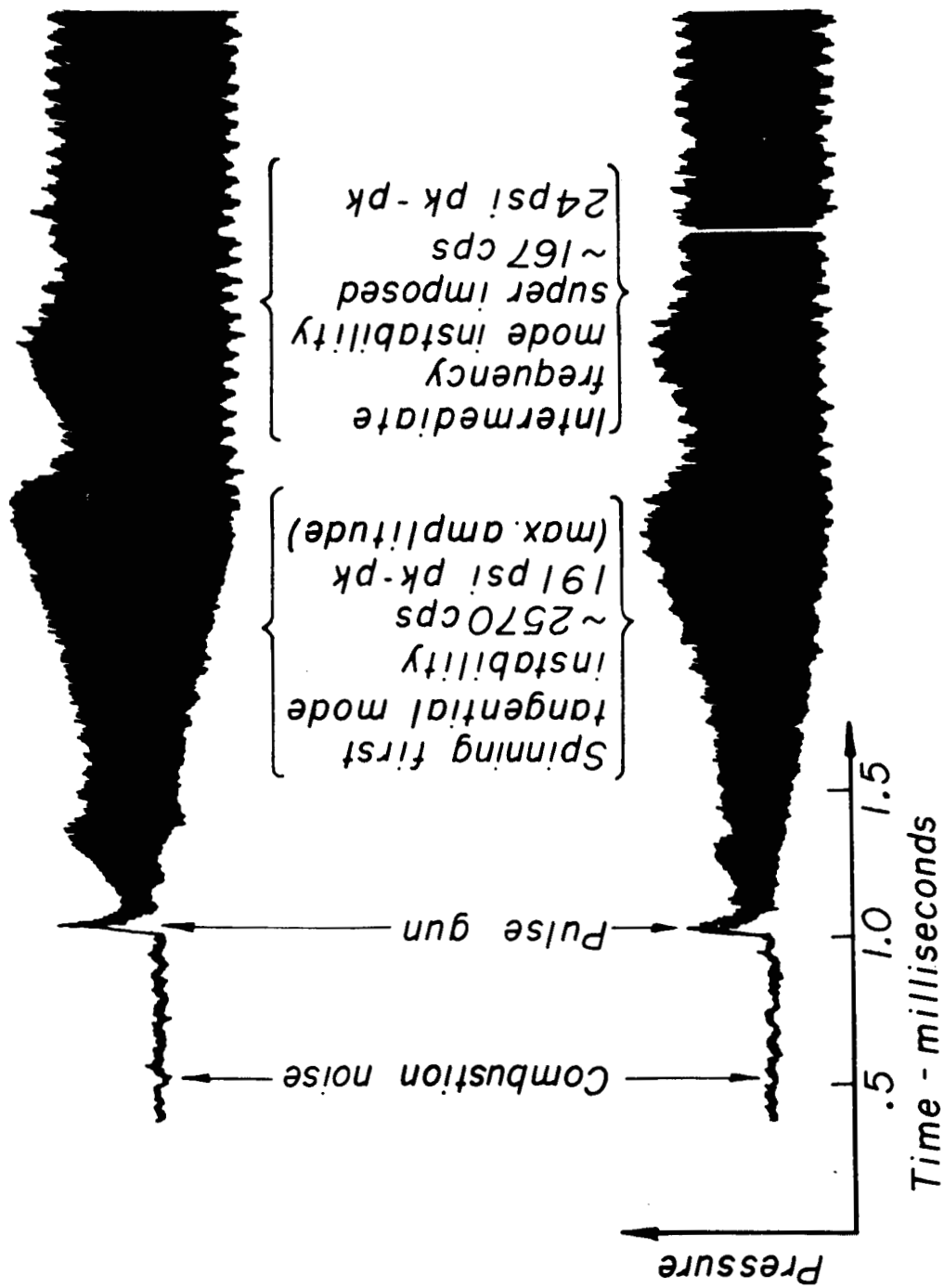


Figure 15

Probe to measure local heat transfer from striated combustion gases

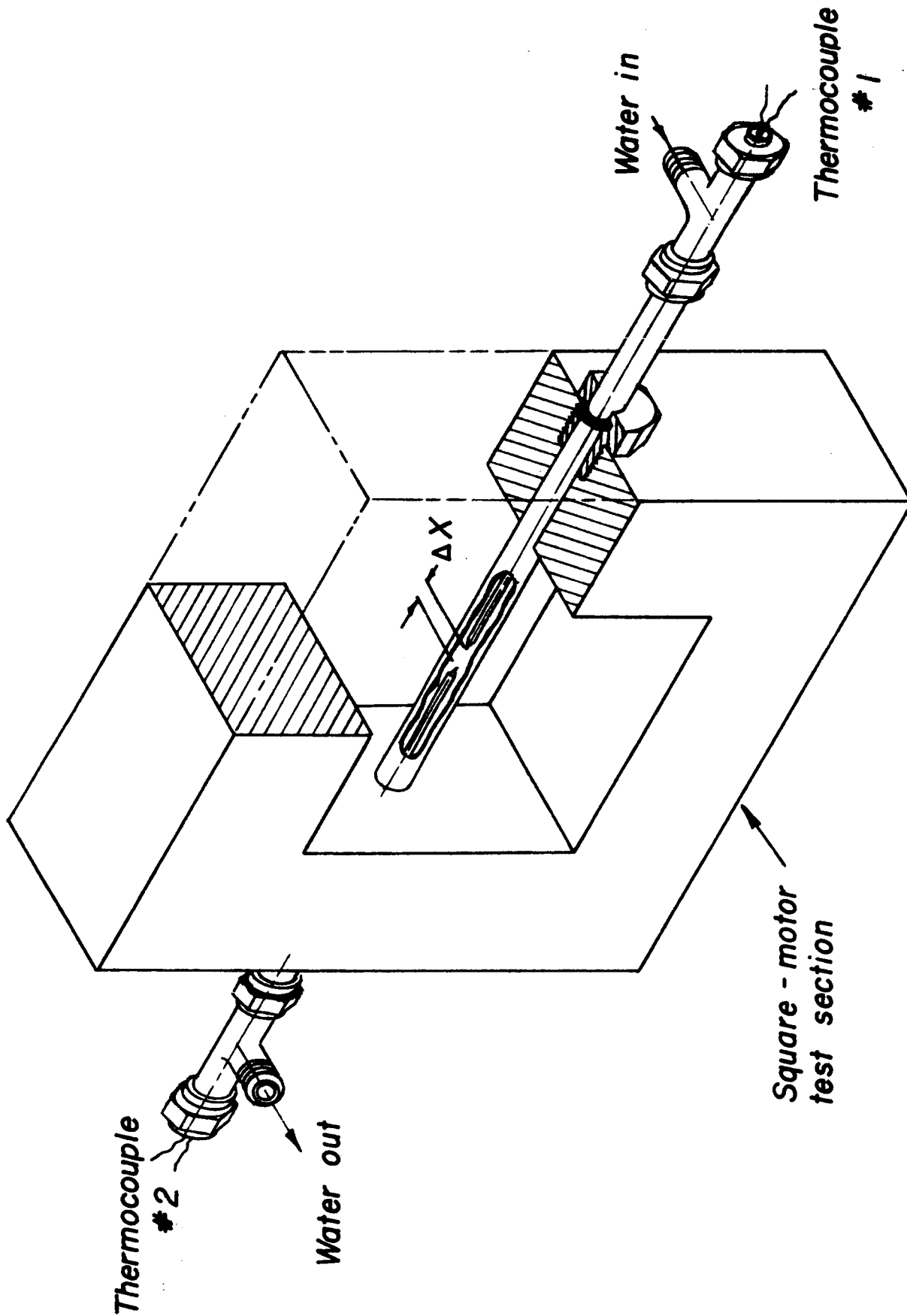


Figure 16

Correction correlation curve

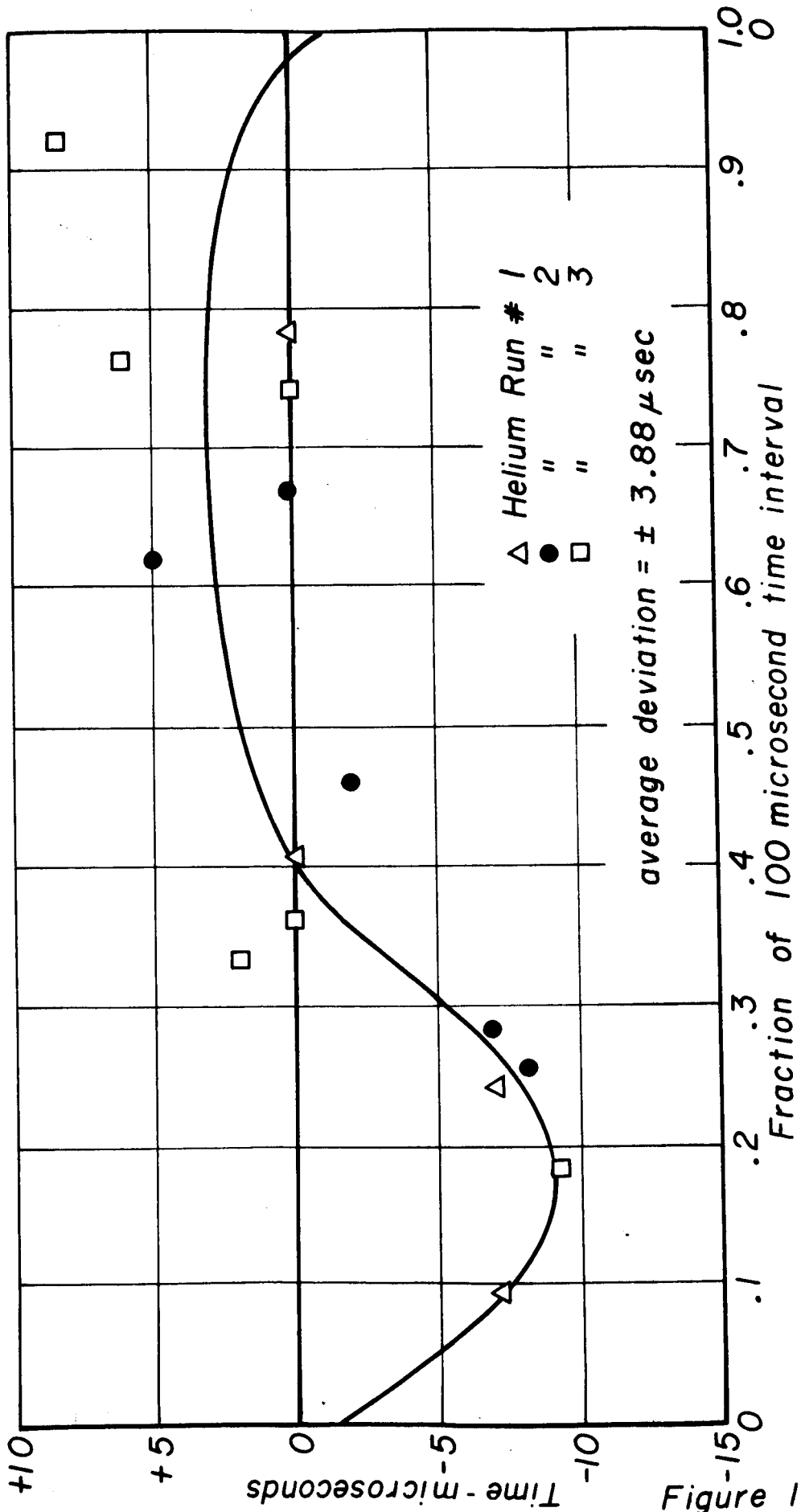


Figure 17

SP21-R4115-66

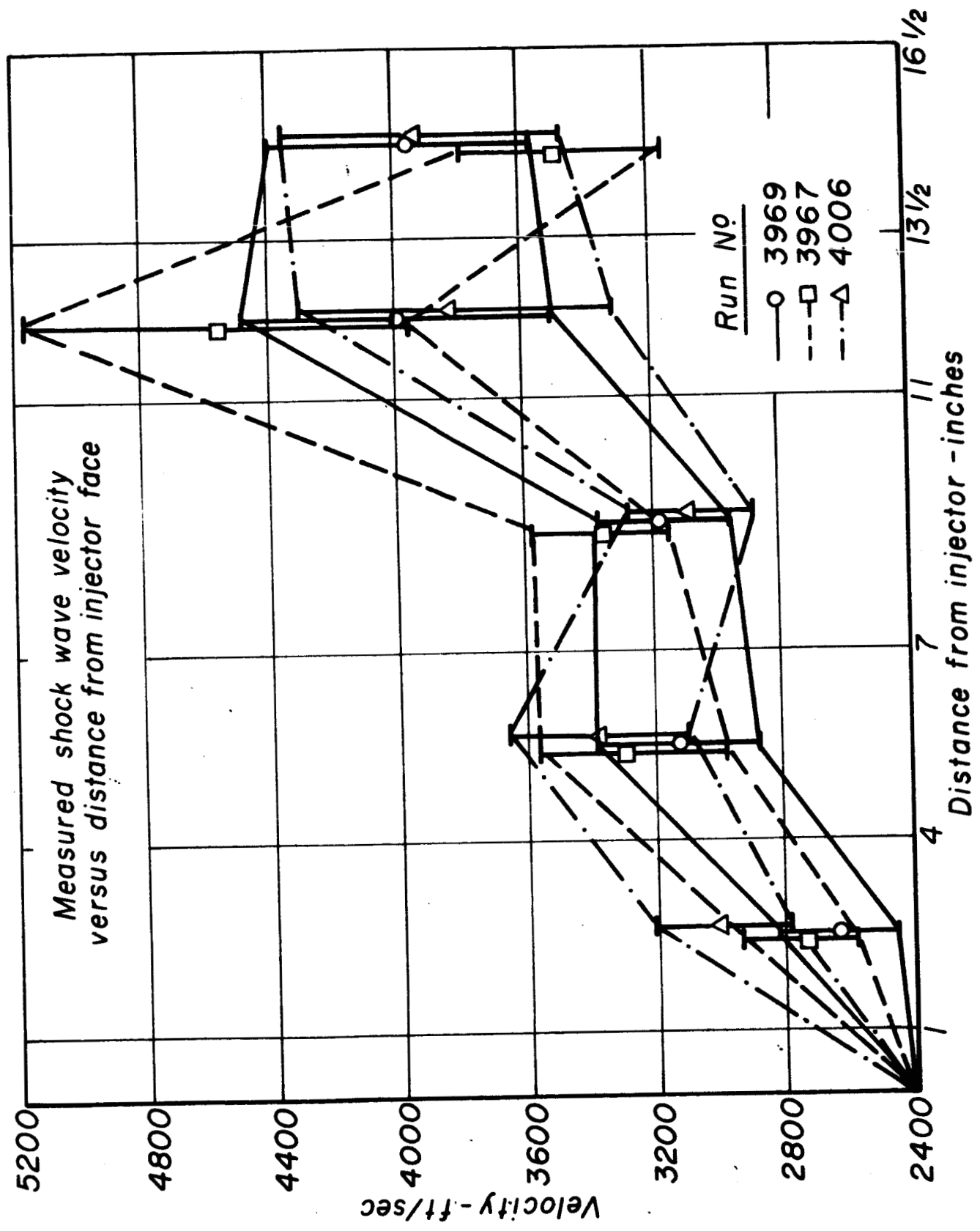
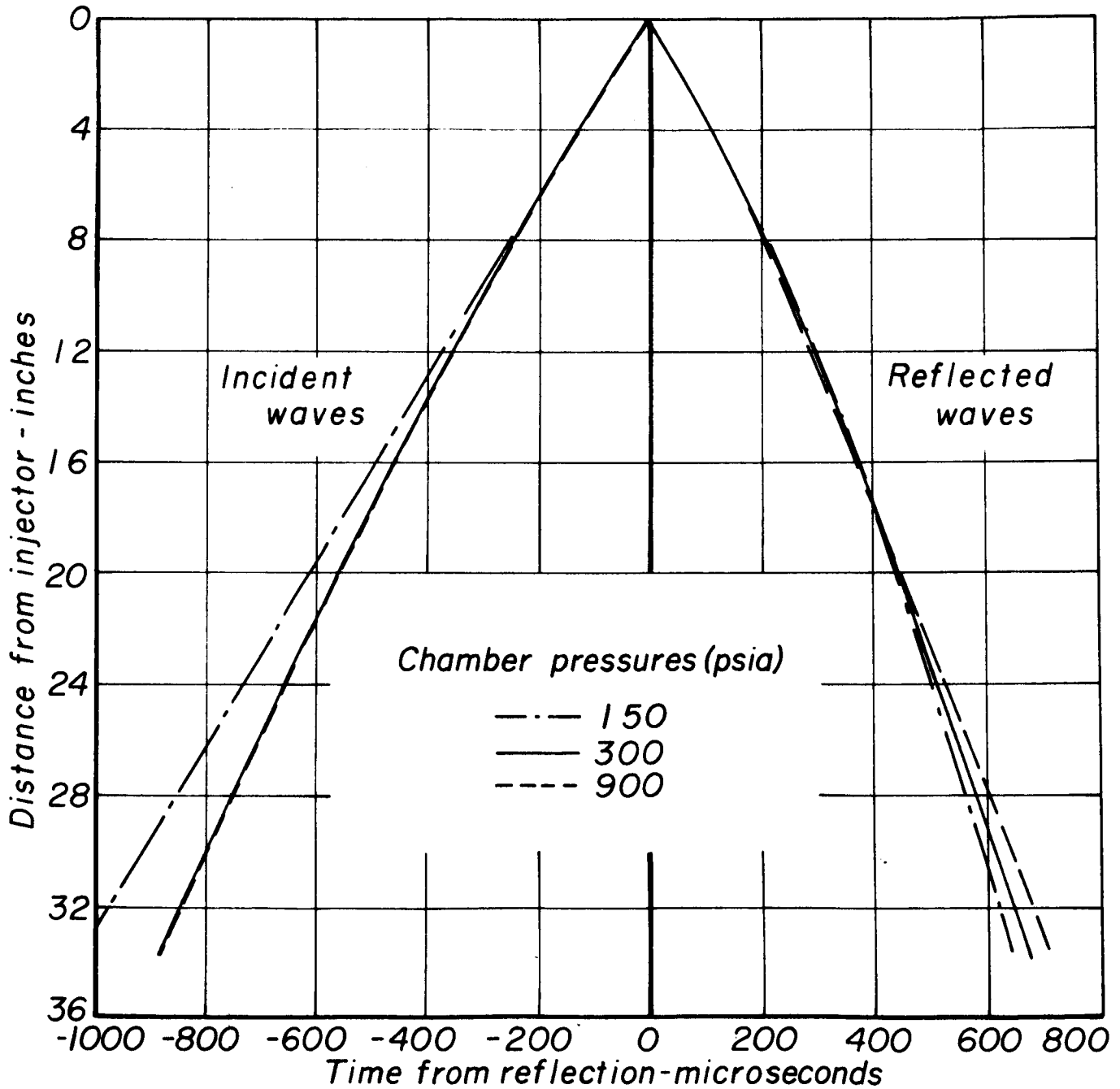


Figure 18

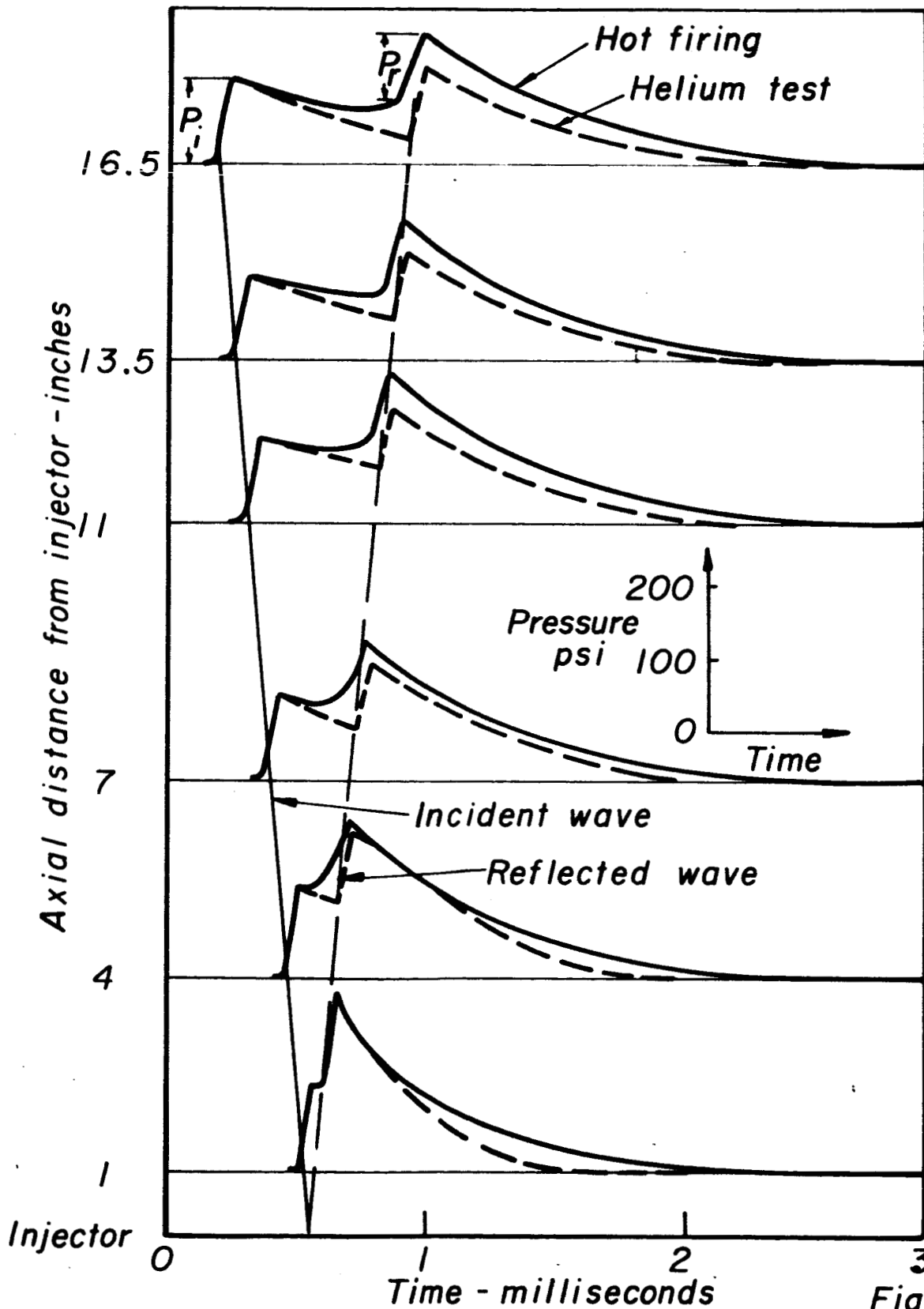
Time-distance history of shock-type wave travel
 for three chamber pressures in a LOX/ALC rocket
 $L = 70$ inches, mass flow = constant, $A_c/A_f = 2, 4 \text{ \& } 12$



VP 24-4116-66

Figure 19

Pressure - time histories at a number of axial stations for a shock - type disturbance



SP21-R1112-66

Figure 20

Amplitude ratio vs location for incident wave, reflected wave and base of reflected wave for LOX/ALC and Helium testing

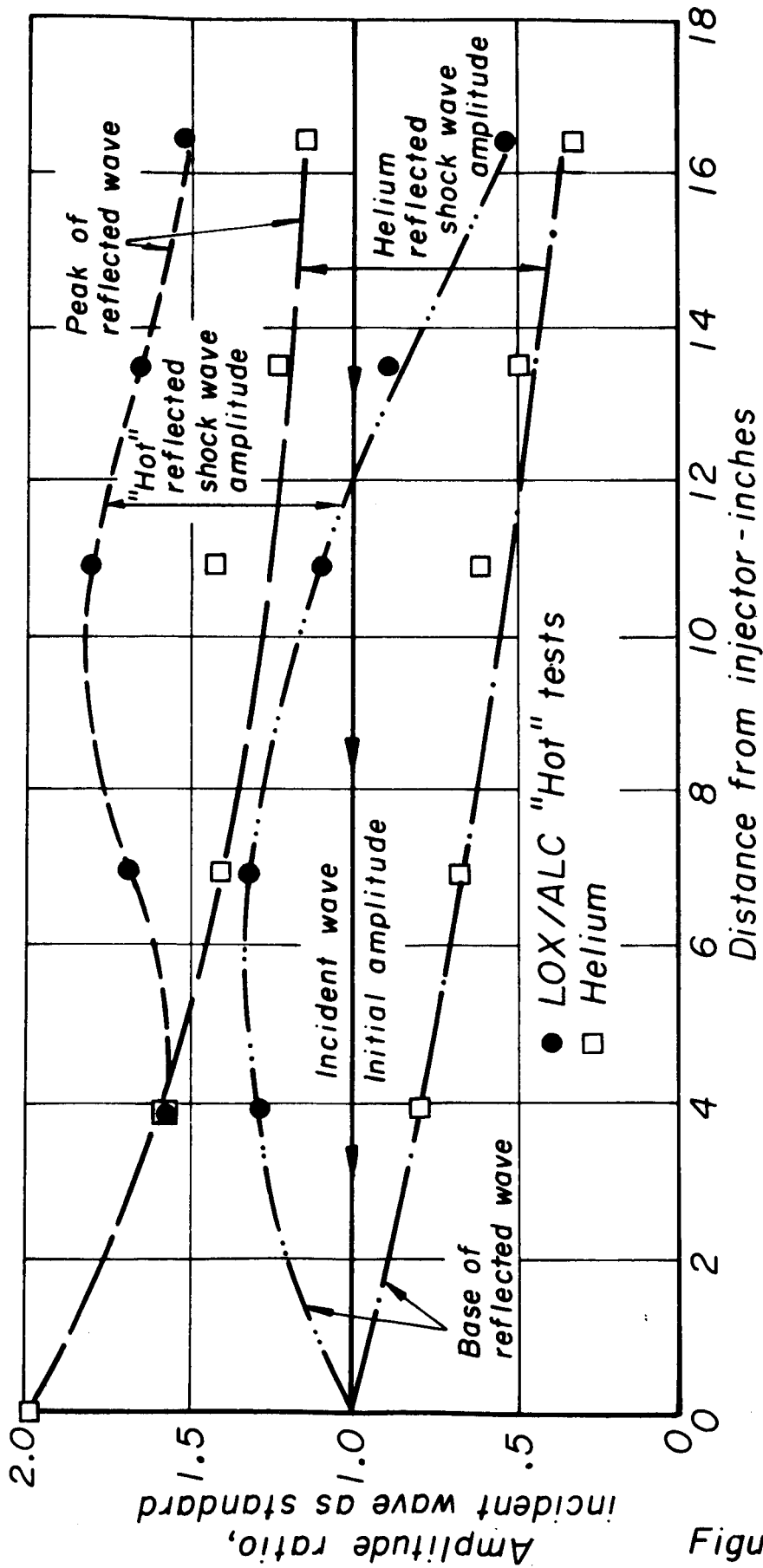


Figure 21

Three tests at 900psia chamber pressure showing the characteristics of the 50th wave

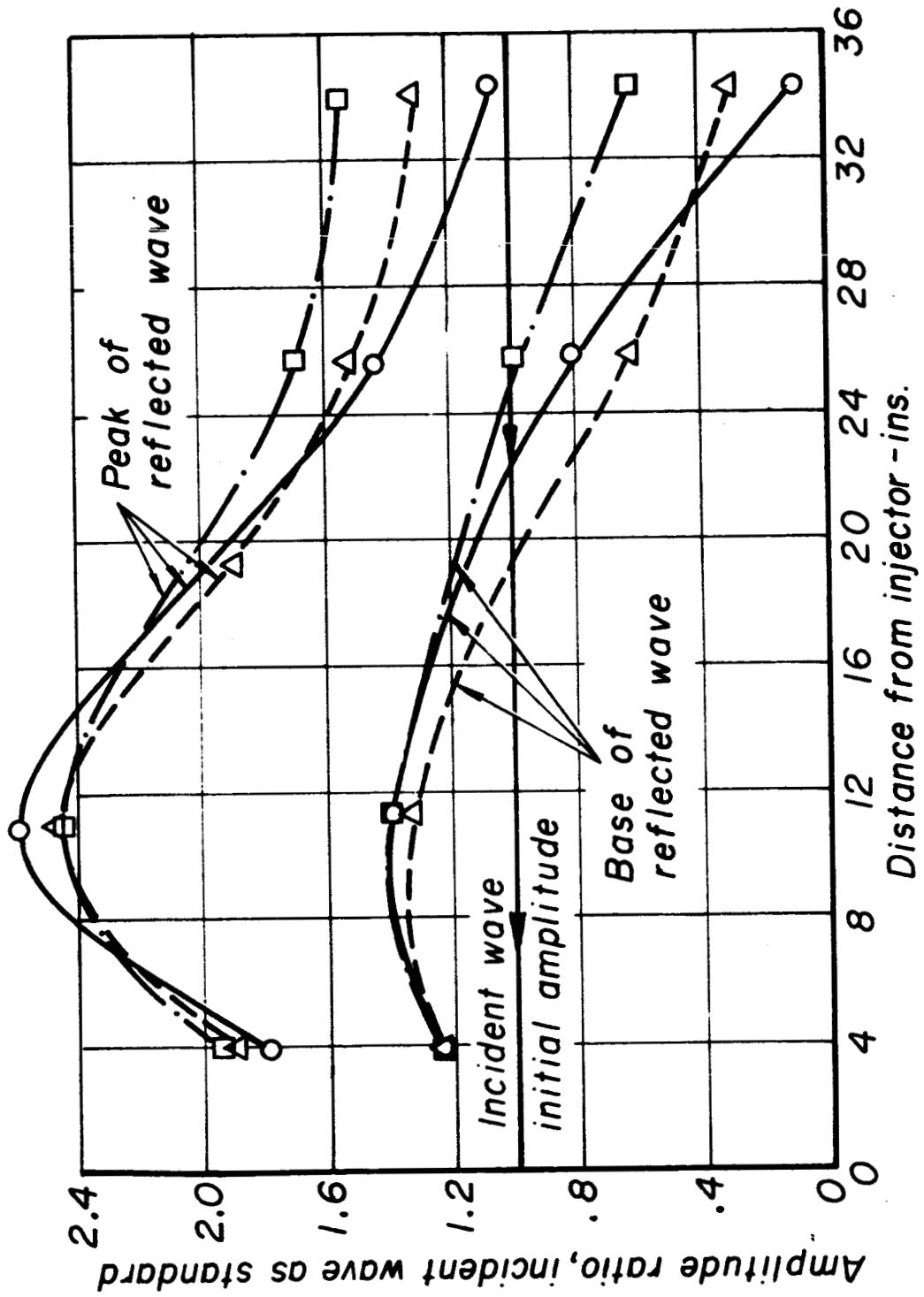


Figure 22

DISTRIBUTION FOR THIS REPORT

NASA

NASA Headquarters
Washington, D.C. 20546
Attn: Alfred Gessow
Robert S. Levine RPL (3)
A.O. Tischler RP

NASA
Universal North Building
Connecticut & Florida Avenues
Washington, D.C.
Attn: T.L. Smull, Director
Grants & Space Contracts (10)

NASA Scientific & Technical
Information Facility
P.O. Box 33
College Park, Maryland 20740 (15)

NASA Headquarters
Washington, D.C. 20546
Attn: E.L. Gray, Director
Advanced Manned Missions, MT
Office of Manned Space Flight

Attn: V.L. Johnson, Director
Launch Vehicles & Propulsion, SV
Office of Space Science

Ames Research Center
Moffett Field
California 94035
Attn: Technical Librarian
Designee: Harold Hornby
Mission Analysis Division

Goddard Space Flight Center
Greenbelt, Maryland 20771
Attn: Technical Librarian
Designee: Merland L. Moseson
Code 620

Jet Propulsion Laboratory
California Institute of Technology
4800 Oak Grove Drive
Pasadena, California 91103
Attn: J.H. Rupe
Attn: Technical Librarian
Designee: Henry Burlage, Jr.
Propulsion Div., 38

Langley Research Center
Langley Station
Hampton, Virginia 23365
Attn: Technical Librarian
Designee: Floyd L. Thompson, Director

NASA
Lewis Research Center
21000 Brookpark Road
Cleveland, Ohio 44135
Attn: M.F. Heidmann (Technical Monitor)
R.J. Priem
E. Conrad

Attn: Technical Librarian
Designee: A. Silverstein, Director

Manned Spacecraft Center
Houston, Texas 77001
Attn: G. Spencer

Attn: Technical Librarian
Designee: Robert R. Gilruth, Director

Marshall Space Flight Center
R-P&VED
Huntsville, Alabama 35812
Attn: Jerry Thomson
R.J. Richmond

Attn: Technical Librarian
Designee: Hans G. Paul

GOVERNMENT INSTALLATIONS

Headquarters, U.S. Air Force
Washington 25, D.C.
Attn: Technical Librarian
Designee: Col. C.K. Stambaugh
AFRST

Aeronautical Systems Division
Air Force Systems Command
Wright-Patterson Air Force Base
Dayton, Ohio 45433
Attn: Technical Librarian
Designee: D.L. Schmidt
Code ASRCNC-2

Air Force Missile Test Center
Patrick Air Force Base
Florida
Attn: Technical Librarian
Designee: L.J. Ullian

Air Force Office of Scientific Research
Propulsion Division
Washington, D.C.
Attn: B.T. Wolfson

Air Force Rocket Propulsion Laboratory
Research & Technology Division
Air Force Systems Command
Edwards, California 93523
Attn: R.R. Weiss, RPRR

Attn: Technical Librarian
Designee: H. Main

Air Force Systems Division
Air Force Unit Post Office
Los Angeles 45, California
Attn: Technical Librarian
Designee: Col. Clark
Technical Data Center

ARL (ARC)
Building 450
Wright-Patterson Air Force Base
Dayton, Ohio
Attn: K. Scheller

Arnold Engineering Development Center
Arnold Air Force Station
Tullahoma, Tennessee
Attn: Technical Librarian
Designee: H.K. Doetsch

Department of the Navy
Bureau of Naval Weapons
Washington, D.C.
Attn: Technical Librarian
Designee: J. Kay
RTMS-41

Department of the Navy
Office of Naval Research
Washington, D.C. 20360
Attn: R.O. Jackel

Defense Documentation Center Headquarters
Cameron Station, Building 5
5010 Duke Street
Alexandria, Virginia 22314
Attn: TISIA

Picatinny Arsenal
Dover, New Jersey 07801
Attn: E. Jenkins

Attn: Technical Librarian
Designee: I. Forsten, Chief
Liquid Propulsion Laboratory
SMUPA-DL

Redstone Scientific Information
Building 4484
Redstone Arsenal
Huntsville, Alabama
Attn: Technical Library

RTNT
Bolling Field
Washington, D.C. 20332
Attn: L. Green, Jr.

U.S. Army Missile Command
Redstone Arsenal
Alabama 35809
Attn: J. Connaughton

Attn: Technical Librarian
Designee: Walter Wharton

U.S. Atomic Energy Commission
Technical Information Services
Box 62
Oak Ridge, Tennessee
Attn: Technical Librarian
Designee: A.P. Huber
Gaseous Diffusion Plant
(ORGDP) P.O. Box P

U.S. Naval Ordnance Test Station
China Lake
California 93557
Attn: E.W. Price

Attn: Technical Librarian
Designee: Code 4562
Chief, Missile Propulsion Div.

CPIA

Chemical Propulsion Information Agency
Applied Physics Laboratory
The John Hopkins University
8621 Georgia Avenue
Silver Spring, Maryland 20910
Attn: T.W. Christian

Attn: Technical Librarian
Designee: Neil Safeer

INDUSTRY CONTRACTORS

Aerojet-General Corporation
P.O. Box 296
Azusa, California 91703
Attn: Technical Librarian
Designee: L.F. Kohrs

Aerojet-General Corporation
P.O. Box 1947
Sacramento, California 95809
Attn: R.J. Hefner
F.H. Reardon
Attn: Technical Librarian
Bldg. 2015, Dept. 2410
Designee: R. Stiff

Aeronutronic
Philco Corporation
Ford Road
Newport Beach, California 92663
Attn: Technical Librarian
Designee: D.A. Carrison

Aerospace Corporation
P.O. Box 95085
Los Angeles, California 90045
Attn: O.W. Dykema
W.C. Strahle

Attn: Technical Librarian
Designee: John G. Wilder
MS-2293
Propulsion Dept.

Astrosystems International, Inc.
1275 Bloomfield Avenue
Fairfield, New Jersey 07007
Attn: Technical Librarian
Designee: A. Mendenhall

Atlantic Research Corporation
Edsall Road and Shirley Highway
Alexandria, Virginia 22314
Attn: Technical Librarian
Designee: A. Scurlock

Battelle Memorial Institute
505 King Avenue
Columbus 1, Ohio
Attn: Charles E. Day,
Classified Rept. Librarian

Bell Aerosystems Company
P.O. Box 1
Buffalo 5, New York 14240
Attn: T. Rossman
J. Senneff

Attn: Technical Librarian
Designee: W.M. Smith

Boeing Company
P.O. Box 3707
Seattle, Washington 98124
Attn: Technical Librarian
Designee: J.D. Alexander

Chrysler Corporation
Missile Division
P.O. Box 2628
Detroit, Michigan 48231
Attn: Technical Librarian
Designee: John Gates

Curtiss-Wright Corporation
Wright Aeronautical Division
Wood-Ridge, New Jersey 07075
Attn: Technical Librarian
Designee: G. Kelley

Defense Research Corporation
6300 Hollister Avenue
P.O. Box 3587
Santa Barbara, California 93105
Attn: B. Gray
C.H. Yang

Douglas Aircraft Company
Missile & Space Systems Division
3000 Ocean Park Boulevard
Santa Monica, California 90406
Attn: Technical Librarian
Designee: R.W. Hallet
Advanced Space Tech.

Douglas Aircraft Company
Astropower Laboratory
2121 Paularino
Newport Beach, California 92663
Attn: Technical Librarian
Designee: George Moc
Director, Research

Dynamic Science Corporation
1445 Huntington Drive
South Pasadena, California
Attn: M. Gerstein

General Dynamics/Astronautics
Library & Information Services (128-00)
P.O. Box 1128
San Diego, California 92112
Attn: Technical Librarian
Designee: Frank Dore

General Electric Company
Advanced Engine & Technology Dept.
Cincinnati, Ohio 45215
Attn: Technical Librarian
Designee: D. Suichu

General Electric Company
Malta Test Station
Ballston Spa, New York
Attn: Alfred Graham, Manager
Rocket Engines

General Electric Company
Re-Entry Systems Department
3198 Chestnut Street
Philadelphia, Pennsylvania 19101
Attn: Technical Librarian
Designee: F.E. Schultz

Geophysics Corporation of America
Technical Division
Bedford, Massachusetts
Attn: A.C. Toby

Grumman Aircraft Engineering Corp.
Bethpage
Long Island, New York
Attn: Technical Librarian
Designee: Joseph Gavin

Ling-Temco-Vought Corporation
Astronautics
P.O. Box 5907
Dallas, Texas 75222
Att: Technical Librarian
Designee: Warren C. Trent

Arthur D. Little, Inc.
20 Acorn Park
Cambridge, Massachusetts 02140
Attn: E. Karl Bastress
Attn: Technical Librarian

Lockheed Missiles & Space Co.
P.O. Box 504
Sunnyvale, California 94088
Attn: Technical Information Center
Designee: Y.C. Lee

Lockheed Propulsion Company
P.O. Box 111
Redlands, California 91409
Attn: Technical Librarian
Designee: H.L. Thackwell

McDonnell Aircraft Corporation
P.O. Box 516
Municipal Airport
St. Louis, Missouri 63166
Attn: Technical Librarian
Designee: R.A. Herzmark

The Marquardt Corporation
16555 Saticoy Street
Van Nuys, California 91409
Attn: Technical Librarian
Designee: Warren P. Boardman, Jr.

Martin Marietta Corporation
Denver Division
P.O. Box 179
Denver, Colorado 80201
Attn: Technical Librarian
Designee: J.D. Goodlette (A-241)

Multi-Tech. Inc.
Box 4186 No. Annex
San Fernando, California
Attn: F.B. Cramer

Northrup Space Laboratories
3401 West Broadway
Hawthorne, California
Attn: Technical Librarian
Designee: William Howard

Rocket Research Corporation
520 South Portland Street
Seattle, Washington 98108
Attn: Technical Librarian
Designee: Foy McCullough, Jr.

Rocketdyne
Division of North American Aviation
6633 Canoga Avenue
Canoga Park, California 91304
Attn: R. Fontaine
R.B. Lawhead

Attn: Technical Librarian
(Library 586-306)
Designee: E.B. Monteath

Space & Information Systems Division
North American Aviation, Inc.
12214 Lakewood Boulevard
Downey, California 90241
Attn: Technical Librarian
Designee: H. Storms

Rohm & Haas Company
Redstone Arsenal
Huntsville, Alabama
Attn: Librarian

Stanford Research Institute
333 Ravenswood Avenue
Menlo Park, California 94025
Attn: Technical Librarian
Designee: Lionel Dickinson

Thiokol Chemical Corporation
Huntsville Division
Huntsville, Alabama
Attn: Technical Librarian
Designee: John Goodloe

Thiokol Chemical Corporation
Reaction Motors Division
Denville, New Jersey 07832
Attn: D. Mann

Attn: Technical Librarian
Designee: Arthur Sherman

TRW Systems
One Space Park
Redondo Beach, California 90278
Attn: G.W. Elverum
Attn: Donald H. Lee
Attn: Technical Librarian

United Technology System
Division of United Aircraft Corporation
P.O. Box 358
Sunnyvale, California 94088
Attn: R.H. Osborn
Attn: Technical Librarian

Pratt & Whitney Aircraft Company
Division of United Aircraft Corp.
West Palm Beach
Florida
Attn: G. Lewis

Pratt & Whitney Aircraft Company
Division of United Aircraft Corp.
Engineering, Building 1-F
East Hartford, Connecticut
Attn: D.H. Utvik

Research Laboratories
Division of United Aircraft Corp.
400 Main Street
East Hartford, Connecticut 06108
Attn: Technical Librarian
Designee: Erle Martin

Walter Kidde and Company
Aerospace Operations
567 Main Street
Belleville, New Jersey 07109
Attn: Technical Librarian
Designee: R.J. Hanville
Director of Research Eng.

Warner-Swasey Company
Control Instrument Division
32-16 Downing Street
Flushing, New York 11354
Attn: R.H. Tourin

UNIVERSITIES

California Institute of Technology
204 Karman Laboratory
Pasadena, California 91109
Attn: Fred E. Culick

Dartmouth University
Hanover
New Hampshire
Attn: P.D. McCormack

Georgia Institute of Technology
Aerospace School
Atlanta 13
Georgia
Attn: Ben T. Zinn

Illinois Institute of Technology
10 W. 35th Street
Chicago, Illinois
Attn: P.T. Torda

The John Hopkins University
Applied Physics Laboratory
8621 Georgia Avenue
Silver Spring, Maryland
Attn: W.G. Berl

Massachusetts Institute of Technology
Cambridge 39
Massachusetts
Attn: T.Y. Toong
Dept. of Mechanical Engineering
Attn: Gail E. Partridge, Librarian
Engineering Projects Laboratory

New York University
Dept. of Chemical Engineering
New York 53, New York
Attn: P.F. Winternitz

Ohio State University
Rocket Research Laboratory
Dept. of Aeronautical & Astronautical Eng.
Columbus 10, Ohio
Attn: Technical Librarian

Polytechnic Institute of Brooklyn
Graduate Center
Route 110
Farmingdale, New York
Attn: V.D. Agosta

Purdue University
School of Mechanical Engineering
Lafayette, Indiana
Attn: J.R. Osborn

Sheffield University
Research Laboratories
Harpur Hill
Buxton, Derbyshire
England
Attn: V.J. Ibberson

University of California
Institute of Engineering Research
Berkeley, California
Attn: A.K. Oppenheim

University of Michigan
Aeronautical & Astronautical Eng. Labs.
Aircraft Propulsion Lab.
North Campus
Ann Arbor, Michigan
Attn: J.A. Nicholls

University of Wisconsin
Dept. of Mechanical Engineering
1513 University Avenue
Madison, Wisconsin
Attn: P.S. Myers

Yale University
Dept. of Engineering & Applied Science
Mason Laboratory
400 Temple Street
New Haven, Connecticut
Attn: B.T. Chu